Bayesian Uncertainty Quantification of Hanger Tension in Arch Bridges Using Modal Frequency Measurements

Konstantina Giakoumi

A thesis submitted in partial fulfillment of the requirements for
the Diploma of Mechanical Engineering

University of Thessaly
School of Engineering
Department of Mechanical Engineering

Volos 2014

Approved by the committee members:

First examiner (Supervisor) Professor Costas Papadimitriou
University of Thessaly, Mechanical Engineering department

Second examiner Professor Nikolaos Aravas
University of Thessaly, Mechanical Engineering department

Second examiner Professor Panos Tsopelas
University of Thessaly, Civil Engineering department

Abstract

The objective of this thesis is to estimate the axial loads of bridge hangers using experimentally identified modal frequencies. A Bayesian structural identification methodology is used to estimate the axial load and its uncertainty. Two different model classes are considered to simulate the vibrations of the hangers: an analytical model based on the Euler-Bernoulli theory, and a high fidelity finite element model of the hanger. The effect of the boundary conditions of the hangers on the estimate of the axial loads and their uncertainties is investigated. It is demonstrated that the boundary conditions have significant impact on the frequencies of hangers used in arch bridges. It is also shown that a fixed-end high fidelity finite element model of the hanger underestimates the axial loads by more than 20%. The simplified beam model with flexible end conditions gives fairly accurate results, close to the ones obtained from the high fidelity finite element model with flexible support conditions. The Bayesian framework for structural identification is effective in estimating the axial loads and boundary conditions in hangers as well as selecting the most appropriate model class to be used for representing the vibrational characteristics of actual hangers.

Acknowledgments

I would like to express my sincere gratitude to my supervisor Professor Costas Papadimitriou for his support, guidance and immense knowledge. In addition, a thank to all the members of the Systems Dynamics Laboratory for their collaboration and their contribution to this thesis. I would also like to thank my family and friends for their support and finally, I want to express my appreciation to Alexios Lorens Vamvakas for his continuous encouragement during the last year and his assistance for the implementation of this work.

Contents

List of Figures

List of Tables

Nomenclature

η_n	Dimensionless parameter=f/f_n^S
ϕ_n	Dimensionless parameter=f/f_n^B
ρ	Density
σ	Prediction error
θ	Model parameters
ξ	Dimensionless parameter $\xi = l\sqrt{\frac{T}{EI}}$
f_n	Measured natural frequency of cable in n-th mode
f_n^B	Theoretical value of nth-order natural frequency of a beam clamped at both ends
f_n^S	Theoretical values of nth-order natural frequency of a string
$u(z,t)$	Deflection in of cable in y-direction due to vibration
A	Area
EI	Flexular rigidity of the cable
f	Theoretical natural frequency of cable
g	Gravitational acceleration
I	Second moment of area
T	Cable force
t	Time
w	Weight of cable per unit length

Chapter 1

Introduction

1.1 Objectives

The objective of this thesis is to estimate the axial loads in hangers using modal frequencies identified from modal tests. The hangers are used as deck support elements in arch bridges. Two general classes of models are introduced to represent the dynamics of the hangers. The first model class is an analytical beam model based on Euler-Bernoulli theory. The second model class is a high fidelity finite element model developed in Abaqus. Both model classes can be used to predict the hanger modal frequencies given the axial load in the hanger. These predictions also depend on the boundary conditions at the end of the hangers. Part of the objective of this thesis is to investigate the effect of the boundary conditions on the estimate of the hanger forces. Bayesian inference [1], [2], [3] is used to identify the values and the uncertainties in the values of the axial force and the boundary conditions based on the measured modal frequencies for a hanger. Finally, Bayesian model selection method [4] is used to select the best model class for representing the dynamics of the hangers.

1.2 Description of Hanger and Experimental Data

The hanger under investigation is one of the hangers used to support the deck of the arch bridge shown in Figure 1.1. The arch bridge consists of 20 hangers in total, ten on each side, symmetrically located, to support the deck. The hanger geometry, along with the geometry of the connections of the hangers to the deck and the arch, is shown in Figure 1.2. All hangers are cylindrical and solid with diameter $D = 0.130$m. They are made out of steel and they are connected to the deck and the arch element with edge plates as shown in Figure 1.3. The edge plates are welded to the hangers and deck or the arch. The connections of the hanger with the deck or the arch with end plates are approximately 1 m long and may affect significantly the boundary conditions of hangers. From the geometry of the plates, shown in Figures 1.2 and 1.3, it is clear that the plate that connects the hanger with the deck has its orientation along the longitudinal direction of the bridge deck, while the plate that connects the hanger to the arch has its orientation along the transverse direction of the bridge deck.

It should be noticed that the hangers considered in this work have many differences from the conventional cables. A conventional cable has small bending stiffness but the

solid plate installed in there hangers contributes significantly to the bending stiffness.

Based on the design plans, the geometry, the material properties and the connection details of the two edge plates of the hanger are identical. The only difference is the orientation of each edge plate. Given that the end conditions of the edge plates can be considered to be fixed, then it is expected that the prediction of the modal frequencies from the analytical or the numerical models in the longitudinal and transverse direction of vibration of the hanger would be identical. Table 1.1 shows the identified eigenfrequencies of hanger 3 in the transversal and longitudinal direction. These eigenfrequencies or modal frequencies were obtained by analysing the force and acceleration time histories obtained from impulse hammer tests performed on the hanger. It is observed that the modal frequencies differ in the two directions (longitudinal and transverse). This is a strong indication that the boundary conditions at the end of the hangers cannot be assumed to be fixed. This study considers the effect of the boundary conditions on the estimation of the axial force.

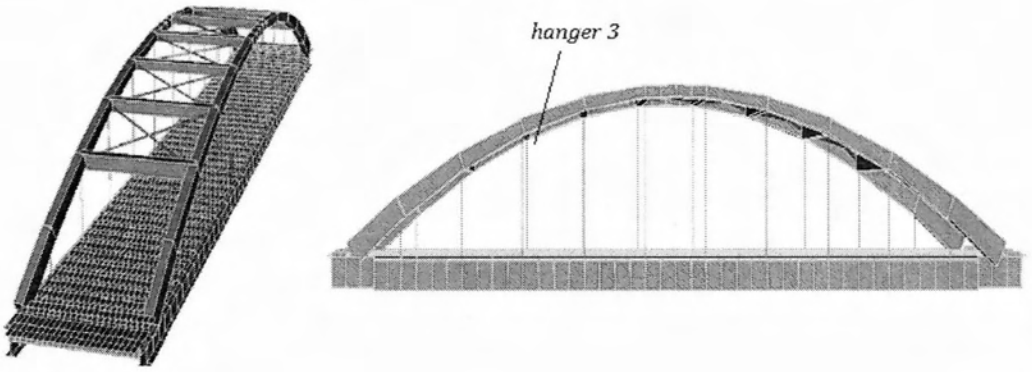

Figure 1.1: The geometry of the bridge

Table 1.1: The experimental frequencies (Hz) of hanger 3 in the transversal and longitudinal direction

	trans	long
Mode 1	5.82	6.09
Mode 2	13.85	14.8
Mode 3	26.17	27.0
Mode 4	40.47	41.8
Mode 5	59.3	61.5
Mode 6	81.3	83.68

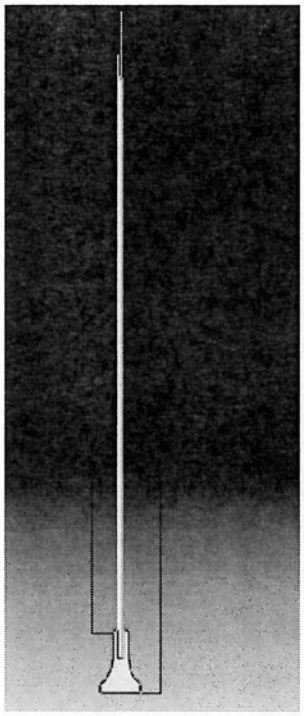

Figure 1.2: The geometry of hanger 3

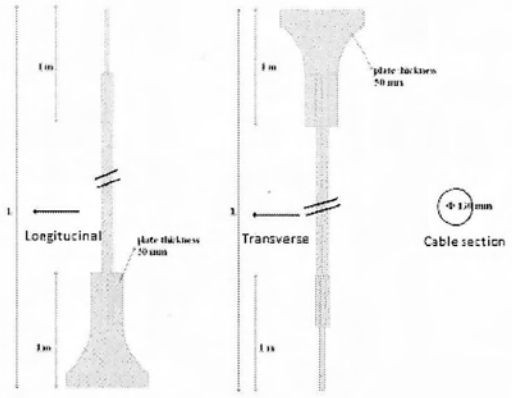

Figure 1.3: The geometry of the plates

1.3 Literature review

Several methods have been proposed for the estimation of the cable tension. One of the first important researches in the field was conducted by Zui et al. [5] with the proposal of practical formulas for the estimation of the tension from the identified natural frequencies. Ren et al. [6] presented a new version of the practical formulas, after having explained the relative influence of the sag-extensibility and the bending stiffness. Ni et al. [7] proposed a method for the analysis of a suspended bridge and a stay-cable bridge. Ceballos and Prato [8] introduced two rotational springs at the cable ends to represent all the possible boundary conditions and the stiffness of the springs is extracted from the first mode that cannot be estimated by the identification procedure. Successively, the axial force of the cable can be calculated. Bellino et al. [9] proposed a method to estimate the cable tension by means of vibration response and moving mass technique. The same authors developed the method [10] by adding springs in order to simulate the different boundary conditions and they introduced the equivalent length.

1.4 Thesis outline

This thesis studies the effect of the model assumptions and the boundary conditions on the estimation of the axial forces. In contrast to existing methods, the present work uses more than one modal frequencies to estimate the axial force and the boundary conditions. Bayesian inference [1] is used for the first time to estimate also the uncertainty in the estimates of the axial force and the boundary conditions as well as to select the best model out of a series of increasingly complex models, including analytical ones as well as high fidelity finite element models with various boundary conditions introduced to represent the support conditions of the hanger.

This thesis is organised as follows. Chapter 2 introduces the beam models based on the Euler-Bernoulli beam theory, in order to predict the modal frequencies of the hanger with various boundary conditions, given the tension on the hanger. Two sets of boundary conditions are considered, one with fixed ends and the other with flexible ends quantified by rotational springs attached at the ends. Analytical transcendental equations are developed and are numerically solved to obtain the modal frequencies. The iterative scheme for solving for the higher order modal frequencies is not trivial and this procedure is also outlined.

In Chapter 3, high fidelity three-dimensional finite element models of the hanger 3 of the arch bridge with different boundary conditions are developed. The purpose is to predict the modal frequencies of the hanger given the axial load and the boundary conditions. For high axial loads large deflections are obtained which introduce geometrical nonlinearities. These nonliearities increase the stiffness of the structure at the equilibrium state and thus affect the modal frequencies. In fact the modal frequencies are obtained by solving the geometrically nonlinear problem for a hanger subjected to large axial loads and then using the tangent stiffness matrix at the final equilibrium position to estimate the modal frequencies. The tangent stiffness matrix depends on the axial force. Only large enough axial forces can give tangent stiffness matrix that is different from the initial stiffness matrix of the hanger. The procedure to estimate the modal frequencies is outlined.

Chapter 4 presents the Bayesian uncertainty quantification and calibration methodology for estimating the axial force and boundary conditions of the hanger based on the two different model classes introduced in Chapters 2 and 3, as well as the twelve experimentally identified modal frequencies shown in Table 1.1. The uncertainties in the estimates are also obtained from the Bayesian methodology. The Transitional Markov Chain Monte Carlo algorithm [1] is used to provide estimates of the axial forces and the boundary conditions, along with the associated uncertainty in their values. Results are presented for five model classes, two are based on the Euler-Bernoulli beam model with fixed and flexible boundary conditions and three are based on the high fidelity finite element model with fixed and flexible boundary conditions. The results are compared and useful conclusions are obtained related to the estimate of the hanger axial force along with its uncertainty, the effect of edge supports and boundary conditions on the prediction of the axial load, as well as the adequacy of each one of the five model class to represent the dynamics of the hanger.

Finally, chapter 5 presents the conclusions of this thesis.

Chapter 2

Modal Frequency Predictions of Hangers based on Beam Theory

The methodology of predicting the modal frequencies of the beam subjected to an axial load is presented in this chapter.

The development of the model is based in Euler-Bernoulli beam theory. This theory is a simplification of the linear theory of elasticity which provides a means of calculating the load-carrying and deflection characteristics of beams. It covers the case for small deflections of a beam that is subjected to lateral loads only. The boundary conditions of the beam are examined. In the first model the ends of the beam are considered fixed, whereas in the second, the ends are considered flexible and are modelled by springs.

2.1 Assumptions

Prior to the formulation of the mathematical model, several assumptions that are presented below have been made in order to simplify the analysis:

- Cable material is homogeneous, isotropic and linearly elastic
- Strains are small, thus shear deformation and Poisson's ratio are neglected
- Beam cross section is infinetely rigid in its own plane
- The cross-section of the beam remains plane after deformation
- The cross-section remains normal to the deformed axis of the beam

2.2 Equation of Motion

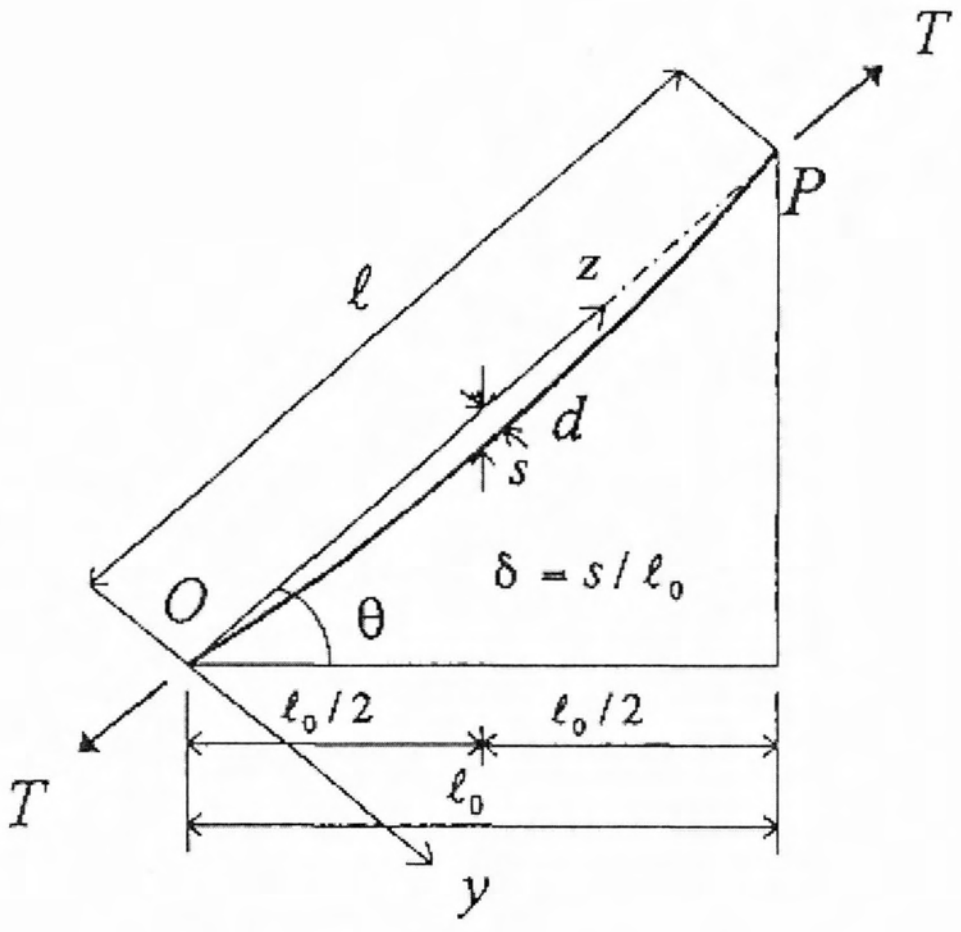

Figure 2.1: Free body diagram of a beam segment

Consider the free body diagram of an element of a beam segment [11] shown in Fig. 2.1 where M(z,t) is the bending moment, V(z,t) is the transverse shear force, f(z,t) is the external force per unit length of the beam and T is the axial force. Gravitational forces are neglected. The inertial force acting on the element of length dz is

$$\rho A dz \left(\frac{\partial^2 u}{\partial t^2}\right) \tag{2.1}$$

The equation of motion of the beam element is

$$-(V + \frac{\partial V}{\partial z}\, dz) + f(z,t)dz + V = \rho A dz \left(\frac{\partial^2 u}{\partial t^2}\right) \tag{2.2}$$

which simplifies to

$$-\frac{\partial V}{\partial z} dz + f(z,t)dz = \rho A dz \left(\frac{\partial^2 u}{\partial t^2}\right) \tag{2.3}$$

and eventually leads to

$$-\frac{\partial V}{\partial z} + f(z,t) = \rho A \left(\frac{\partial^2 u}{\partial t^2}\right) \tag{2.4}$$

The equation of motion for moments about the x axis at the left end of the beam element in Fig. 2.1 is given as:

$$(M + \frac{\partial M}{\partial z} dz) - V dz + f(z,t)\frac{dz^2}{2} - T\theta dz = 0 \tag{2.5}$$

Disregarding terms that include second orders of dz we can write equation (2.5) as

$$\frac{\partial M}{\partial z} - V(z,t) - T\theta = 0 \tag{2.6}$$

or equivalently

$$V = \frac{\partial M}{\partial z} - T\theta = 0 \tag{2.7}$$

Substituting (2.7) into (2.4) one readily derives the equation :

$$-\frac{\partial^2 M}{\partial^2 z} + T\frac{\partial \theta}{\partial z} + f(z,t) = \rho A \left(\frac{\partial^2 u}{\partial t^2}\right) \tag{2.8}$$

For small deflections,

$$tah(\theta) = \theta = \frac{\partial u}{\partial z} \tag{2.9}$$

and from the Euller-Bernouli beam theory, the relationship between bending moment and deflection can be expressed as [12]

$$M(z,t) = EI(z,t) \left(\frac{\partial^2 u}{\partial t^2}\right) \tag{2.10}$$

where E is the Modulus of Elasticity and I is is the moment of inertia of a beam cross

section about the y-axis. By inserting (2.9) and (2.10) into (2.8) we obtain the equation of motion of the cable:

$$EI\frac{\partial^4 u}{\partial z^4} - T\frac{\partial^2 u}{\partial z^2} + \rho A\left(\frac{\partial^2 u}{\partial t^2}\right) = 0 \tag{2.11}$$

2.3 Eigenproblem Solution

The method of separation of variables is applied to the equation (2.11) assuming that the solution has the following form :

$$u(z,t) = u^*(z)q(t) \tag{2.12}$$

Then (2.11) yields the following equation for $u^*(z)$

$$EI\frac{\partial^4 u*}{\partial z^4} - T\frac{\partial^2 u*}{\partial z^2} - \frac{w}{g}\omega^2 = 0 \tag{2.13}$$

The general solution of (2.13) is:

$$u^*(z) = Asinh(bz) + Bcosh(bz) + Csin(az) + Dcos(az) \tag{2.14}$$

2.4 Boundary Conditions

Two different sets of boundary conditions will be applied creating two problems: the fixed ends and the flexible ends.

2.4.1 Problem A:Euler-Bernoulli beam with Fixed ends

In problem A the beam is considered to have both ends fixed. The boundary conditions are the following:

$$\begin{aligned} u(0,t) &= 0 \\ u(l,t) &= 0 \\ u'(0,t) &= 0 \\ u'(l,t) &= 0 \end{aligned} \tag{2.15}$$

By applying (2.12) to the boundary conditions for $u^*(z)$ become

$$\begin{aligned} u^*(0) &= 0 \\ u^*(l) &= 0 \\ u^{*'}(0) &= 0 \\ u^{*'}(l) &= 0 \end{aligned} \tag{2.16}$$

From the general solution (2.14) and the boundary conditions, the following 4x4 linear algebraic equation is satisfied:

$$\begin{pmatrix} 0 & 1 & 0 & 1 \\ b & 0 & a & 0 \\ sinh(bl) & cosh(bl) & sin(al) & cos(al) \\ bcosh(bl) & bsinh(bl) & acos(al) & -asin(al) \end{pmatrix} \begin{pmatrix} A \\ B \\ C \\ D \end{pmatrix} = 0 \tag{2.17}$$

which is of the form $\bar{A}x = \bar{0}$ where

$$\bar{A} = \begin{pmatrix} 0 & 1 & 0 & 1 \\ b & 0 & a & 0 \\ sinh(bl) & cosh(bl) & sin(al) & cos(al) \\ bcosh(bl) & bsinh(bl) & acos(al) & -asin(al) \end{pmatrix} \tag{2.18}$$

To obtain non trivial solutions of (2.18) we set the determinant of $\bar{A}$ to 0 and the following characteristic equation (2.20) arises :

$$det \begin{pmatrix} 0 & 1 & 0 & 1 \\ b & 0 & a & 0 \\ sinh(bl) & cosh(bl) & sin(al) & cos(al) \\ bcosh(bl) & bsinh(bl) & acos(al) & -asin(al) \end{pmatrix} = 0 \tag{2.19}$$

which is also written as:

$$detA = 2(al)(bl)[1 - cos(al)cos(bl)] + [(bl)^2 - (al)^2]sin(al)sinh(bl) = 0 \tag{2.20}$$

where the parameter al and bl are given with respect to the parameters ζ, γ as

$$al = l\sqrt{\sqrt{\zeta^4 + \gamma^4} - \zeta^2} \tag{2.21}$$

$$bl = l\sqrt{\sqrt{\zeta^4 + \gamma^4} - \zeta^2} \tag{2.22}$$

$$\zeta^2 = \sqrt{\frac{T}{EI}} \tag{2.23}$$

$$\gamma^4 = \frac{w\omega^2}{gEI} \tag{2.24}$$

The unknown ω is contained on γ and the axial force T is contained in ζ. The problem of estimating ω given the axial force T is turned into the problem of estimating γ given the value of ζ. The values of γ can be obtained by the numerical solution of (2.13). This equation gives as many modal frequencies γ (equivalent of ω) as they are desired by the analysis.

Normalization

The following dimensionless parameter ξ is introduced:

$$\xi = \sqrt{\frac{T}{EI}}l \tag{2.25}$$

The value of ξ according to literature [5] has a significant role at the dynamic behaviour of the cable. For large values of ξ (> 20) the dynamic characteristics of the cable are similar to those of a string. When ξ becomes small the solution of (2.20), increases very rapidly, and it becomes difficult to obtain exact solutions. Thus, these equations are not suitable for the region of small values of ξ. When ξ is small the characteristics of a cable are similar to that of a beam. two different normalizations are next proposed depending on the range of ξ values

Large ξ

For large values of ξ introduce the normalized parameter η_n:

$$\eta_n = \frac{f}{f_n^s} \tag{2.26}$$

where f_n^s is the theoretical values of the nth order natural frequency of a string [13] given by:

$$f_n^s = \frac{n}{2l}\sqrt{\frac{Tg}{w}} \tag{2.27}$$

By substituting them to (2.21) and (2.22) we obtain:

$$al = \frac{\xi}{\sqrt{2}}\sqrt{-1 + \sqrt{1 + (\frac{2n\pi\eta_n}{\xi})^2}} \tag{2.28}$$

$$bl = \frac{\xi}{\sqrt{2}}\sqrt{1 + \sqrt{1 + (\frac{2n\pi\eta_n}{\xi})^2}} \tag{2.29}$$

By substituting (2.28) and (2.29) in (2.20) we obtain the characteristic equation in the form

$$2n\eta_n(1 - cos(al)cosh(bl)) + \xi sin(al)sinh(bl) = 0 \tag{2.30}$$

The normalized modal frequencies η_n are obtained by solving the characteristic equation (2.30) for a given value of ξ.

Small ξ

For small ξ (< 20)we introduce the dimensionless parameter ϕ_n:

$$\phi_n = \frac{f}{f_n^B} \tag{2.31}$$

where f_n^B is the theoretical values of the n-th order natural frequency of a beam fixed at both ends [13] and is given as follows:

$$f_n^B = \frac{a_n^2}{2\pi l^2}\sqrt{\frac{EIg}{w}} \tag{2.32}$$

The values of a_n are the solutions of $cos(a)cosh(a) = 1$. The first ten solutions are the following:

$$\begin{pmatrix} a_1 = 4.73 \\ a_2 = 7.8532 \\ a_3 = 10.9956 \\ a_4 = 14.1372 \\ a_5 = 17.2788 \\ a_6 = 20.4204 \\ a_7 = 23.5619 \\ a_8 = 26.7035 \\ a_9 = 29.8451 \\ a_{10} = 32.9867 \end{pmatrix}$$

When the beam force approaches to zero ($\xi = 0$) , ϕ_n becomes 1. By substituting (2.32) and (2.32) into (2.21) and (2.22) , al and bl are transformed into

$$al = \frac{\xi}{\sqrt{2}}\sqrt{-1 + \sqrt{1 + f_{al}^2}} \tag{2.33}$$

where $f_{al} = \frac{2\alpha_n^2}{\xi^2}\phi_n$

$$bl = \frac{\xi}{\sqrt{2}}\sqrt{1 + \sqrt{1 + f_{bl}^2}} \tag{2.34}$$

where $f_{bl} = \frac{2\alpha_n^2}{\xi^2}\phi_n^2$

By substituting (2.33) and (2.34) into (2.20) we obtain:

$$2a_n^2\phi_n(1 - cos(al)cosh(bl)) + \xi^2 sin(al)sinh(bl) = 0 \tag{2.35}$$

The normalized model frequencies ϕ_n are obtained by solving (2.35) for a given value of ξ.

2.4.2 Problem B:Euler-Bernoulli beam with flexible supports

In Problem B the assumption of the fixed ends of Problem A is removed and the end conditions of the beam are replaced by rotational springs supports. The torsional springs k_1 and k_3 are applied a shown on igure 2.2 are applied to restrict the bending around y direction.

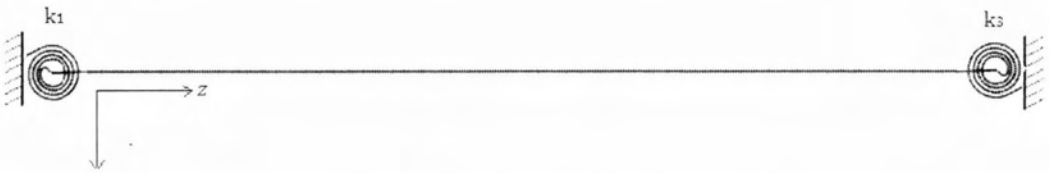

Figure 2.2: The rotational springs at y direction

The eigenproblem and the general solution have been defined previously, given by equations the (2.13) and (2.14).
The boundary conditions are now given by:

$$\begin{aligned} u(0,t) &= 0 \\ EIu''(0,t) - k_1 u'(0,t) &= 0 \\ u(l,t) &= 0 \\ EIu''(l,t) + k_3 u'(l,t) &= 0 \end{aligned} \tag{2.36}$$

By applying (2.12) to (2.36) we obtain the boundary conditions for u^* as follows:

$$\begin{aligned} u^*(0) &= 0 \\ EIu^{*''}(0) - k_1 u^{*'}(0) &= 0 \\ u^*(l) &= 0 \\ EIu^{*''}(l) + k_3 u^{*'}(l) &= 0 \end{aligned} \tag{2.37}$$

To implement the equation we first differentiate (2.14) :

$$u^{*'}(x) = Abcosh(bx) + Bbsinh(bx) + Cacos(ax) - Dasin(ax) \tag{2.38}$$

$$u^{*''}(x) = Ab^2sinh(bx) + Bb^2cosh(bx) - Ca^2sin(ax) - Da^2cos(ax) \tag{2.39}$$

$$u^{*'''}(x) = Ab^3cosh(bx) + Bb^3sinh(bx) - Ca^3cos(ax) + Da^3sin(ax) \tag{2.40}$$

By substituting (2.38), (2.39), (2.40) to (2.37) the following for linear algebraic equations are observed:

$$\begin{aligned}
bB + dD &= 0 \\
(-k_1)A + (EIb^2)B + (-k_1)C - EIa^2D &= 0 \\
Absin(bl) + Bbcos(bl) + C\alpha sin(al) + D\alpha cos(al)) &= 0 \\
(EIb^2sinh(bl) + k_3bcosh(bl))A + (EIb^2cosh(bl) + k_3bsinh(bl))B + & \\
(-EIa^2sin(al) + k_3acos(al))C + (-EIa^2cos(al) - k_3asin(al))D &= 0
\end{aligned} \tag{2.41}$$

In matrix form this system is given as:

$$\begin{pmatrix} a_{11} & a_{12} & a_{13} & a_{14} \\ a_{21} & a_{22} & a_{23} & a_{24} \\ a_{21} & a_{22} & a_{23} & a_{24} \\ a_{41} & a_{42} & a_{43} & a_{44} \end{pmatrix} \begin{pmatrix} A \\ B \\ C \\ D \end{pmatrix} = 0 \tag{2.42}$$

where:
$a_{11} = 0$
$a_{12} = b$
$a_{13} = 0$
$a_{14} = a$
$a_{21} = -k_1$
$a_{22} = EIb^2$
$a_{23} = -k_1$
$a_{24} = EIa^2)$
$a_{31} = bsinh(bl)$
$a_{32} = bcosh(bl)$
$a_{33} = asin(al)$
$a_{34} = acos(al)$
$a_{41} = EIb^2sinh(bl) + k_3cosh(bl)$
$a_{42} = EIb^2cosh(bl) + k_3sinh(bl)$
$a_{43} = -EIa^2sin(al) + k_3cos(al)$
$a_{44} = -EIa^2cos(al) - k_3sin(al)$

Note that al and bl are given as before in equations (2.21) and (2.22)

Normalization

The normalization procedure of problem B is identical to problem A, with additional normalized parameters due to the different boundary conditions. Specificaly, the following normalised parameters for the spring constants are introduced.

$$k_a = \frac{k_2 l}{EI} \tag{2.43}$$

$$k_c = \frac{k_3 l}{EI} \tag{2.44}$$

By insterting k_a, k_c and ξ as given in (2.25), (2.42) the elements of matrix in (2.42) get the following form

$a_{11} = 0$

$a_{12} = 1$

$a_{13} = 0$

$a_{14} = 1$

$a_{21} = -(bl)$

$a_{22} = \frac{(bl)^2}{k_a}$

$a_{23} = -(al)$

$a_{24} = -\frac{(al)^2}{k_a}$

$a_{31} = sinh(bl)$

$a_{32} = cosh(bl)$

$a_{33} = sin(al)$

$a_{34} = cos(al)$

$a_{41} = \frac{(bl)^2 sinh(bl)}{k_c} + (bl)cosh(bl)$

$a_{42} = \frac{(bl)^2 cosh(bl)}{k_c} + (bl)sinh(bl)$

$a_{43} = -\frac{(al)^2 sin(al)}{k_c} + (al)cos(al)$

$a_{44} = -\frac{(al)^2 cos(al)}{k_c} - (al)sin(al)$

The solution of (2.42) is obtained by setting the determinant of matrix A to zero, for the normalized elements described above.

$$det \begin{pmatrix} a_{11} & a_{12} & a_{13} & a_{14} \\ a_{21} & a_{22} & a_{23} & a_{24} \\ a_{21} & a_{22} & a_{23} & a_{24} \\ a_{41} & a_{42} & a_{43} & a_{44} \end{pmatrix} = 0 \tag{2.45}$$

2.4.3 Numerical estimation of modal frequencies

The dimensionless frequencies η_n and ϕ_n of problem A are calculated from the equations (2.30) and (2.35) for large and small values of ξ respectively and from equation (2.45) for problem B. All of them are transcendental equations and for their solution the "fzero" function was used, which is built-in into Matlab. Fzero is a hybrid method that combines bisection, secant and reverse quadratic interpolation [14].
The method finds a root of an equation with one variable, within an interval of two points, where the function changes sign. If one starting point is given instead of an interval, the function attempts to find an interval with a sign change close to that point. In order for this function to work, a change of sign is required. In order to minimise the probability of losing possible solutions, the solution starts from large values of ξ, where the solution approaches the known values. Subsequently, the solution advances to smaller ξ values, using the previous step solution as an initial value for the current step. Using the method described above, equations (2.30) and (2.35) have been solved. Figures (2.3) and (2.4) indicate the first seven solutions in the case of small and large ξ respectively.

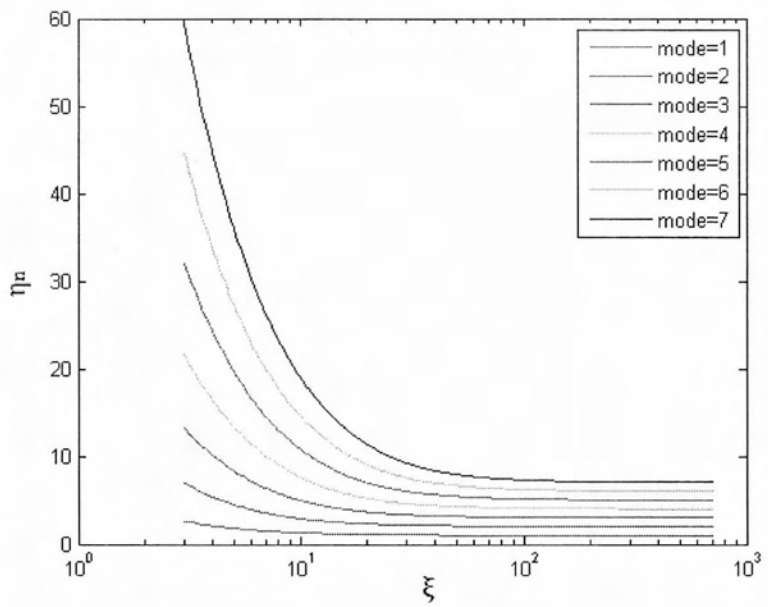

Figure 2.3: The dimensionless solutions η_n versus ξ for large values of ξ for problem A

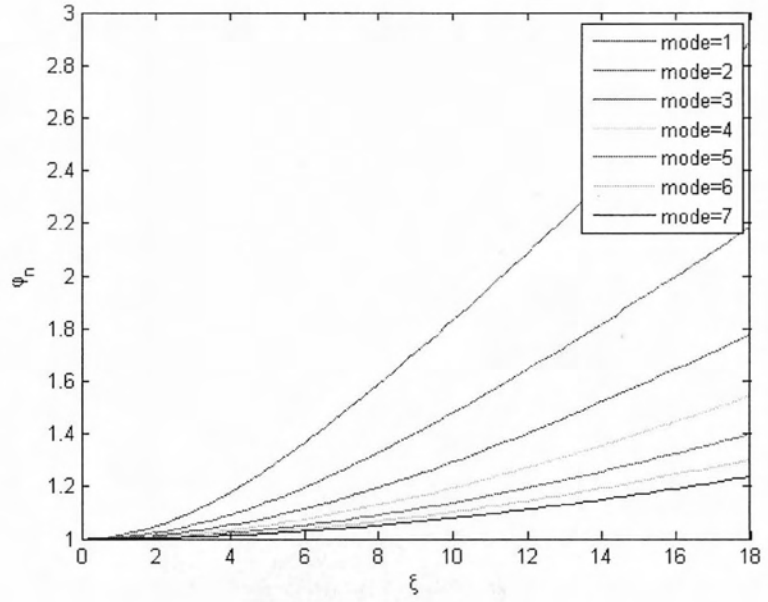

Figure 2.4: The dimensionless solutions ϕ_n versus ξ for small values of ξ for problem A

The behaviour of the beam with flexible ends under large values of spring constants

In the case of problem B, when k_a, k_b, k_c, k_d become very large, the first term of the elements a_{31} , a_{32} , a_{33} , a_{34} ,a_{41} , a_{42} , a_{43} , a_{44} in matrix (2.42) does no longer contribute and (2.42) becomes equal to (2.18) for problem A, thus the behaviour leads to the model with the fixed ends. Figure 2.5 shows the solutions of problem B for small ξ when the springs obtain large values. Figure 2.6 shows the solutions of problem B when ξ becomes large. By observing Figure 2.6 we notice that the estimation of the modes is not accurate. The plot is noisy and the modes are not consistent for the total range ok ξ. The problem appears to have high sensitivity to initial guesses used for the application of "fzero" function.

For the solution of this issue it is recommended to split the range of ξ in smaller intervals and apply appropriate initial guesses to each set. For the investigated hanger, the values of ξ will not exceed 20 so the algorithm will not enter into the case of large ξ but for any other application, further investigation regarding initial guesses is suggested.

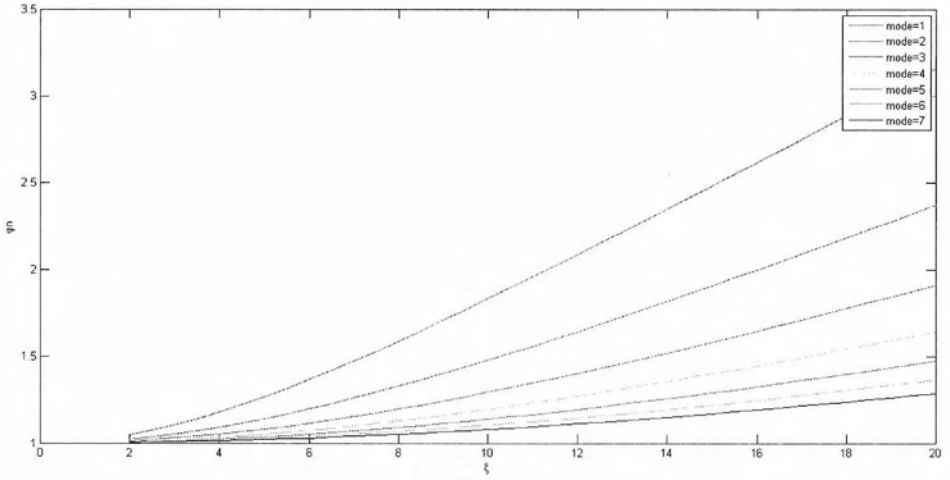

Figure 2.5: The dimensionless solutions of problem B, ϕ_n , versus ξ for large spring stiffness and small values of ξ

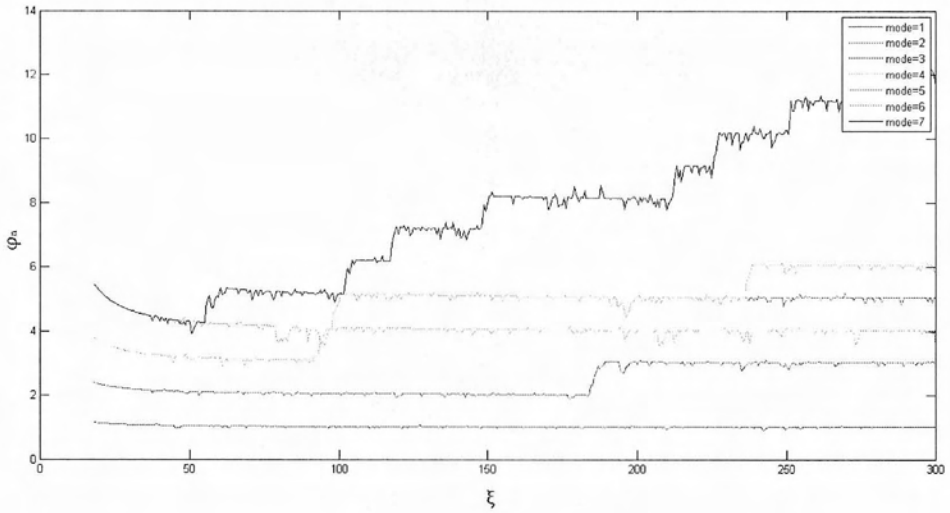

Figure 2.6: The dimensionless solutions of problem B, ϕ_n , versus ξ for large spring stiffness and small values of ξ

2.4.4 Selected Model Classes

We now introduce the selected model classes based on the Euler-Bernoulli beam theory:

- Beam 1: Fixed ends
- Beam 2: Flexible ends

Model class beam 1 is the beam model with fixed ends descibed in section 2.4.1. Model class beam 2 is a beam model with flexible ends simulated by for rotational springs, two at each side of the beam.

These models are implemented in the TMCMC algorithm for the qualitication of the hanger's tension. As seen in Table 1.1 the frequencies of the hanger along the transient and longitudinal direction differ. Thus the application of two rotational springs, as described in section 2.4.2, along the y axis is not sufficient in order to approach the experimental frequencies. By applying rotational springs, one frequency is obtained for each mode and corresponds to the transient and/of the longitudinal direction. For this reason, the model described in section 2.4.2 is being implemented twice, once for the springs k_1, k_3 and once for the springs k_2, k_4. The application of springs k_2, k_4 is shown in Figure 2.7 and the normalised stiffnesses are given by (2.46) and (2.47) as follows

$$k_b = \frac{k_2 l}{EI} \tag{2.46}$$

$$k_d = \frac{k_4 l}{EI} \tag{2.47}$$

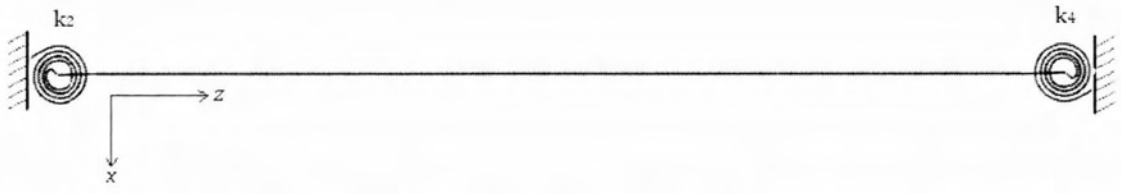

Figure 2.7: The dimensionless solutions ϕ_n , versus ξ for small values of ξ for problem A

The problem is solved two consecutive times, one for k_1,k_3 and one for k_2,k_4. Thus we are able to obtain different frequencies along the transverse and longitudinal direction of the beam by applying different spring constants.

Chapter 3

Modal Frequency Predictions of Hangers based on Finite Element Models

In this Chapter the complete geometry of an existing bridge hanger is analysed. High fidelity finite element models with various boundary condition cases are developed in order find the most appropriate model to simulate the behaviour of an existing hanger. Furthermore two simple beam models are developed as well in order to validate the analytical models described in Chapter 2. The finite element models are the following:

- Model class s1: Simple 12 m beam with fixed ends as shown in Figure 3.1(a)
- Model class s2: Simple 9.817 m beam with fixed ends as shown in Figure 3.1(b)
- Model class 0: Hanger 3 with fixed ends as shown in Figure 3.1(c)
- Model class 1: Hanger 3 with fixed central nodes of the two edges and springs at x,y,z as shown in Figure 3.1(c)
- Model class 2: Hanger 3 with fixed central nodes of the two edges in z direction, fixed perimetric nodes at x,y and springs at z direction as shown in Figure 3.1(c)

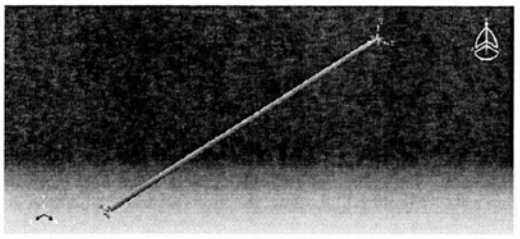

(a) Model class s1: Simple 12 m beam

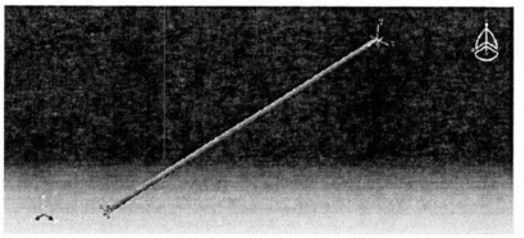

(b) Model class s2: Simple 9.817 m beam

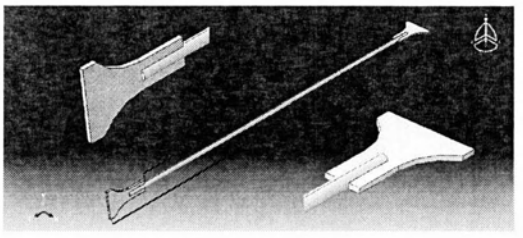

(c) Hanger 3 geometry

Figure 3.1: The geometric models

3.1 Finite element models with fixed ends

There are three different models with fixed ends. Model class s1 is a simple solid beam model with 12m length, which is the total length of the real hanger including the plates. Model class s2 is a simple solid beam model with 9.817 m length which is the lenght between the plates of the real hanger. Model class 0 is the model with the complete geometry of hanger 3. Prior to the analysis, the analysis technique and the selection of the pre processing parameters is described bellow. The goal of pre-processing analysis is to develop an appropriate finite element mesh, assign suitable material properties, and apply boundary conditions in the form of restraints and loads.

3.1.1 The analysis technique of the models with fixed ends

In this paragraph, the analysis technique of the models with fixed ends is described. All of them are subjected to a tension load that is applied on the left edge. The load is a distributed force and the area of application is the end face of each model. Comparing the model results for the same load, it is implied that the axial force is the same but the distributed load differ, since the loas is applied at different section of each model

Finite element type

In order to cover the geometry of all models efficiently, detailed finite element models using ten-node tetrahedral element (C3D10) element were created. The C3D10 element , shown in Figure 3.2, is a general purpose solid tetrahedral , stress/displacement element (4 integration points). The acive degrees of freedom of the element are 1,2,3 as follows:
DoF 1: x direction
DoF 2: y direction
DoF 3: z direction

C3D10 is a solid 10-node tetrahedron element and it is commonly used because of the existence of fully automatic tetrahedral meshers. Among other existing element types, hexaedrical elements can also be used as well but then the geometry cannot be meshed as it is and needs to be partitioned. As a result, C3D10 element has been used for the analysis of all the models with fixed ends.

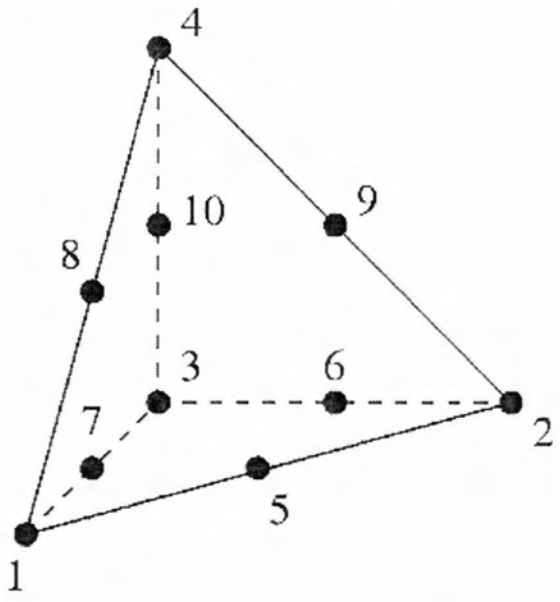

Figure 3.2: The 10-node tetrahedral element

Modal analysis in Abaqus for fixed ends BC

The evaluation of a modal analysis in Abaqus consists of a certain sequence of actions. The aim is to obtain the frequencies of the system after an axial load has been applied. The analysis is separated in two steps.

Step 1: Step 1 is a static deformation step. A load is applied to the left edge of the model. The load is a distributed pressure and the boundary conditions are applied only at the right end of the hanger, in order to allow the deformation of the hanger.

Step 2: Step 2 is a eigenfrequency calculation step. After the hanger has been elongated in Step 2, the boundary conditions of the left end are activated again and the hanger is kept in its deformed state. At this step the model outputs the eigenfrequencies of the loaded hanger.

In the case that we are interested in the natural frequencies of the model an additional step before step 1 is nescessary.This step is a frequency step like step 1 but the eigenproblem is solved before the application of the load.

The load application

The load applied in each model is a distributed force. The load is applied on the left end of each model as shown in Figure 3.3. Comparing different models under the same load, the magnitude that is constant is the axial force. The pressure load varies, since as each model has different area of load application. For nominal load we consider the load calculated with numerical models when the bridge was measured. For hanger 3 the tension was estimated to be 711 kN 835 kN in the longitudinal and transverse direction respectively. The aim is to use an initial value for the load that is close to the actual in order to save computational time. The load of 711 kN has been selected as nominal. This is translated to 1.67 e7 Pa for the geometry of hanger 3 and to 5.35 e7 Pa for the geometry of the simple beam.

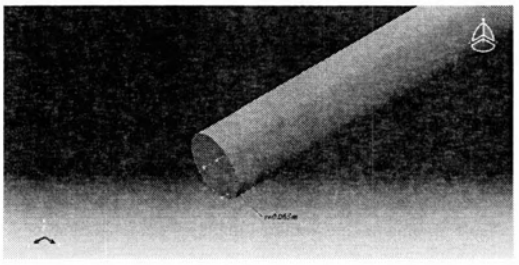

(a) The load application section in the simple beam models

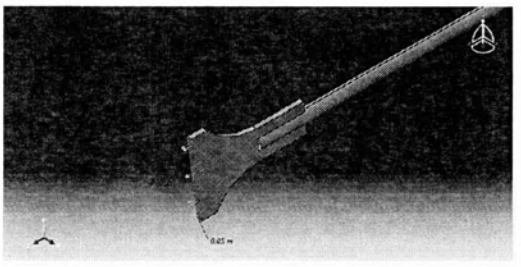

(b) The load application section in models with the geometry of hanger 3

Figure 3.3: The load application section

The definition of fixed Boundary Condition

Before proceeding with any further analysis , it is important to define the fixed boundary condition (BC). In Abaqus there are several types of BC. Regarding the mechanical BC we can either use the encastre BC which is applied to a geometry set (veertice/edge/face)or the displacement/rotation BC which is applied to a node set. The encastrate BC restricts all the degrees of freedom of the region of application (U1=U2=U3=UR1=UR2=UR3=0) and in displacement/rotation BC the upper degrees of freedom are restricted independently . The question is if the rotational DoF affect the results. For this purpose, two analyses with different BC have been conducted in the geometry of hanger 3. A tensile load of 1.67e7 Pa has been applied on the left section of the model at z rirection. The mesh for this test is fine enough to give reliable results.

It is evident from Table 3.1 that the rotational DoFs do not affect the results for the specific load direction. Taking under consideration the above results, with respectto the fixed BC is, it is implied that U1=U2=U3=0.

3.1.2 Convergence test for the fixed ends models

Mesh convergence tests were conducted in order to determine of the most suitable mesh size ragne for saving computational time and simultaneously reducing the error. Model class s1, s2 and 0 have been analysed in various mesh densities in order to decide for the most appropriate mesh size for each one. The applied load is $1.67e7\ Pa$ for model class

Table 3.1: The effect of the rotational DoF on fixed BC in the hanger's 3 frequencies (Hz) under the tension of 1.67$e7$ Pa

	Encastrate BC	U1=U2=U3=0
	x - y	x - y
Mode 1	5,97	5,97
Mode 2	14,68	14,68
Mode 3	27,10	27,10
Mode 4	43,27	43,27
Mode 5	62,94	62,94
Mode 6	85,85	85,85

0 and 3.35$e7$ Pa for model class s1 and s2. The mesh technique used for all the models, is the free mesh tool that Abaqus has, with the use of C3D10 tetrahedron elements. At this point we have to mention that the mesh amaylsis could be extended with the use of partitions and other mesh techniques, but the extended study of the mesh density exceeds the scope of this project.

Model class s1

Model class s1 is a simple solid beam cable with the following characteristics.

- Lenght 12 m
- Diameter 0.13 m
- Modulus of elasticity $E = 200Gpa$
- Mass density 7800 kg/m^3
- Poisson's ratio 0.3
- Element type : C3D10 three dimensional solid quadratic tetrahedron elemet
- Clamped ends boundary condition(U1=U2=U3=0)

The diameter of this model is the same with the diameter of the existing hanger and the length represents the total length of the real hanger including the edges

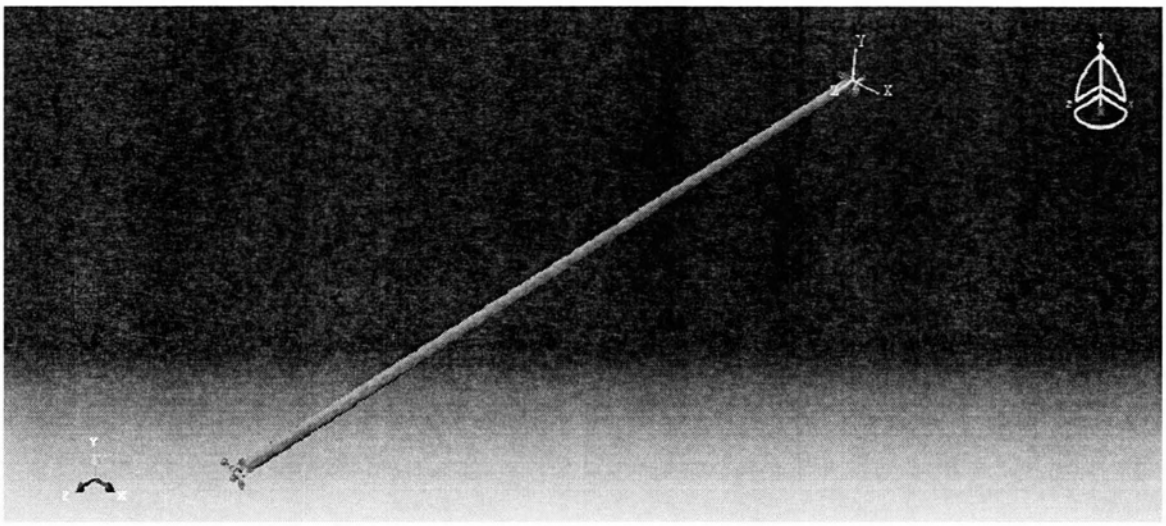

Figure 3.4: Model class s1: 12 m simple solid beam model with fixed ends

The model has been analysed in various mesh densities under the load of $5.35e7\ Pa$. This load is equivalent to the nominal load that has been measured in hanger 3. Figure 3.5 presents the results of the model. These results are based on the table A.1 in appendix A1. For a mesh with 3500 elements and more, the solution converges for all the modes of interest therefore this mesh will be used for further analysis.

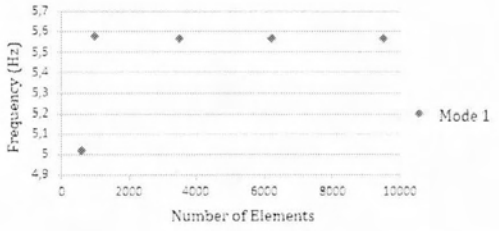

(a) Mode 1

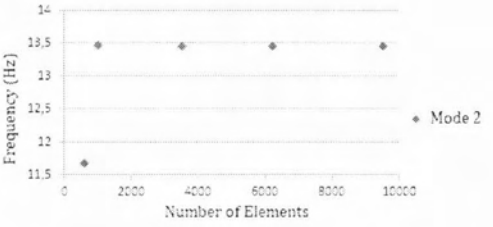

(b) Mode 2

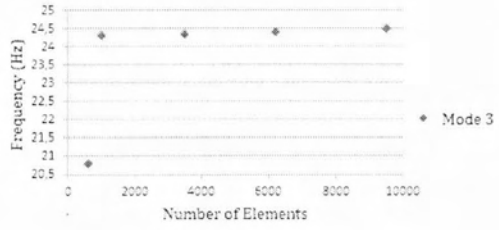

(c) Mode 3

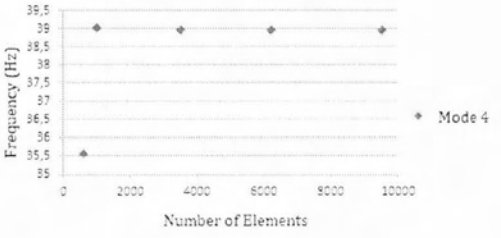

(d) Mode 4

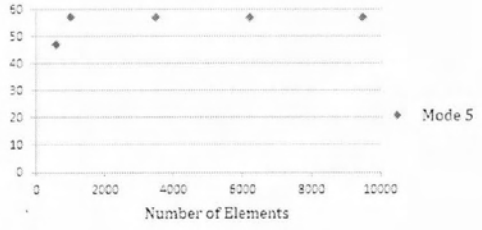

(e) Mode 5

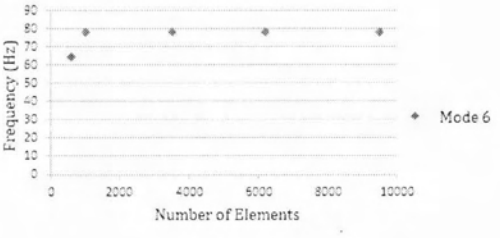

(f) Mode 6

Figure 3.5: The frequency (Hz) of the 6 first modes of model class s1 under the tension of $P = 5.35e7\ Pa$ in various mesh densities

Model class s2

Model class s2 is a simple solid beam cable with the following characteristics.

- Lenght 9.817 m
- Diameter 0.13 m
- Modulus of elasticity $E = 200\ Gpa$
- Mass density 7800 kg/m^3
- Poisson's ratio 0.3
- Element type : C3D10 three dimensional solid quadratic tetrahedron elemet
- Clamped ends boundary condition (U1=U2=U3=0)

The diameter of this model is the same with the diameter of the real existing hanger and the length represents the length of the hanger 3 without including the edges.

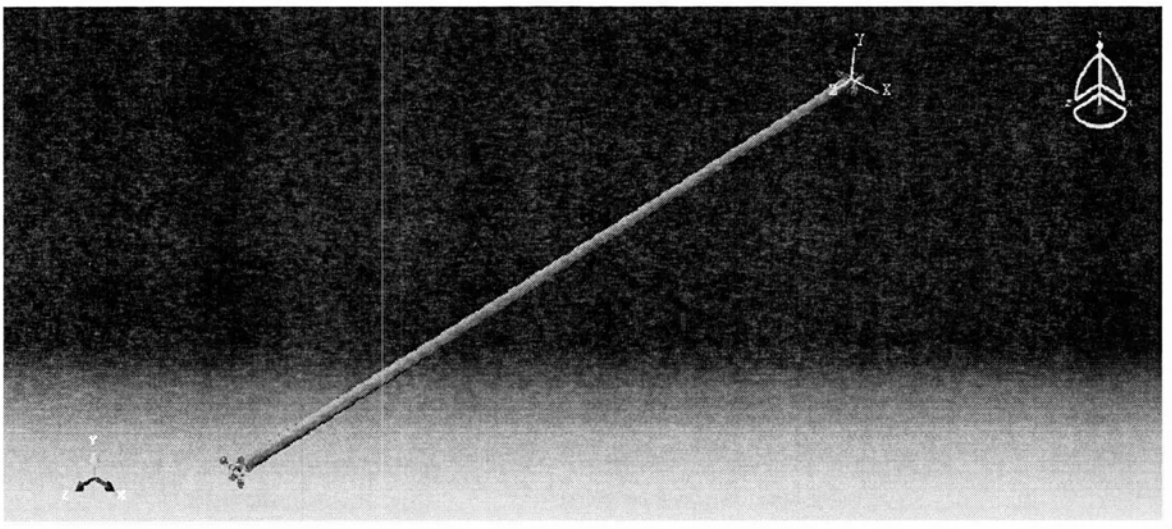

Figure 3.6: Model class s2: 9.817 m simple solid beam model with fixed ends

Figure 3.7 shows the frequencies of model class s2 under the tension of $5.35e7\ Pa$ in various mesh densities. The results are based in table A.2 in Appendix A2. It is noticed that the solution converges for the model with 13000 elements for all the modes of interest and this model is selected for further analysis.

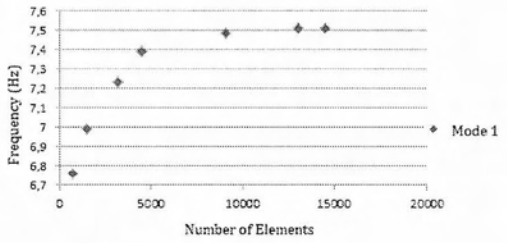

(a) Mode 1

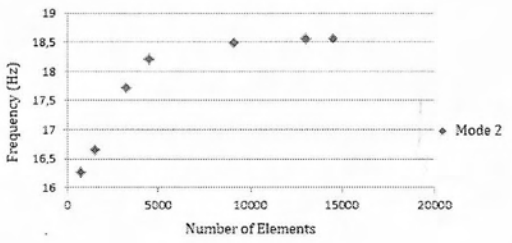

(b) Mode 2

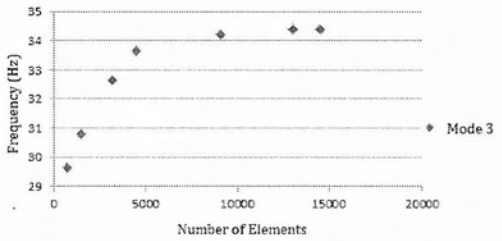

(c) Mode 3

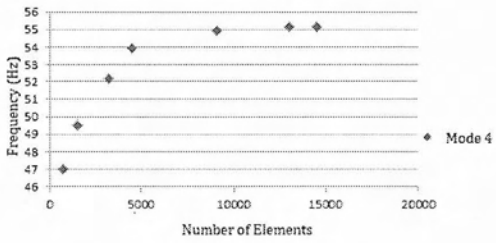

(d) Mode 4

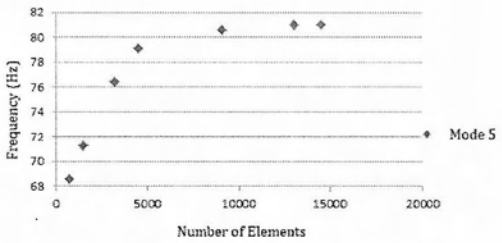

(e) Mode 6

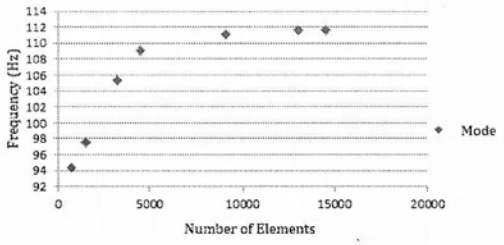

(f) 6th mode

Figure 3.7: The frequency of the 6 first modes of model class s2 under the tension of $P = 5.35e7Pa$ in various mesh densities

Model class 0

Model class 0 consists of the complete geometry of hanger 3 as shown in Figure 3.8 The parameters of the analysis are the following

- Frequency analysis
- Lanczos Eigensolver
- Nonlinear analysis
- Element type : C3D10 three dimensional solid quadratic tetrahedron elemet
- Boundary conditions: Right side:U1=U2=U3=0, Left side U1=U2=0 for all steps,U3=0 after the load has been applied and the hable has been derofmed
- Modulus of elasticity $E = 200Gpa$
- Mass density $7800kg/m^3$
- Poisson's ratio 0.3

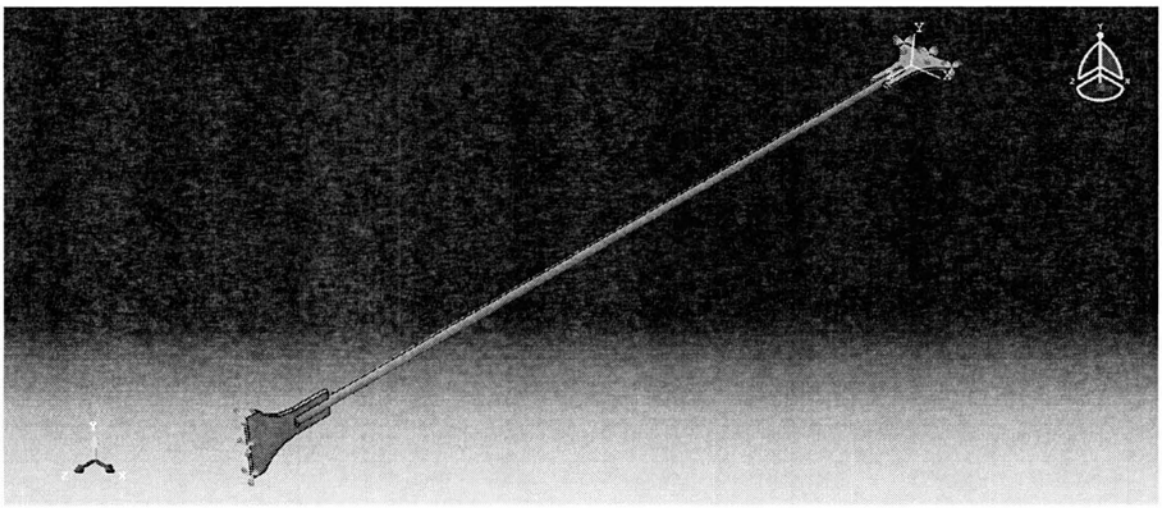

Figure 3.8: Model 3:Hanger 3 geometry with fixed ends

Model class 0 has been analysed in the mesh densities listed bellow. Case A with 3492 elements represents the coarser mesh that Abaqus allows for this geometry. Case G with 118000 elements represents a very fine mesh where the frequencies in x and y direction match. This result is expected based on the theory for this model. The mesh densities that have been studied are the following.

- A:3500 elements
- B:6200 elements
- C:11800 elements
- D:16800 elements
- E:25000 elements
- F:44000 elements
- G:118000 elements

Figure 3.9 shows the freequencies of the model in the above mesh densities. These results are based on Tables A.3 and A.3 in Appendix A3. The analysis of cases A and B ended with distorted elements and this might affect the results, as a result the selection of one of these models is not safe. Moreover the computational time for Model G is extremely high. Since the solutions converges for more than 25000 elements, as it is shown in Figure 3.9, case E is selected for the mesh.

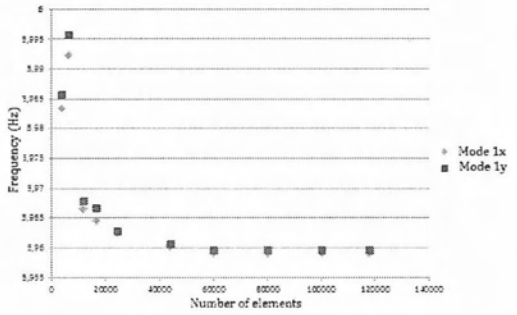

(a) Mode 1

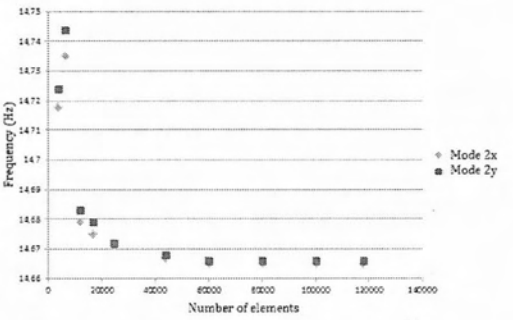

(b) Mode 2

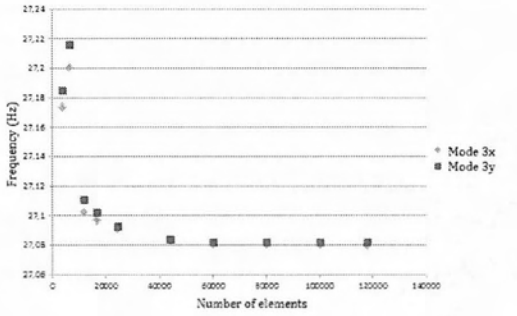

(c) Mode 3

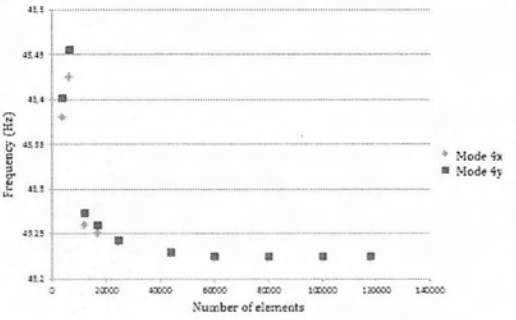

(d) Mode 4

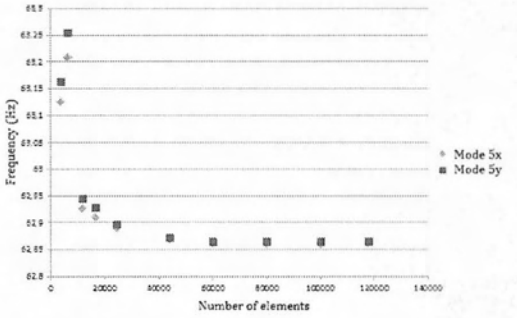

(e) Mode 5

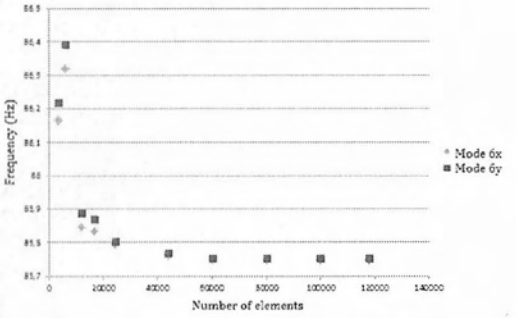

(f) Mode 6

Figure 3.9: The frequencies (Hz) of model class 0 under the tension of $P = 1.37e7\ Pa$ in various mesh densities

3.2 Geometric model with springs

In this section the fixed ends of hanger 3 are replaced by springs. The following models have been developed, with the geometry of hanger 3 and different boundary conditions.

- Model class 1
- Model class 2

Model class 1 has springs with stiffness at x,y,z direction and model class 2 has springs with stiffness at at z direction only. The springs are implemented in such a way that they simulate the behavior of a torsional spring.

3.2.1 Mesh selection

Eventhought the geometry of the models with springs is identical to the models with the fixed ends, the selection of the mesh density is more complicated in the case of flexible ends simulated by springs. The initial approach was to keep the mesh of model class 0 which has been validated but in contrast to the fixed displacement/rotation BC of model class 0, which is a BC applied to the geometry of the model (surfaces,edges etc) springs must be applied to a node or a node set. The role of the mesh in this analysis is not only to give a converged solution but also to give sufficient available nodes for the springs application. The distribution of any boundary bondition such as springs or fixed points plays important role. As we saw in model class 0, 25000 elements are enough to give a converged solution but as long as we need to add springs the number of elements arise to 44000 in order to create sufficient number of nodes for the springs application and to avoid warnings for distrorted elements that occured when springs were applied to the model with 25000 elements. The issue of the distorted elements has been quite serious as it can lead to an inaccurate solution. In genera a way to solve the issue of distorted elements is the to adaptive mesh techniques but in Abaqus, nodes with springs are non-adaptive, thus the increase of mesh density has been a good solution. The model has been analysed within the desirable range of spring stiffness and load for a mesh density of 44000 elements . Figure 3.11 indicates the distribution of the elements. At this point it is important to notice that there are various available mesh techniques that can be used for this problem. For instance we could create a coarser mesh localy to apply the springs and not just increase the number of the elements but the extended study of the mesh density exceeds the scope of this project.

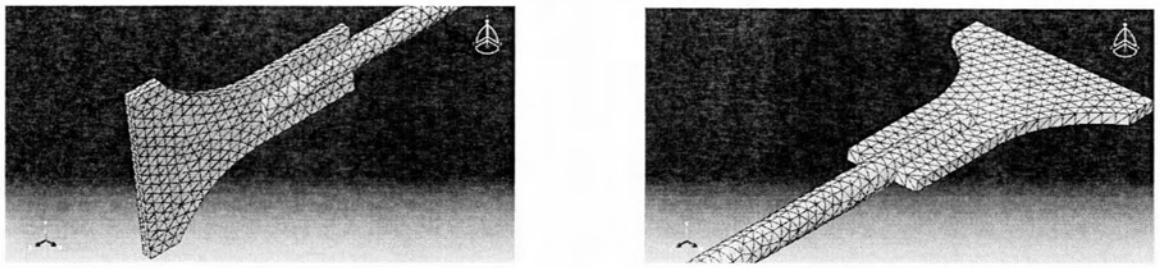

(a) Mesh on the left edge of model 4

(b) Mesh on the right edge of model 4

Figure 3.10: The 44000 element mesh of model class 0

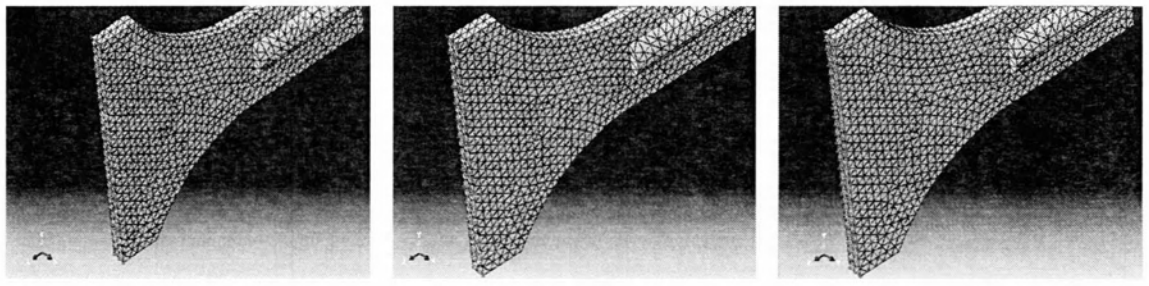

(a) 24 fixed nodes

(b) 45 fixed nodes

(c) 87 fixed nodes

Figure 3.11: The location of the fixed nodes in different distribution cases

Table 3.2: The effect of the number of fixed nodesn in the frequencies (Hz) of the model in comparisson to the fixed BC

	24 nodes	45 nodes	87 nodes	fixed surface
Mode 1	5,85	5,91	5,94	5,95
Mode 2	14,40	14,55	14,63	14,66
Mode 3	26,54	26,84	27,00	27,08
Mode 4	42,20	42,76	43,01	43,22
Mode 5	61,09	62,05	62,6	62,86
Mode 6	83,26	84,45	85,3	85,74

3.2.2 The analysis technique for flexible ends BC

The steps of modal analysis with springs

In order to evaluate the analysis we need to deactivate the springs on the left side to allow the hanger to elongate and reactivate them at the final step where the eigenproblem is solved. This procedure though is not quite straight forward in Abaqus. Springs are described as interactions and the way they are added in the model via the Abaqus Graphic User Interface, they are kept active in the model for all the analysis steps. At this point it was better to handle the model through its input file. Springs for Abaqus are

springs elements, so what should be done is deactivating the element set of the springs we want and reactivate them in the last step. This was obtained using the *Model,change command. The analysis step sequence must change as well as *Model,change cannot be added in a Linear perturbation step, such as the frequency step, but only in a static step. For this purpose, in model class 1 the analysis has the four following steps.

Step-1: Step 1 is a static step where the load is being applied.*Model, change, remove is used at this step to deactivate the desirable degrees of freedom of the left edge.For this step the right ends at x ,y ,z and the left end at x, y are always fixed. These BC can change in step 3 accordingly to the test we want to evaluate.

Step-2:Step 2 is a static step with only purpose to reactivate the deactivated objects of step 2. *Model,change,add is used here to activate the desirable degrees of freedoms of the springs.

Step-3:Step 3 is the final frequency step where the eigenfrequencies are calculated. The mesh density is still a parameter here and for each change of the mesh , the node sets of the springs should be redefined.

The effect of rotational degrees of freedom

Before the model goes to any further analysis, the effect of the rotational degrees of freedom of the springs needs to be investigated. In the analysis of the models with fixed ends we saw that the rotational DoFs do not have any effect on the model, but in that case the BC are placed in the geometry following and equal distribution on each face.In the models with springs the same test needs to be evaluated in order to see if the distribution of the springs on each side is good enough to give as the same results and how we will simulate the fixed BC with large stiffness springs.

Table 3.2.2 shows the frequencies of the finite element model of hanger 3 with springs at both sides. The stiffness of the springs is applied at z direction and is large enough to simulate the fixed boundary condition. The load applied is $1.64e7Pa$ along the z axis.

- Case A: Springs at x,y,z,rx,ry,rz at both sides
- Case B: Springs at x,y,z at both sides

From the results of Table 3.2.2 we notice that Case A and B give exactly the same frequencies, therefore the rotational DoF, do not play any role at this study and no springs are needed.

3.2.3 The effect of the springs stiffness

Model class 1

In model class 1 , the central node of each side of the hanger is fixed in z direction. Two spring sets are applied in each side of the model. On the right side k1 is a set of distributed

Table 3.3: The effect of the rotational degrees of freedom of the springs

	Case A		Case B	
	x	y	x	y
Mode 1	5,96	5,96	5,96	5,96
Mode 2	14,68	14,68	14,68	14,68
Mode 3	27,11	27,11	27,11	27,11
Mode 4	43,26	43,27	43,26	43,27
Mode 5	62,93	62,94	62,93	62,94
Mode 6	85,85	85,89	85,85	85,89

springs in the large edges and k2 in the small as shown in 3.12 a, b. Equivalently k3 and k4 spring sets are applied on the left side as shown in Figure 3.12 c, d. Each spring set has three DoFs at x, y, z directions. Totally the model has the following spring sets:

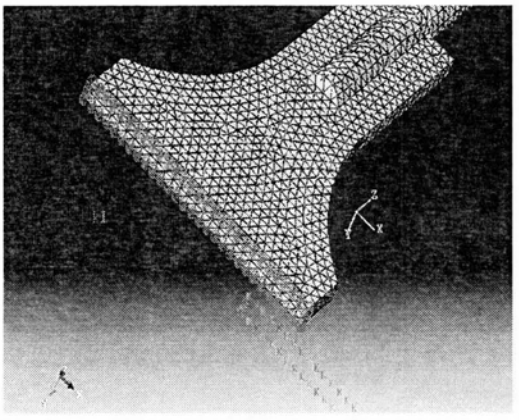

(a) Location of spring k1 (right end)

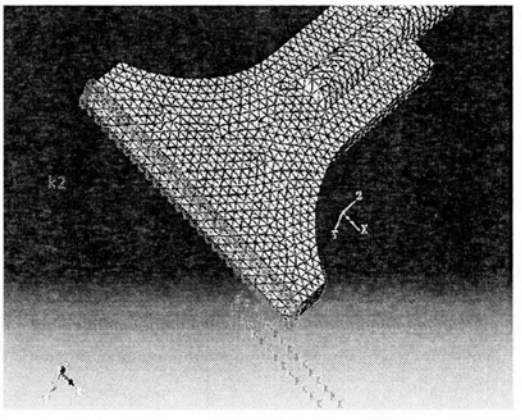

(b) Location of spring k2 (right end)

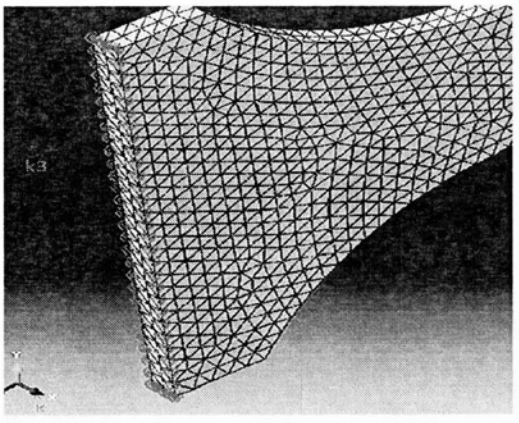

(c) Location of spring 3 (left end)

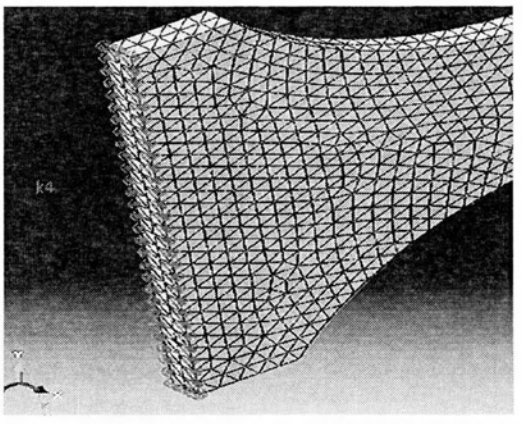

(d) Location of spring k4 (left end)

Figure 3.12: The location of springs k1, k2, k3, k4 in model class 1

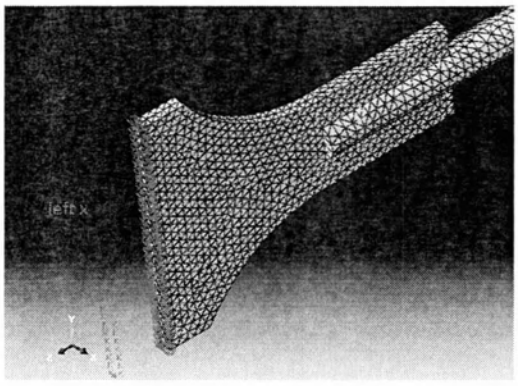

(a) Location of spring left x

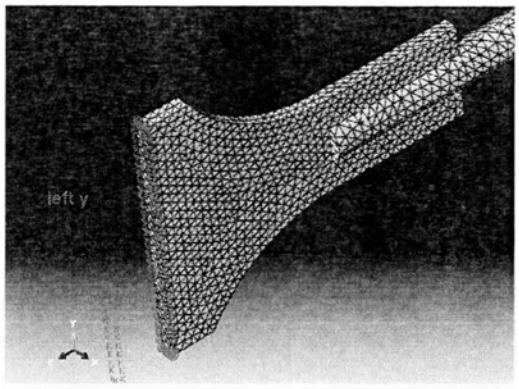

(b) Location of spring left y

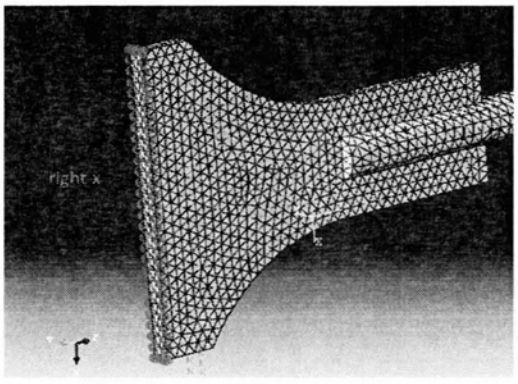

(c) Location of spring right x

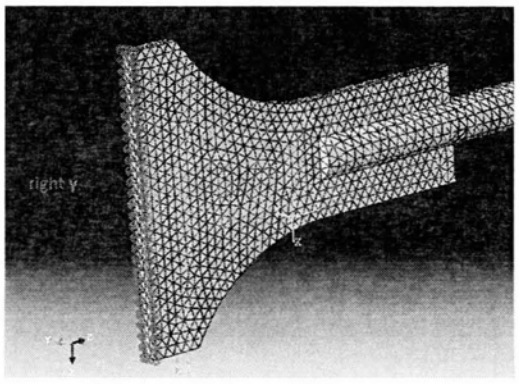

(d) Location of spring right y

Figure 3.13: The location of springs k_3 and k_4 on the left side of the hanger

Fixed boundary condition at z direction is applied to the central node of each side as shown in Figure 3.2.3.

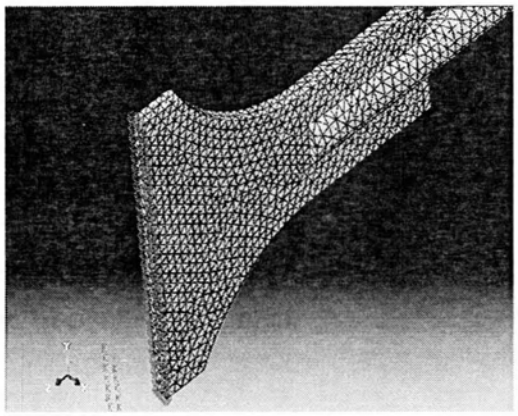

(a) The central fixed node of the left side

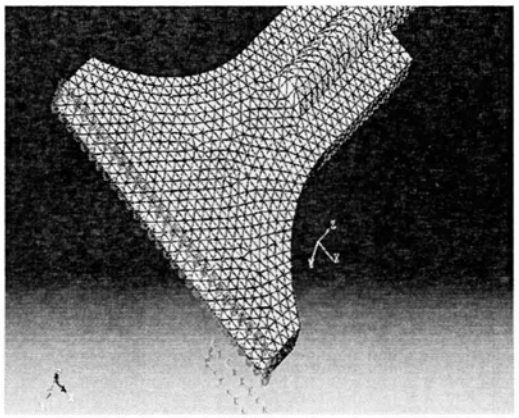

(b) The central fixed node on the right side

Figure 3.14: The application points of the fixed BC at z direction

Model class 1 parameters :

- Frequency analysis
- Lanczos Eigensolver
- Nonlinear analysis
- Element type : C3D10 three dimensional solid quadtatic element
- Modulus of elasticity $E = 200\ Gpa$
- Mass density 7800 kg/m^3
- Poisson's ratio 0.3

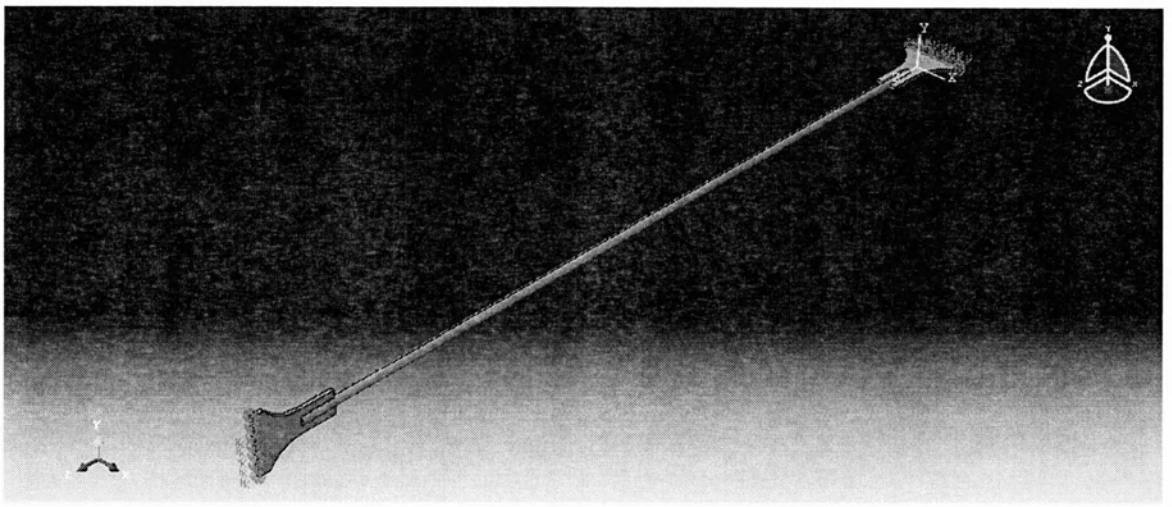

Figure 3.15: Model class 1: Hanger 3 model with springs at both sides

Figure 3.16 shows the frequencies of model class 1 under the tension of P=1.67e7 Pa in various spring stiffnesses in comparisson to the experimental results and the results of model class 0. These graphs are based on the results of the tables A.4 and A.4 in Appendix A4. To obtain these results all the springs of the model have the same stiffness. The aim is to find the spring constant that simulates the fixed end condition and also the range of k that will be tested within the Transitional Markov Chain Monte Carlo in order to reach the experimental frequencies. The behavior of all modes must be taken under consideration in order to ensure that the solution converges. As the spring constant increases the solution converges to a value which is close to this of the fixed ends model. For spring constants larger that $e12\ N/m$ the solution is consistant. The experimental results appear to have a significant unsymmetry betweeen x and y direction.In order to reach the experimental frequencies , the lowest value of the spring constant is $e7\ N/m$ while the frequency in x direction of model class 1 is smaller than the experimental. Ideally there should be a spring stiffness value large enough to give frequency larger than the experimental in y direction. The larger value of k in which the

model runs without errors is $e26\ N/m$ and the frequency occurs in this value is consistant in the range $k \in [e11, e26]\ N/m$.

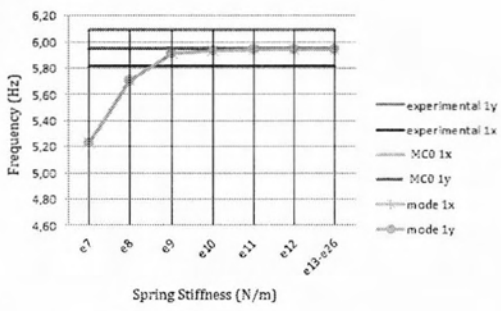

(a) Mode 1

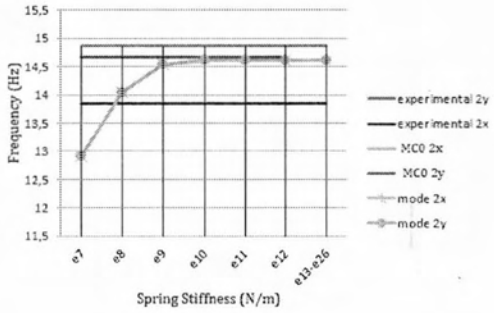

(b) Mode 2

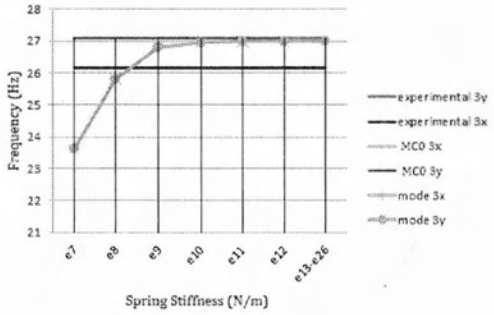

(c) Mode 3

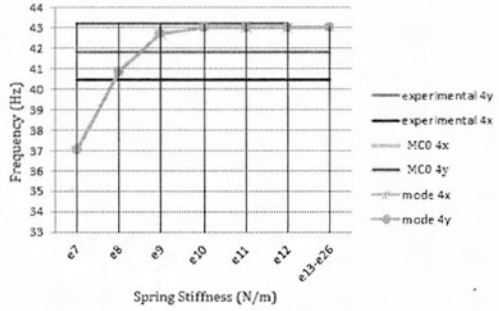

(d) Mode 4

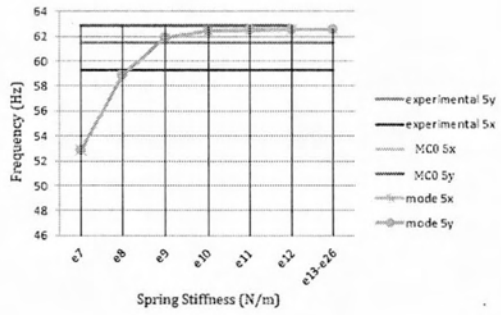

(e) Mode 5

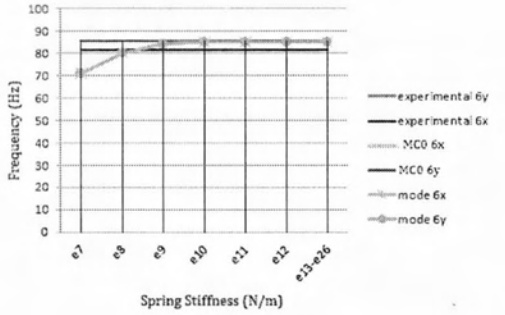

(f) Mode 6

Figure 3.16: The frequencies of model class 1 under various spring stiffnesses in comparisson to the frequencies of model class 0 (MC0) and to the experimental frequencies

Model class 2

Model class 2 is a sub model of model class 1, where the springs at x,y directions are substituted by fixed BC. The springs of the model are k_1, k_2, k_3, k_4 with stiffness only at z direction and the application points are the same as in model class 1 .
Figure 3.17 shows the frequencies of model class 2 under different values of the springs stiffnesses in comparison to the fixed model and the experimental results. All the springs are supposed to have the same stiffness. These graphs are based on the results of the tables A.5 and A.4 in Appendix A4. It can be seen from the results as k increases, the frequencies of the model come closer to those of the fixed model. For k values larger than $e13\ N/m^2$ the results are consistent.

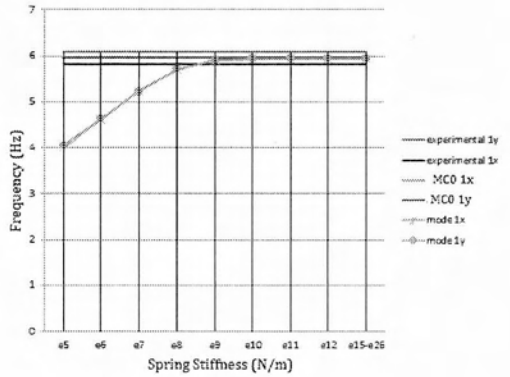

(a) Mode 1

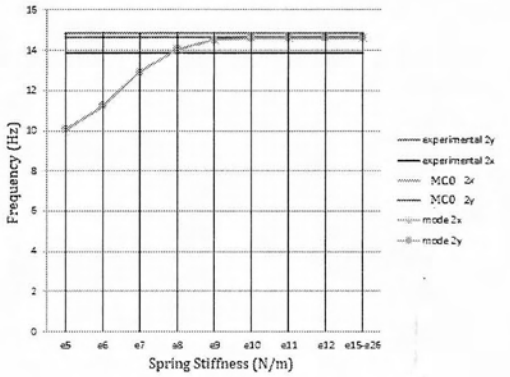

(b) Mode 2

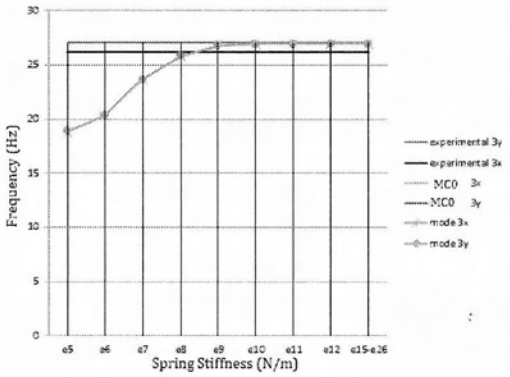

(c) Mode 3

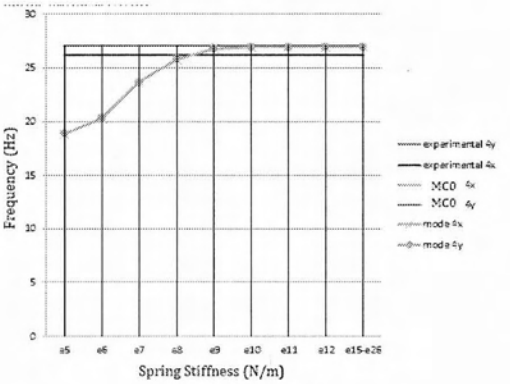

(d) Mode 4

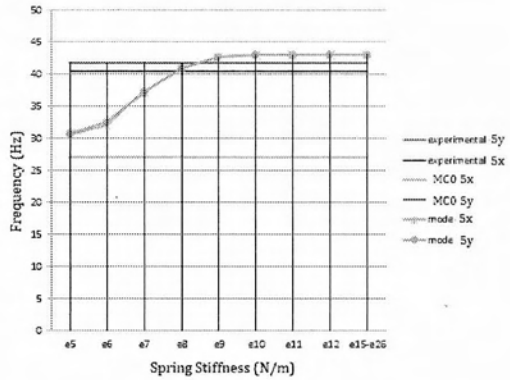

(e) Mode 5

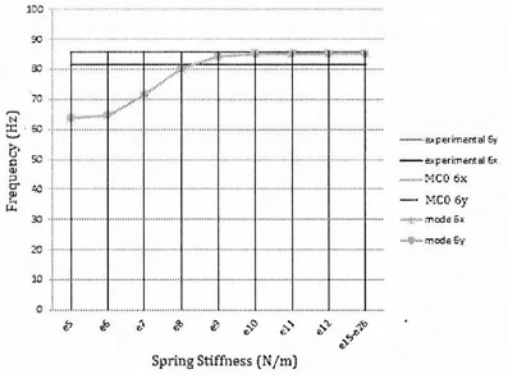

(f) Mode 6

Figure 3.17: The frequencies of model class 2 under various spring stiffnesses in comparisson to the frequencies of model class 0 and to the experimental frequencies

3.3 Model results

With regard to understand which model describes better hanger 3, the results of all the models have been combined. Figure 3.18 presents the frequencies (Hz) for all the models at x and y direction. All the models have been tested under the nominal load and for model class 1 and 2, that include springs, the spring constants have very large values. From the results it is evident that the behavior of the hanger is between the two simple beam models and closest to model class s1. This implies that if we want to use a fixed model to simulate the hanger, the term of the modal length needs to be inserted. Modal length is the length that gives the best fitting in a fixed model. By noticing the first modes, all the models give similar results but as we step into higher modes, the differences become clear. By focusing on mode 6 (11 and 12 values on x axis) we notice that the longitudinal experimental frequency is described very preciselly by model class 2 but there is not a model to simulate the thansverse frequency yet. For this reason we need to start changing the spring values of the models. This procedure will be done through the TMCMC algorithm, described in Chapter 4.

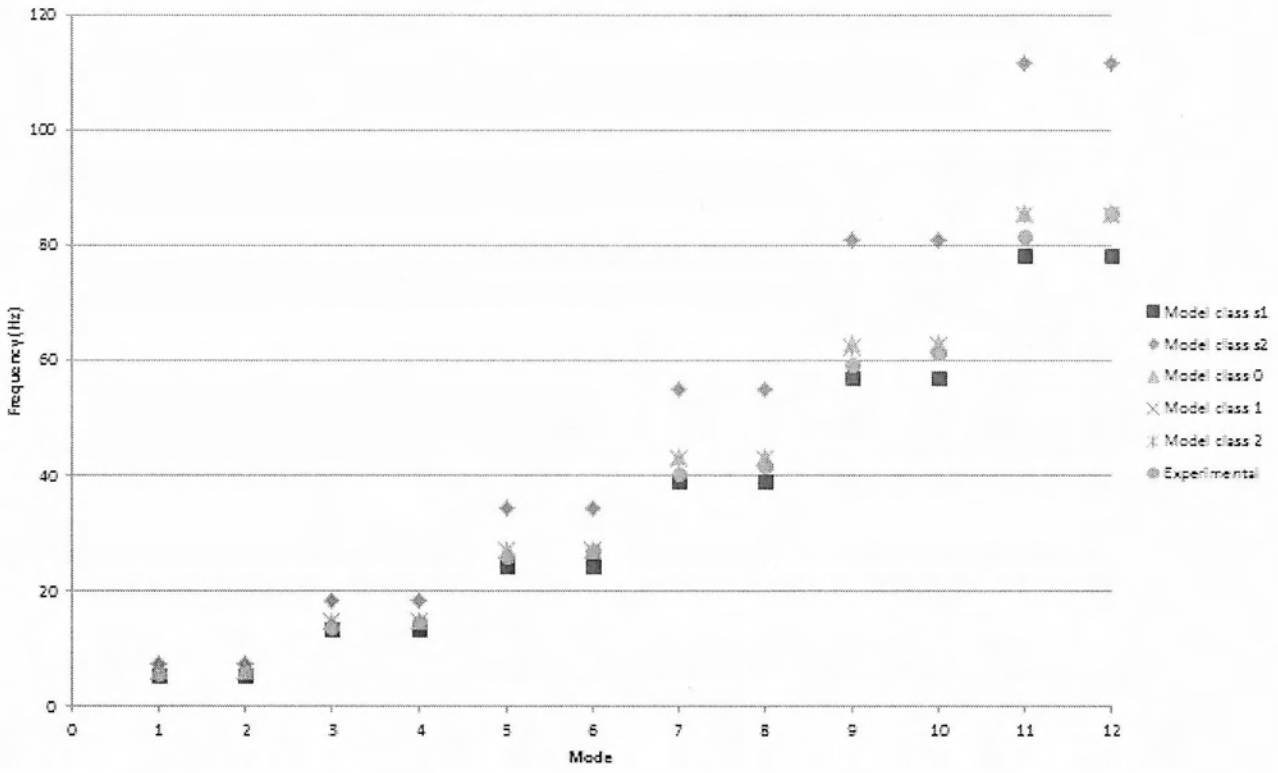

Figure 3.18: The frequencies (Hz) of all models under the act of the nominal load in comparison to the experimental

Numerical models compared to Finite Element models

The simple FE models, model class s1 and s2, have been built in order to be compared to the numerical models in Matlab. Figures 3.19 and 3.20 present the results of Matlab numerical models versus the FE models model class s1 and model class s2 under the effect of the nominal load. The graphs are based on the results of tables A.6 and A.7 in appendix A5. In Figure 3.19 we notice that the frequencies have a good match. This proves that the numerical model has been evaluated correctly, the selected initial guesses are the suitable and all the modes of the vibration have been calculated. In Figure 3.20 the frequencies are close but the fit is not as good as in the first case. The numerical models are not expected to give very precise results due to the assumptions of the theory. Furthermore it is evident that the numerical models do not work efficiently for a wide parameter range.

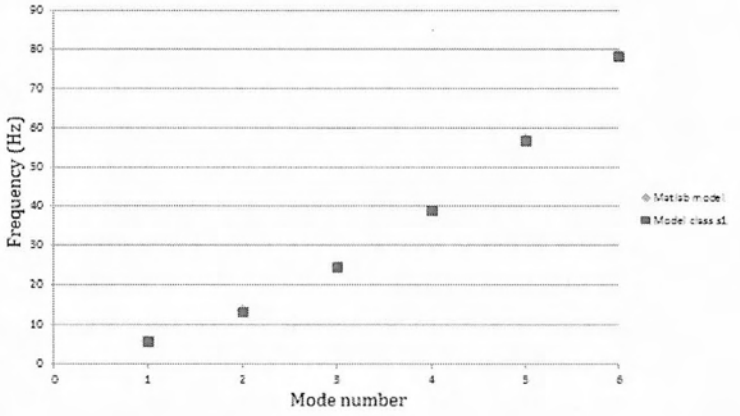

Figure 3.19: The frequencies (Hz) of Matlab numerical model vs. the frequencies of Model class s1 under the act of $5.35e7\ Pa$

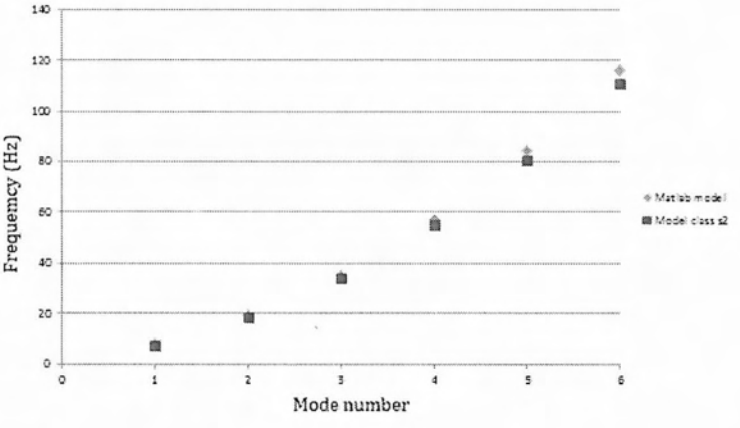

Figure 3.20: The frequencies (Hz) of Matlab numerical model vs. the frequencies of Model class s2 under the act of $5.35e7\ Pa$

Chapter 4

Bayesian Inference for Estimation of Hanger Axial Load

4.1 The purpose of model updating

There are two main purposes of model updating or system identification. One common goal is to identify physical parameters, e.g. stiffness of a structural element. The identified parameters can be further used as indicator for the status of the system or phenomenon. For example, the stiffness parameter of a structural member can be monitored from time to time and an abnormal reduction indicates possible damage of the member. However, reduction may be simply due to statistical uncertainty. Therefore, it is necessary to quantify the uncertainty of the estimation so that one can distinguish whether the parameter change is due to deterioration of the structural member. In this case, it is desirable to obtain a narrow distribution of the parameter so that small changes can be detected with a high level of confidence. Another purpose of model updating is to obtain a mathematical model to represent the underlying system for future prediction. Even though there are parameters to be identified as in the previous case, these parameters may not necessarily be physical, e.g., coefficients of auto-regressive models. In this situation, the identified parameters are not necessarily as important as the previous case provided that the identified model provides an accurate prediction for the system output. Using the quantified uncertainty obtained from Bayesian methods, there are two important types of applications. The first category is robust reliability analysis. Another type of important applications is structural vibration control. This area has received great attention in the last several decades. Because complete information about a dynamical system and its environment is never available, the system and excitation can not be modeled exactly. Classical control design methods based on a single nominal model of the system may fail to create a controlled system that provides satisfactory and robust performance [15].

4.2 Bayesian Parameter Estimation and Uncertainty Propagation Utilizing Modal Data

4.2.1 Bayesian formulation for the posterior PDF

The Bayesian framework for parameter estimation [1] is used to address the problem of estimating the uncertainty in the values of the parameters of structural dynamics models based on the measured modal data. The model class used to represent the structural behavior is considered to be linear. Prediction errors, measuring the fit between the measured and the model predicted modal properties, are modeled by Gaussian distributions.

Let $D = \left\{\omega_r^{(k)}\right\}, r = 1, ..., m, k = 1, ..., N_D$ be the measured modal frequencies of the hanger, where m is the number of experimentaly identified modal frequencies and N_D is the number of modal data sets available. Consider a parameterized class of linear structural models used to model the dynamic behavior of the structure and let $\theta \in R^{N_\theta}$ be the set of free structural model parameters to be identified using the measured modal data. Let also $\omega_r(\theta), \phi_r(\theta) \in R^{N_d}$ where N_d is the number of model degrees of freedom (DOF), be the predictions of the modal frequencies and modeshapes obtained for a particular value of the parameter set by solving the eigenvalue problem corresponding to the model mass and stiffness matrices $M(\theta)$ and $K(\theta)$, respectively, that is

$$[K(\theta) - \omega_r^2(\theta)M(\theta)]\phi_r(\theta) = 0 \tag{4.1}$$

The objective in a modal-based Bayesian structural identification methodology is to estimate the uncertainties in the values of the parameter set θ that the modal data $\omega_r(\theta), \phi_r(\theta)$ predicted by the linear class of models best matches, in some sense, the experimentally obtained modal data in D. The Bayesian approach uses probability distributions to quantify the plausibility of each possible value of the model parameters $\boldsymbol{\theta}$. Using Bayes theorem, the updated (posterior) probability distribution $p(\theta|D, \sigma, M)$ of the model parameters $\boldsymbol{\theta}$ based on the inclusion of the measured data D, the modelling assumptions M and the value of a parameter set $\boldsymbol{\sigma}$, is obtained as follows:

$$p(\theta|D, \sigma, M) = cp(D|\theta, \sigma, M)p(\theta|\sigma, M) \tag{4.2}$$

where $p(D|\theta, \sigma, M)$ is the probability of observing the data (likelihood function) from a model M corresponding to a particular value of the parameter set $\boldsymbol{\theta}$ and the value of $\boldsymbol{\sigma}$, $p(\theta|\sigma, M)$ is the initial (prior) probability distribution of a model, and c is a normalizing constant selected such that the PDF $p(\theta|D, \sigma, M)$ integrates to one. The reciprocal of this term is called the evidence of the model M and for parameter estimation purposes it is just a normalization constant (does not depend on the parameters). For model selection, however, this term plays a crucial role. Herein, the modeling assumptions M refer to the structural modeling assumptions as well as those used to derive the probability distributions $p(D|\theta, \sigma, M)$ and the prior $p(\theta|\sigma, M)$. The parameter set $\boldsymbol{\sigma}$ contains all parameters that need to be defined in order to completely specify the prediction error model of the model M. Measured data are accounted for in the updated estimates through the likelihood term $p(D|\theta, \sigma, M)$, while any available prior information is reflected in the term $p(\theta|\sigma, M)$. From the experience it is usually assumed that $p(\theta|\sigma, M) = \pi(\theta) =$

constant (a non-informative prior distribution). Other prior distribution can be assumed as well. In order to simplify the notation, the dependence of the probability distributions on M is dropped in the analysis that follows.

The form of $p(D|\theta,\sigma,M) \equiv p(D|\theta,\sigma)$ is derived by using a probability model for the prediction error vector $e^{(k)} = [e_1^{(k)},...,e_m^{(k)}], k = 1,...,N_D$, defined as the difference between the measured modal quantities involved in D for all m modes and the corresponding modal quantities predicted from a model that corresponds to a particular value of the parameter set $\boldsymbol{\theta}$. Specifically, the prediction error $e_r^{(k)} = [e_{\omega_r}^{(k)}]$ is given for the modal frequencies by the prediction error equations:

$$e_{\omega r}^{(k)} = \widehat{\omega}_r^{(k)} - \omega_r(\boldsymbol{\theta}), r = 1,...,m \tag{4.3}$$

where $e_{\omega_r}^{(k)}$ is the prediction error for the modal frequency of the r-th mode. Following the Bayesian methodology, the predictions errors are modeled by zero-mean Gaussian vector variables. Specifically, the prediction error $e_{\omega_r}^{(k)}$ for the r-th modal frequency is assumed to be a zero mean Gaussian variable $e_{\omega_r}^{(k)} \sim N(0, \sigma_{\omega_r}^2 \widehat{\omega}_r^{(k)^2})$, with standard deviation $\sigma_{\omega_r}\widehat{\omega}_r^{(k)}$.The prediction error parameter σ_{ω_r} represents the fractional difference between the measured and the model predicted frequency of the r-th mode. The formulation for $p(D|\theta,\sigma)$ is developed as follows

$$p(D|\boldsymbol{\theta},\boldsymbol{\sigma}) = p(\widehat{\omega}_1^{(k)},...,\widehat{\omega}_r^{(k)}) = \prod_{k=1}^{N_D}\prod_{r=1}^{m} p(\widehat{\omega}_r^{(k)}|\boldsymbol{\theta},\boldsymbol{\sigma}) \tag{4.4}$$

Since $\omega_r(\boldsymbol{\theta})$ in 4.4 is is a deterministic quantity and the predictions errors $e_{\omega_r}^{(k)}$ are modeled by zero-mean Gaussian scalar variables so that $e_{\omega_r}^{k} \sim N(0, \sigma_{\omega_r}^2 \widehat{\omega}_r^{(k)2})$, the measured modal frequencies $\widehat{\omega}_r^{(k)}$are also implied to be Gaussian variables, that is $\widehat{\omega}_r^{(k)2} \sim N(\omega_r(\theta), \sigma_{\omega_r}^2 \widehat{\omega}_r^{(k)2})$, with mean $\omega_r(\theta)$ and variance $\sigma_{\omega_r}^2 \widehat{\omega}_r^{(k)2}$. Therefore, the probability density function (PDF) of $\widehat{\omega}_r^{(k)}$ involved in 4.4 given the values of $\boldsymbol{\theta}$ and $\boldsymbol{\sigma}$, is given by

$$p(\widehat{\omega}_r^{k}|\boldsymbol{\theta},\boldsymbol{\sigma}) = \frac{1}{(\sqrt{2\pi})\sigma_{\omega_r}\widehat{\omega}_r^{k}} exp\{-\frac{1}{2}\frac{(\widehat{\omega}_r^{(k)2} - \omega_r(\boldsymbol{\theta}))^2}{\sigma_{\omega_r}^2 \widehat{\omega}_r^{(k)^2}}\} \tag{4.5}$$

By subsituting 4.5 into 4.4 we get

$$p(D|\boldsymbol{\theta},\boldsymbol{\sigma}) = \prod_{k=1}^{N_D}\prod_{r=1}^{m} \frac{1}{(\sqrt{2\pi})^{N_0}\sigma_{\omega_r}\widehat{\omega}_r^{(k)}} exp\{-\frac{1}{2\sigma_{\omega_r}^2}\frac{(\widehat{\omega}_r^{(k)2} - \omega_r(\boldsymbol{\theta}))^2}{\widehat{\omega}_r^{(k)}}\} \tag{4.6}$$

which simplifies to

$$p(D|\boldsymbol{\theta},\boldsymbol{\sigma}) = \frac{1}{(\sqrt{2\pi})^{mN_D}\prod_{k=1}^{N_D}\prod_{r=1}^{m}\widehat{\omega}_r^{(k)}\prod_{r=1}^{m}(\sigma_{\omega_r})^{N_D}} exp\{-\frac{1}{2}\sum_{r=1}^{m}\frac{1}{\sigma_{\omega_r}^2}\sum_{k=1}^{N_D}\frac{(\widehat{\omega}_r^{(k)} - \omega_r(\boldsymbol{\theta}))^2}{\sigma_{\omega_r}^2\widehat{\omega}_r^{(k)2}}\} \tag{4.7}$$

Equation (4.7) can be rewritten in the form

$$p(D|\theta,\sigma) = \frac{1}{b(\sqrt{2\pi})^{NN_D}\rho(\boldsymbol{\sigma})} exp\{-\frac{NN_D}{2} J_D(\boldsymbol{\theta};\boldsymbol{\sigma})\} \tag{4.8}$$

where

$$J_D(\theta;\sigma) = \sum_{i=1}^{m} \frac{\alpha_i}{\sigma_i^2} J_i(\theta) \tag{4.9}$$

with $J_i(\boldsymbol{\theta}) = J_{\omega_i}(\boldsymbol{\theta})$, $i = 1, ..., m$, represents the weighted measure of fit between the measured frequencies and frequencies predicted by a particular model within the selected model class, $J_{\omega_i}(\theta)$ is defined by

$$J_{\omega_r}(\boldsymbol{\theta}) = \frac{1}{N_D} \sum_{k=1}^{N_D} \frac{[\omega_r(\boldsymbol{\theta}) - \widehat{\omega}_r^{(k)}]^2}{[\widehat{\omega}_r^{(k)}]^2} \tag{4.10}$$

respectively,

$$\rho(\boldsymbol{\sigma}) = \prod_{i=1}^{m} (\sigma_i)^{\alpha_i NN_D} \tag{4.11}$$

is a function of the prediction error parameters $\boldsymbol{\sigma}$, $N = m \times N_D$ is the total number of measured data assuming equal number of data in each set. $\alpha_r = 1/N$, $r = 1, ..., m$, satisfying $\sum_{i=1}^{n} \alpha_i = 1$, represent the number of data contained in each modal group in relation to the total number N of data, and

$$b = \prod_{k=1}^{N_D} \prod_{r=1}^{m} (\widehat{\omega}^{(k)_r} ||_{N_D}^{N_D}) = constant \tag{4.12}$$

Optimal Value of Structural Model Parameters given the Prediction Error Parameters

Given the values of the prediction error parameters $\boldsymbol{\sigma}$, the optimal value of the model parameter set $\boldsymbol{\theta}$ corresponds to the most probable model maximizing the updated PDF $p(\theta|D,\sigma,M)$ given in 4.8. In particular, using 4.8 and assuming a noninformative prior distribution $p(\theta|D,\sigma,M) = \pi(\theta) = constant \ \forall \ \theta$ in Θ where $\boldsymbol{\Theta}$ is the domain of the definition of $\boldsymbol{\theta}$, the oprimal values of $\widehat{\boldsymbol{\theta}}$ of the model parameters $\boldsymbol{\theta}$ are equivalently obtained by minimizing the measure of fit $J_D(\boldsymbol{\theta};\boldsymbol{\sigma})$ in 4.9, i.e.

$$\widehat{\boldsymbol{\theta}} = arg_{\theta} min J_D(\boldsymbol{\theta};\boldsymbol{\sigma}) \tag{4.13}$$

The notation $\widehat{\boldsymbol{\theta}(\sigma)}$ is used to show that the optimal value $\widehat{\boldsymbol{\theta}}$ depends on the values of the prediction error parameter set $\boldsymbol{\sigma}$. Hybrid algorithms based on evolution strategies and gradient methods are well-suited optimization tools for solving the resulting non-convex optimization problem and identifying the global optimum from multiple local ones.

4.2.2 Parameter estimation

The closed form of the posterior (4.2) is not always straight forward to calculate as in many real cases there is not even an analytical formula available for the model predictions, instead the posterior PDF is represented by samples in the parameter space $\boldsymbol{\theta}_i, i = 1, ..., N$, where N is the number of samples. This method requires only point-wise evaluation of the posterior, which must been known only up to proportionality constant. The samples are generated by the Transitional Markov Chain Monte Carlo (TMCMC) algorithm, which is a variant of the Markov Chain Monte Carlo (MCMC) class of algorithms [3]. These samples are used to estimate the uncertainties in the parameters $\boldsymbol{\theta}$ and possible correlations between the parameters. Markov Chain Monte Carlo (MCMC) methods are a class of algorithms for sampling from probability distributions based on constructing a Markov chain that has the desired distribution as its equilibrium distribution [3]. The state of the chain after a large number of steps is then used as a sample of the desired distribution. The quality of the sample improves as a function of the number of steps [16]. The Transitional Markov Chain Monte Carlo has been proposed to address the problem of choosing the right adaptive proposal PDF in MCMC methods for accelerating convergence to the posterior PDF. This can be a serious problem when the support of the posterior PDF is very peacked and isolated in a small region in the parameter space. Due to a large number of independent parallel chains involved, TMCMC is efficient in terms of parallel implementation.

4.2.3 Uncertainty propagation

The uncertainty in the model parameters $\boldsymbol{\theta}$ is propagated through the model to estimate the uncertainty in output quantities of interest. The samples $\boldsymbol{\theta}_i, i = 1, ..., N$ are also used for that purpose, except for parameter estimation. Specifically, the expected value of an output quantity of interest $Q_1(\theta)$ is approximated using the TMCMC samples by

$$E[Q_1(\theta)] = \frac{1}{N} \sum_{i=1}^{N} Q_1(\theta_i) \tag{4.14}$$

For each sample, the quantity of interest (modal frequencies in this study) is calculated from the corresponding model. In this study, the folowing models, described in Chapters 2 and 3 are investigated.

- Model class beam 1
- Model class beam 2
- Model class 0
- Model class 1
- Model class 2

4.3 Bayesian Model selection

The Bayesian framework can be used to select the best model class among a family of alternative model classes. Specifically, let M1, M2, be competitive model classes. Let $P(M1)$, $P(M2)$ be the prior probabilities of the model classes, these represent initial states of knowledge for each model and are usually considered equal. Using the Bayes theorem, the posterior probabilities $P(M1|D)$ and $P(M2|D)$ of the model classes given the data are obtained from

$$P(M1|D) = \frac{P(D|M1)P(M1)}{P(D)} \tag{4.15}$$

$$P(M2|D) = \frac{P(D|M2)P(M2)}{P(D)} \tag{4.16}$$

then

$$\frac{P(M1|D)}{P(M2|D)} = \frac{P(D|M1)}{P(D|M2)} \tag{4.17}$$

where $P(D|M1)$ is the evidence of M1 and $P(D|M2)$ is the evidence of M2.

Assuming that the model classes are equally probable prior to the use of the data, then the most probable model class based on the data corresponds to the model class with the highest evidence [3]. One more merit of using the TMCMC algorithm for Bayesian purposes is the calculation of the evidence integral given by

$$P(D|M) = \int_{\theta} P(D|M,\theta)P(\theta)d\theta \tag{4.18}$$

Chapter 5

Results

5.1 Numerical models

Model class beam 1

Model class beam 1 is the analytical beam model with fixed ends. The structural parameters are the length L and the axial load F of the beam. In order to obtain a smooth parameter space, the model parameters were defined as the multiplying coefficients of the nominal values of the respective patameters which were determined independently. The prior distributions for these parameters was chosen to be uniform in the following ranges:

- Load F (Newton): $F = F_{nom} * \theta_F$, $F_{nom} = 711000N$, $\theta_F \in [0.5, 5]$
- Length L (m): $L = L_{nom} * \theta_L$, $L_{nom} = 12m$, $\theta_L \in [0.5, 1.5]$
- Prediction error $\sigma : \sigma \in [0, 1]$, assumed the same for all modes

Paramater estimation results were obtained by using the TMCMC algorithm. Figure 5.1 presents the marginal distributions of the parameters. The most probable value for θL is 0.97 and the most probable value for θF is 1.1 which indicates that the value of the parameters is close to the nominal values. By observing the marginal distributions alone it is not possible to assess for correlation between the parameters. For this purpose the two dimensional projection of the samples is presented in Figure 5.2. The colour indicates the value of the posterior. In this Figure we can note the correlation between the length and load of the beam which is expected as while the length is increased, the frequencies tend to decrease and the load must be increased in order to maintain the fit with the experimental frequencies. Figure 5.3 presents the uncertainty propagation of the parameters to the output frequencies of the model based on equation (4.14). The frequencies are normalized with respect to the experimental frequencies. We can see that the expected value of the model predicted frequencies is quite close to the observed experimental frequencies (values close to 1).

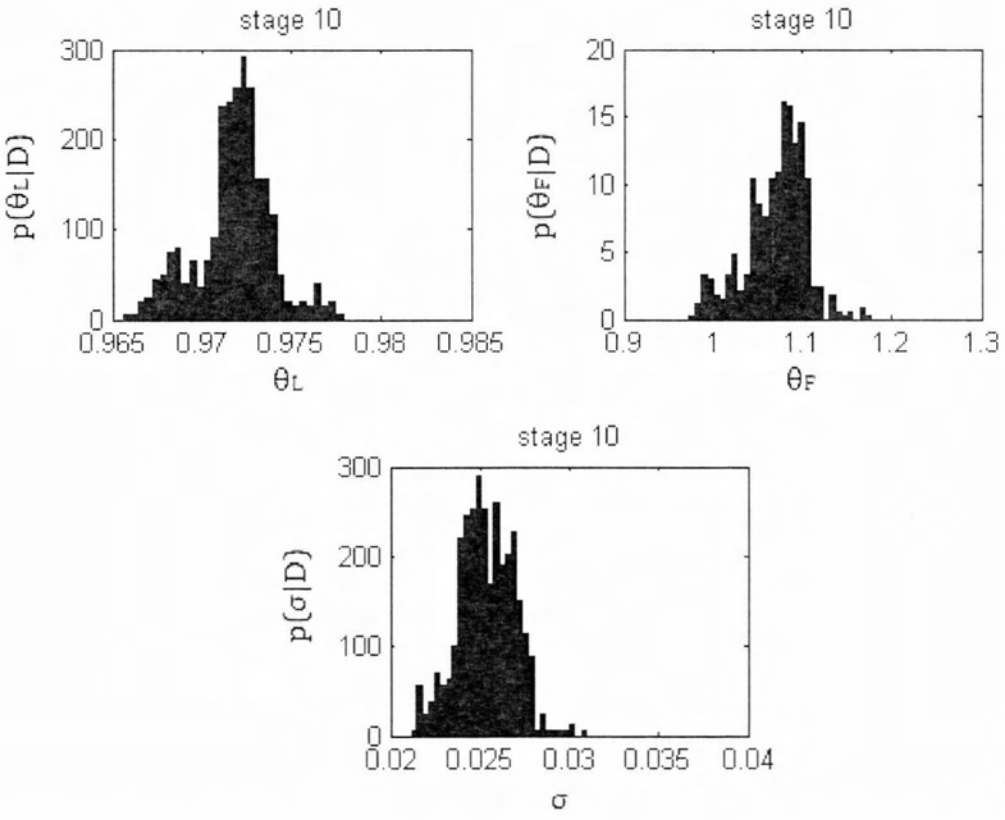

Figure 5.1: The marginal distribution of model class beam 1 parameters θ_L, θ_F, σ

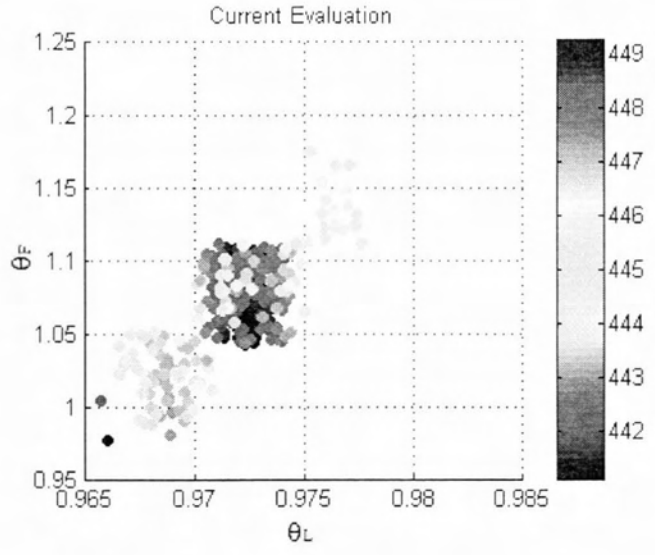

Figure 5.2: 2D sample projection of model class beam 1

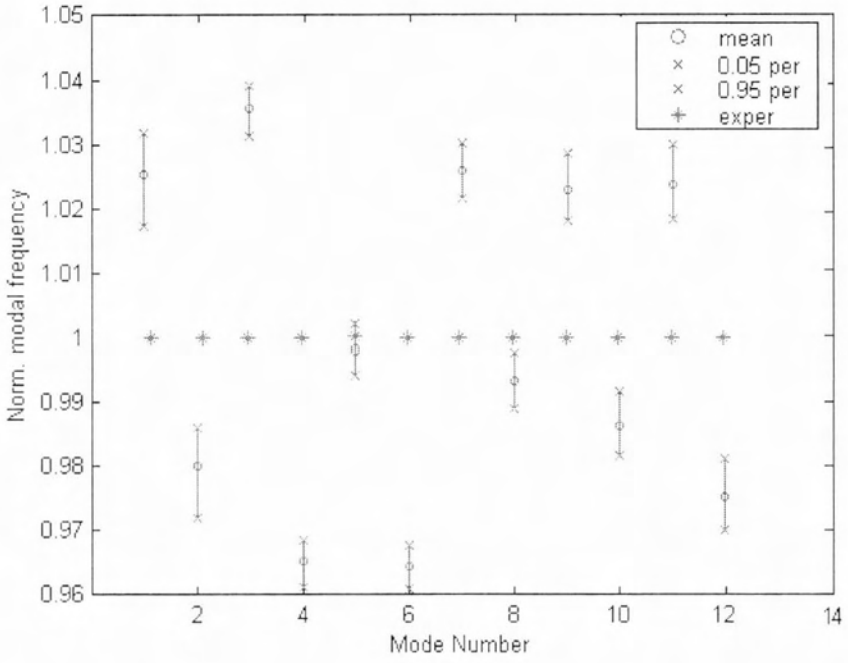

Figure 5.3: Uncertainty propagation to the output frequencies of model class beam 1

Model class beam 2

Model class beam 2 has flexible supports modeled by four springs, two in each direction, transverse and longitudinal. As a result it has four additional parameters compared to model class beam 1, the four spring constants. In order to keep the parameter space smooth, the parameters associated with the springs were defined as the exponents of 10. Uniform priors were assigned for the model parameters.

- Load F (Newton): $F = F_{nom} * \theta_F$, $F_{nom} = 711000N$, $\theta_F \in [0.5, 5]$
- Length L (m): $L = L_{nom} * \theta_L$, $L_{nom} = 12m$, $\theta_L \in [0.5, 1.5]$
- Spring stiffness k_1 (N/m): $k_1 = 10^{\theta_{k1}}$, $\theta_{k1} \in [5, 12]$
- Spring stiffness k_2 (N/m): $k_2 = 10^{\theta_{k2}}$, $\theta_k 2 \in [5, 12]$
- Spring stiffness k_3 (N/m): $k_3 = 10^{\theta_{k3}}$, $\theta_{k3} \in [5, 12]$
- Spring stiffness k_4 (N/m): $k_4 = 10^{\theta_{k4}}$, $\theta_{k4} \in [5, 12]$
- Prediction error $\sigma : \sigma \in [0, 1]$ assumed the same for all modes

Figures 5.4 and 5.5 present the marginal distributions of the model parameters. Figures 5.6-5.17 show selected 2D sample projections for various parameter combinations. Figure 5.18 presents the uncertainty propagation to the predicted frequencies of model class beam 2, normalized by the experimental frequencies. The axial force in this model

appears to be closer to the nominal value compared to model beam 1. The spring stiffnesses appear to cover a range from 10^8 to 10^{12} which implies that the model is insensitive to these parameters. However, their inclusion in the model results in a better fit with the experimental frequencies as we can see in Figure 5.18. The effect of the springs is important as their stiffness constants are not large compared to the Modulus of Elasticity of the beam which is assumed to be $E = 200GPa$.

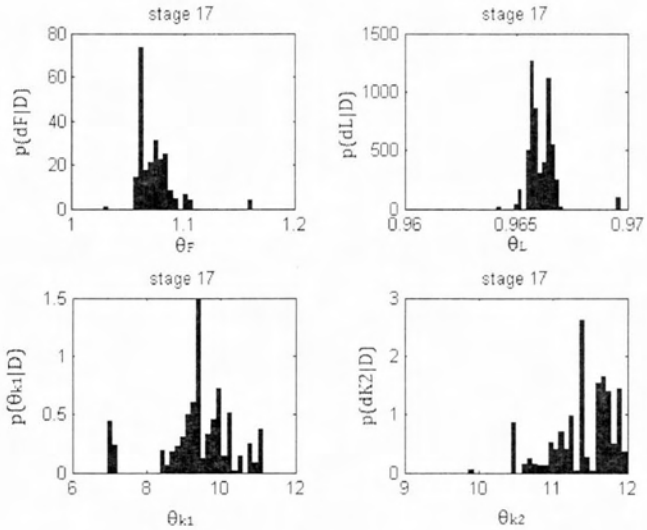

Figure 5.4: The marginal distribution of model class beam 2 parameters $\theta_F, \theta_L, \theta_{k1}, \theta_{k2}$

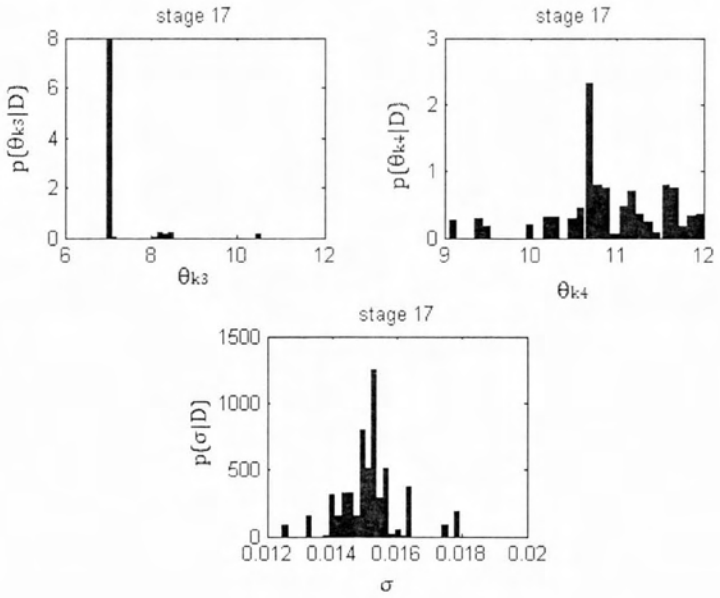

Figure 5.5: The marginal distribution of model class beam 2 parameters $\theta_{k3}, \theta_{k4}, \sigma$

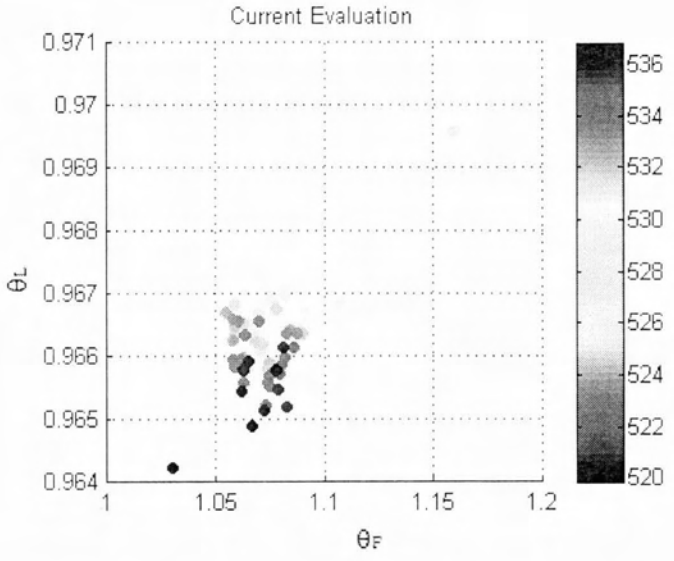

Figure 5.6: 2D sample projection of model class beam 2, θ_L vs. θ_F

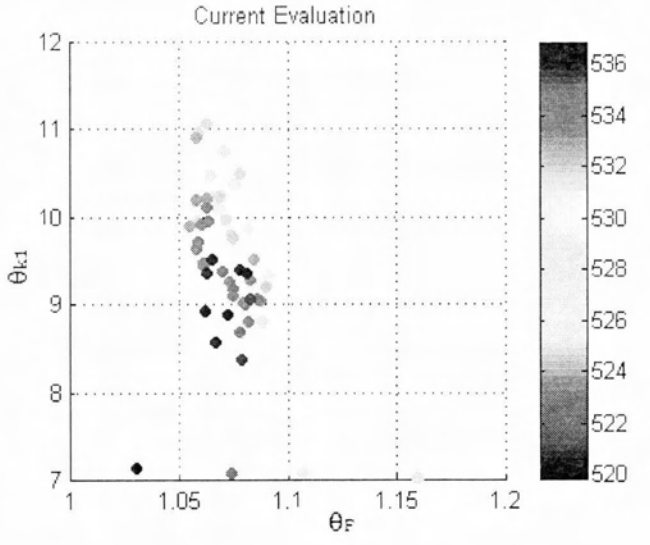

Figure 5.7: 2D sample projection of model class beam 2, θ_{k1} vs. θ_F

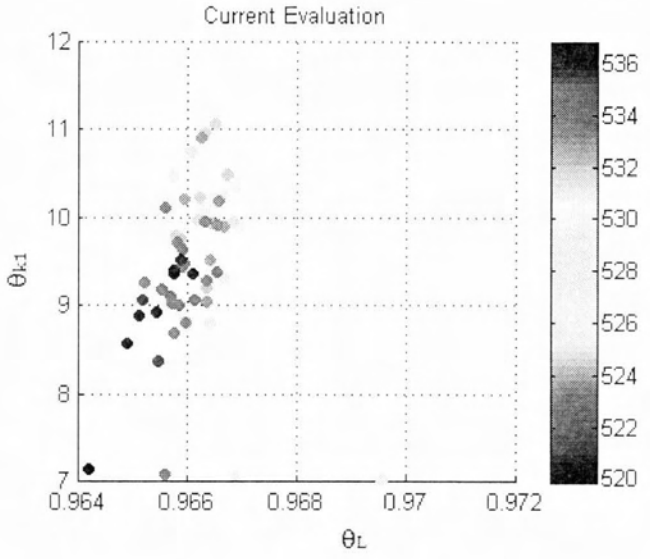

Figure 5.8: 2D sample projection of model class beam 2, θ_{k1} vs. θ_L

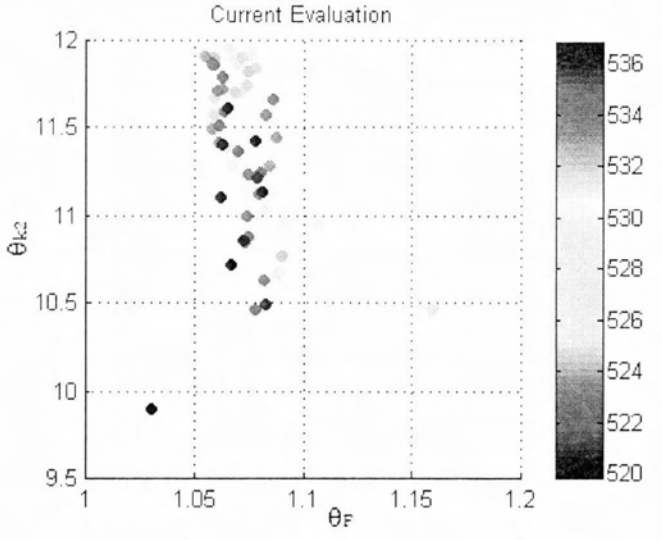

Figure 5.9: 2D sample projection of model class beam 2, θ_{k2} vs. θ_F

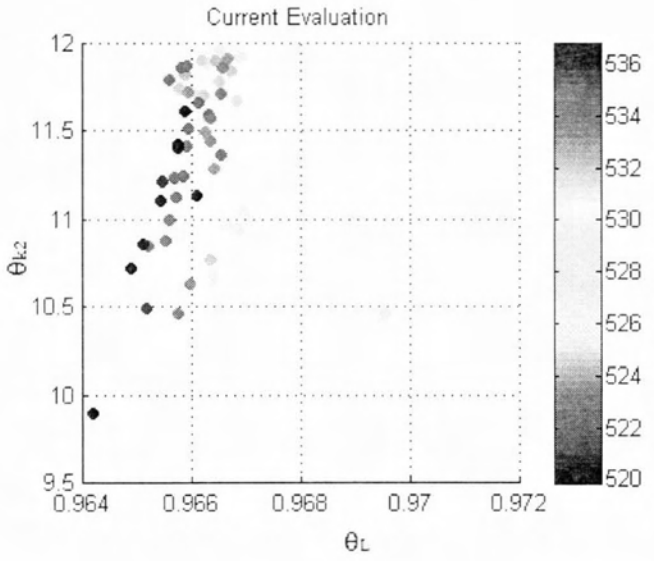

Figure 5.10: 2D sample projection of model class beam 2, θ_{k2} vs. θ_L

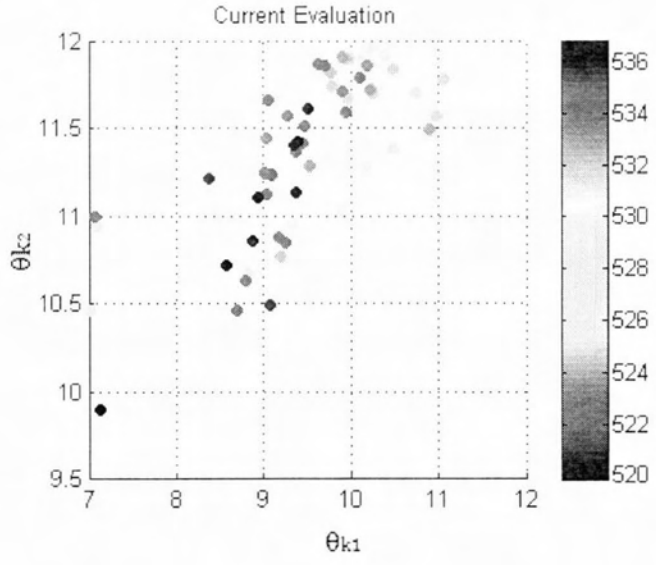

Figure 5.11: 2D sample projection of model class beam 2, θ_{k2} vs. θ_{k1}

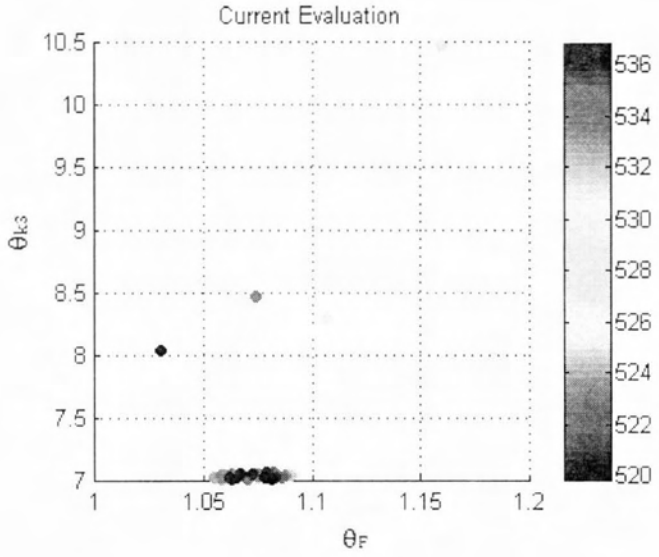

Figure 5.12: 2D sample projection of model class beam 2, θ_{k3} vs. θ_F

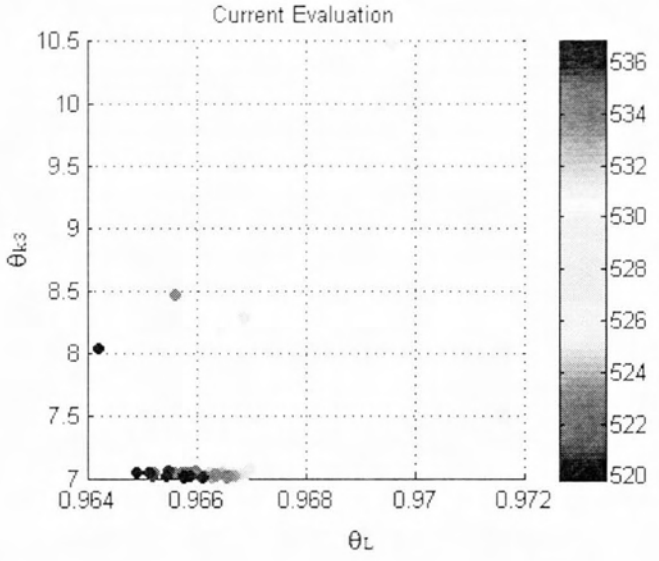

Figure 5.13: 2D sample projection of model class beam 2, θ_{k3} vs. θ_L

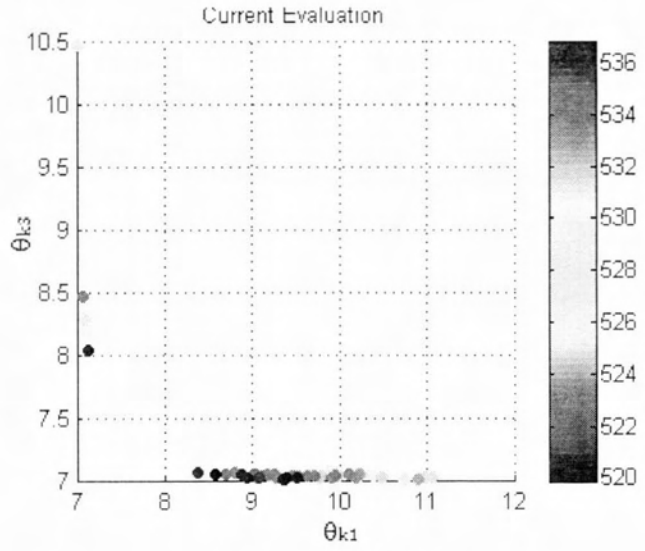

Figure 5.14: The 2D sample projection of model class beam 2, dk_3 vs. θ_{k1}

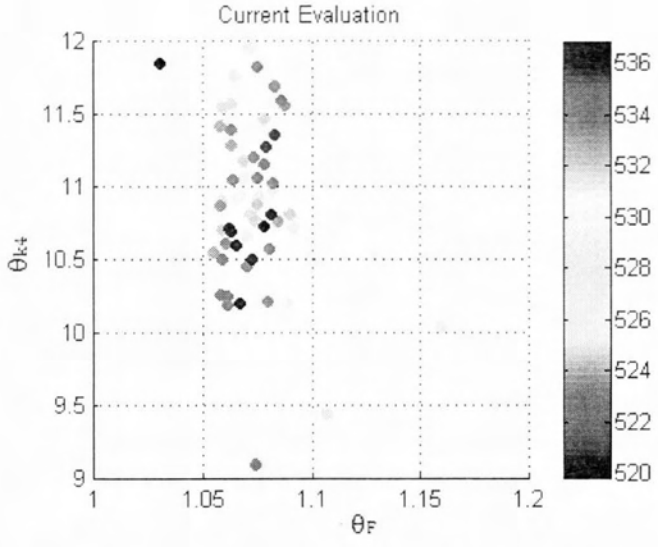

Figure 5.15: The 2D sample projection of model class beam 2, θ_{k4} vs. θ_F

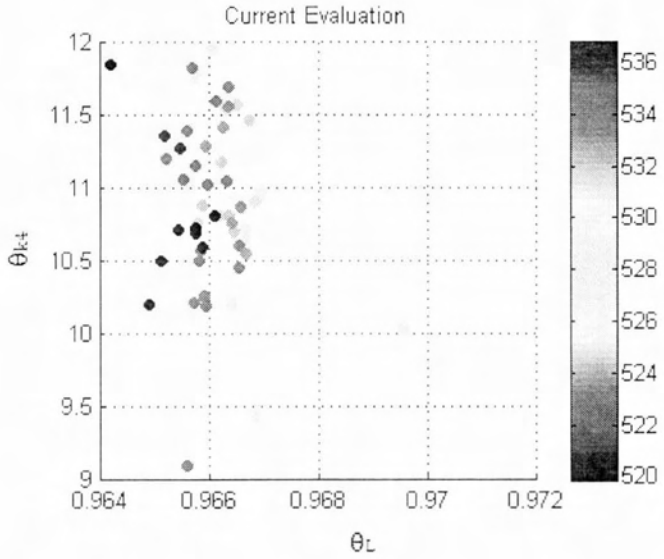

Figure 5.16: The 2D sample projection of model class beam 2, θ_{k4} vs. θ_L

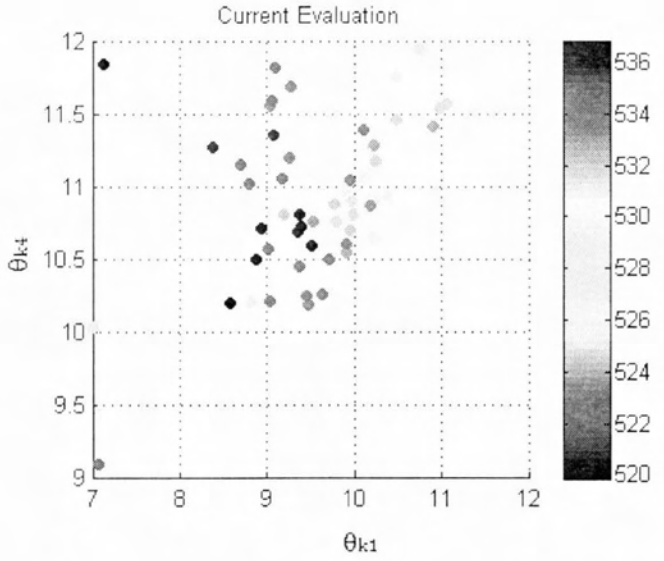

Figure 5.17: The 2D sample projection of model class beam 2, θ_{k4} vs. θ_{k1}

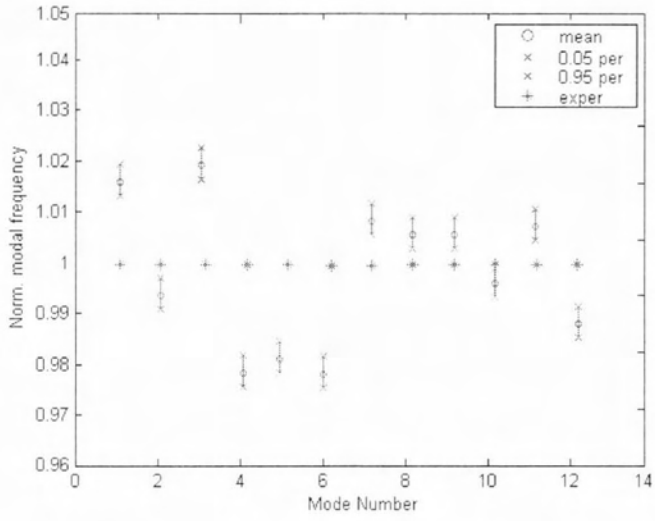

Figure 5.18: Uncertainty propagation to the output frequencies of model class beam 2

5.2 FEA models

Model class 0

Model class 0 is a high fidelity finite element model of the hanger developed in Abaqus. The model has fixed ends and the only parameter is the axial load. The prior distribution for the load was considered uniform.

- Load P (Pa): $P = P_{nom} * \theta_P$, $P_{nom} = 1.37e7Pa$, $\theta_P \in [0.2, 2]$
- Prediction error $\sigma : \sigma \in [0, 1]$ assumed the same for all modes

Figure 5.19 presents the marginal distributions of model class 0 parameters. Figure 5.20 presents the two dimensional projection of the samples. Figure 5.21 shows the uncertainty propagation to the output frequencies of the model. We can see that this model with fixed ends underestimates the axial load by almost 20%, and provides a worse fit with the experimental frequencies compared to the model class beam 2 which has flexible supports.

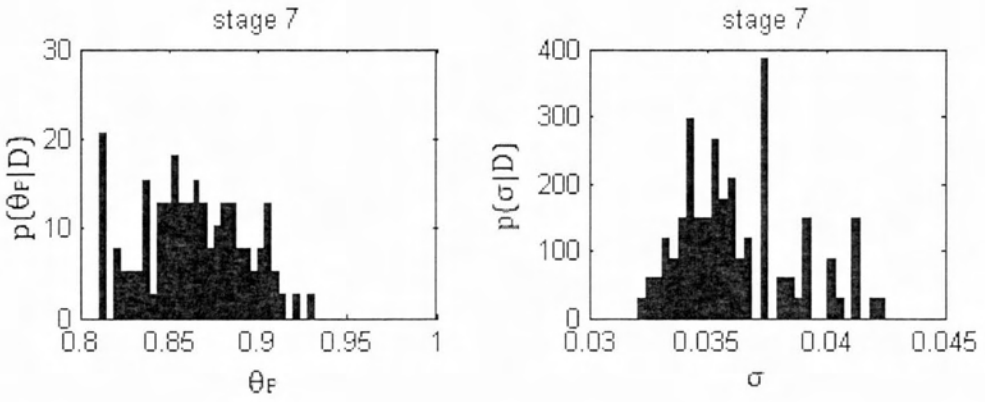

Figure 5.19: The marginal distribution of of model class 0 parameters θ_P , σ

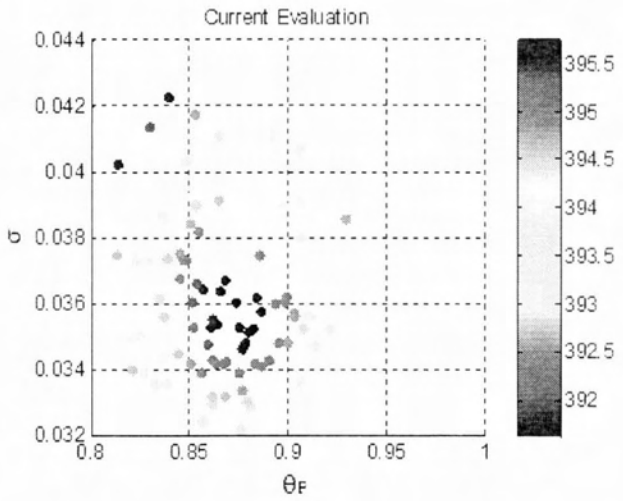

Figure 5.20: 2D sample projection for model class 0, σ vs. θ_P

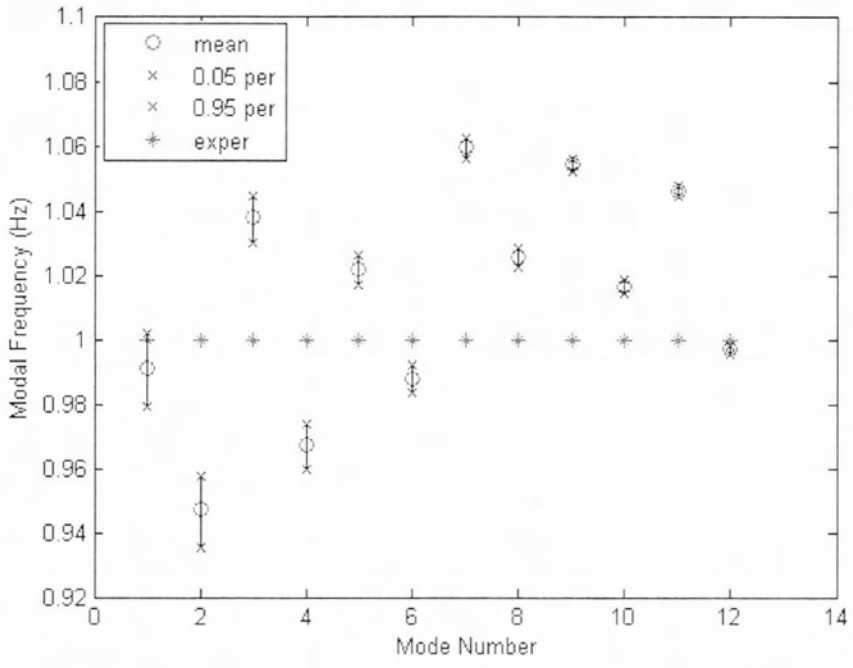

Figure 5.21: Uncertainty propagation to the output frequencies of model class 0

Model class 1

This model is a high fidelity finite element model with flexible supports, model by 8 springs resulting in a total number of 10 parameters. The prior distributions for these parameters were considered uniform in the following ranges.

- Load P (Pa): $P = P_{nom} * \theta_P, P_{nom} = 5.35e7Pa, \theta_P \in [0.5, 5]$
- Spring stiffness k_1 (N/m): $k_1 = 10^{\theta_{k1}}, \theta_{k1} \in [5, 12]$
- Spring stiffness k_2 (N/m): $k_2 = 10^{\theta_{k2}}, \theta_{k2} \in [5, 12]$
- Spring stiffness k_3 (N/m): $k_3 = 10^{\theta_{k3}}, \theta_{k3} \in [5, 12]$
- Spring stiffness k_4 (N/m): $k_4 = 10^{\theta_{k4}}, \theta_{k4} \in [5, 12]$
- Spring stiffness k_{lx} (N/m): $k_{lx} = 10^{\theta_{klx}}, \theta_{klx} \in [5, 12]$
- Spring stiffness k_{ly} (N/m): $k_{ly} = 10^{\theta_{kly}}, \theta_{kly} \in [5, 12]$
- Spring stiffness k_{rx} (N/m): $k_{rx} = 10^{\theta_{krx}}, \theta_{krx} \in [5, 12]$
- Spring stiffness k_{ry} (N/m): $k_{ry} = 10^{\theta_{kry}}, \theta_{kry} \in [5, 12]$
- Prediction error $\sigma : \sigma \in [0, 1]$ assumed the same for all modes

Figures 5.22, 5.23 and 5.24 present the marginal distributions of model class 1 parameters. Figures 5.20 - 5.28 present the two dimensional projection of the samples. The spring stiffnesses appear to cover a range from 10^8 to 10^{12} which implies that the model is insensitive to these parameters. Figure 5.29 presents the uncertainty propagation to the model class 1 output frequencies, which are closer to the experimental frequencies than model class 0. We can clearly see the impact of the flexible foundations in predicting the frequencies compared to model class 0 which is fixed. This means that even if the model is insensitive to the spring constants, they affect the predictions.

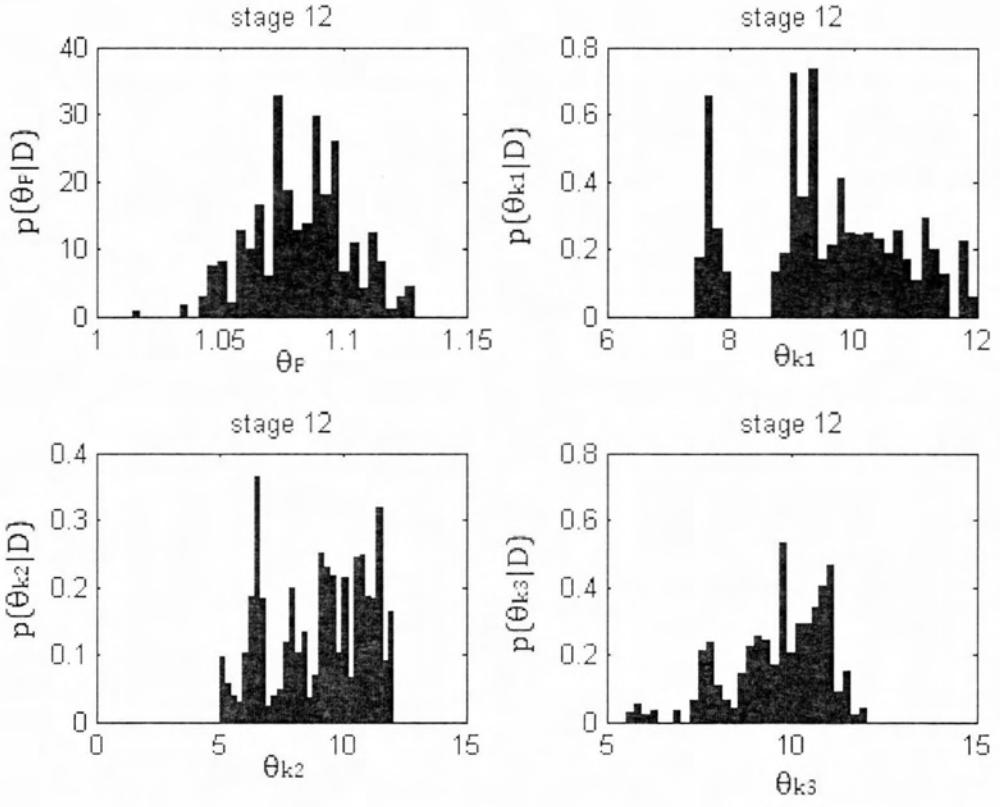

Figure 5.22: The marginal distribution of model class 1, parameters θ_P , θ_{k1}, θ_{k2}, θ_{k3}

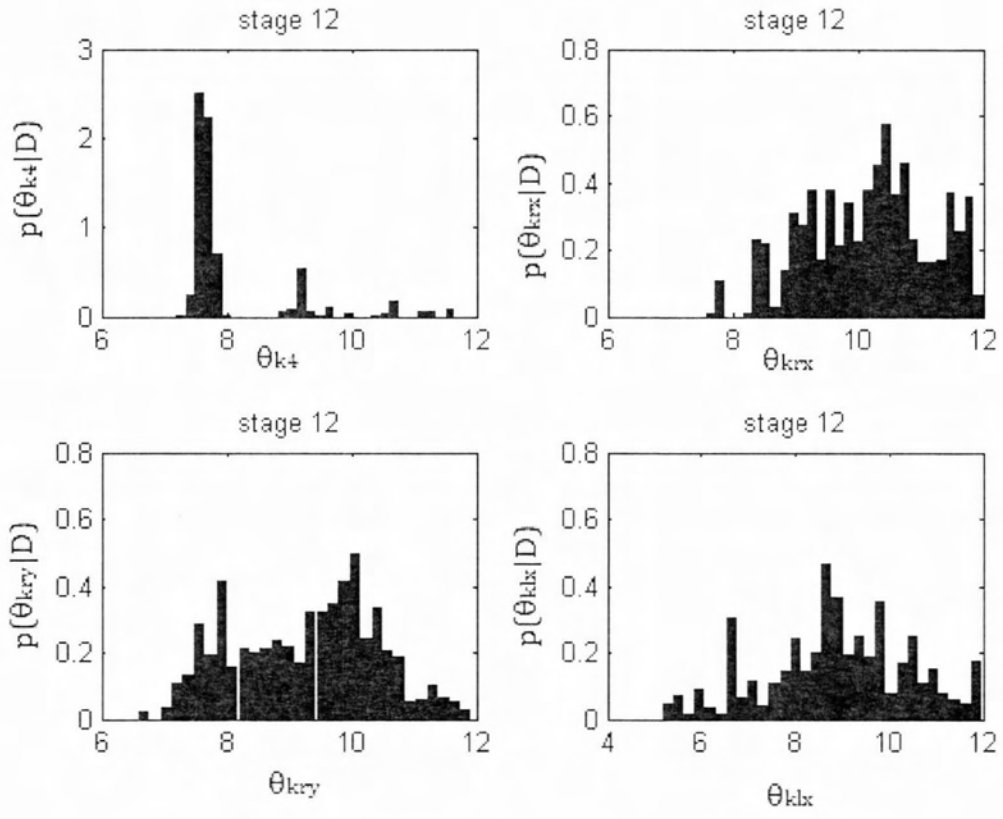

Figure 5.23: The marginal distribution of model class 1, parameters θ_{k4}, θ_{kly}, θ_{krx}, θ_{kry}

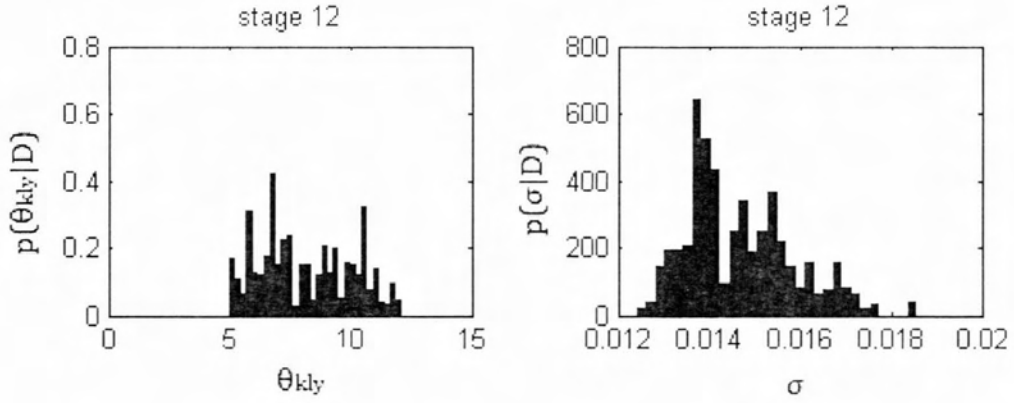

Figure 5.24: The marginal distribution of model class 1, parameters θ_{kly}, σ

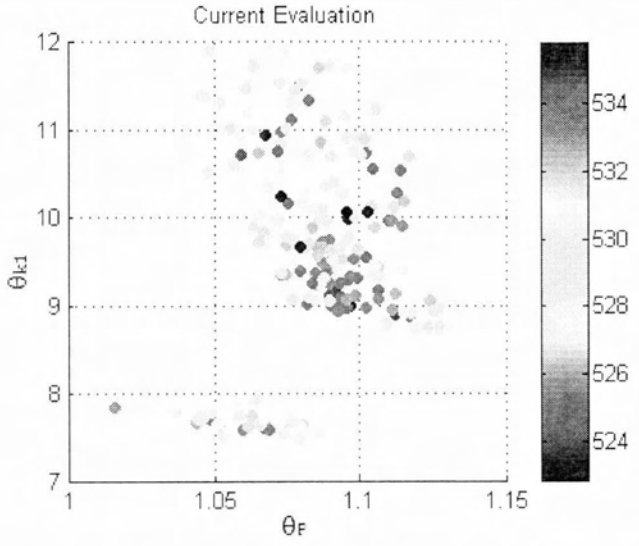

Figure 5.25: 2D sample projection for model class 1, θ_{k1} vs. θ_P

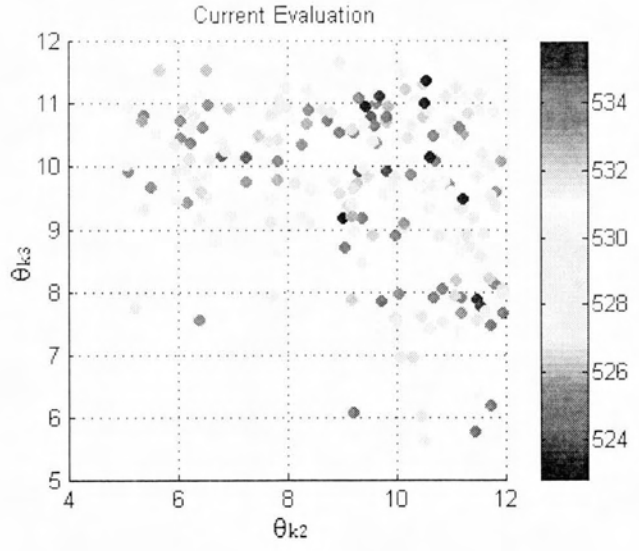

Figure 5.26: The 2D sample projection for model class 1, θ_{k3} vs. θ_{k2}

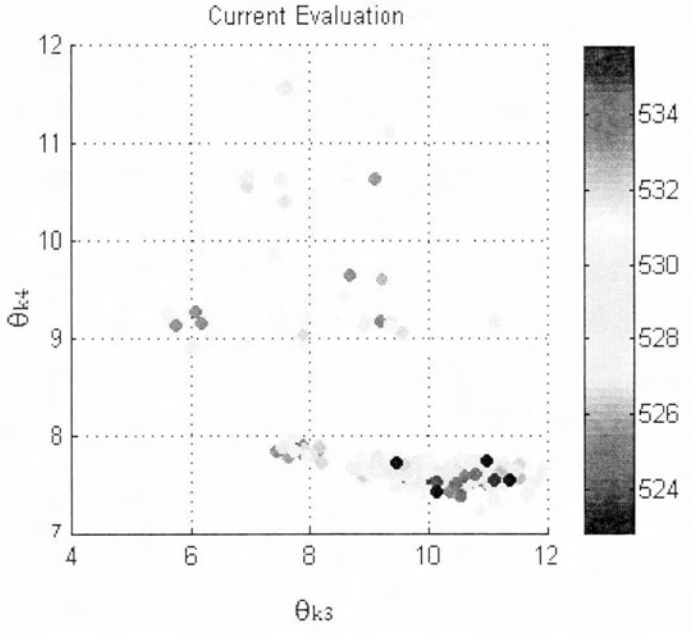

Figure 5.27: 2D sample projection for model class 1, θ_{k4} vs. θ_{k3}

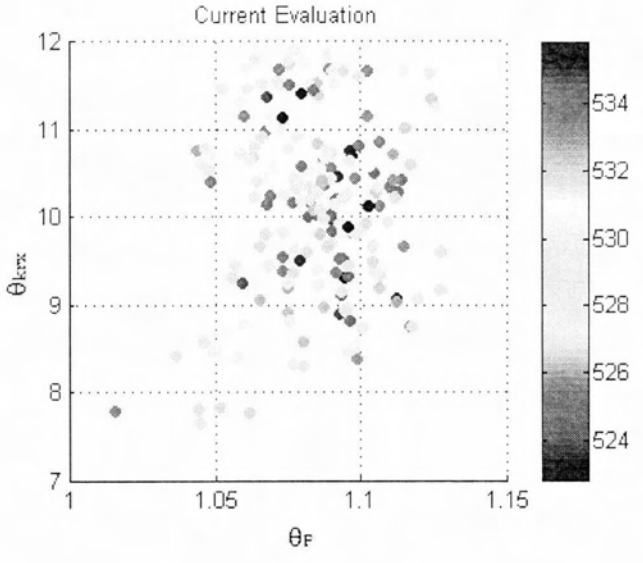

Figure 5.28: 2D sample projection for model class 1, θ_{krx} vs. θ_{k3}

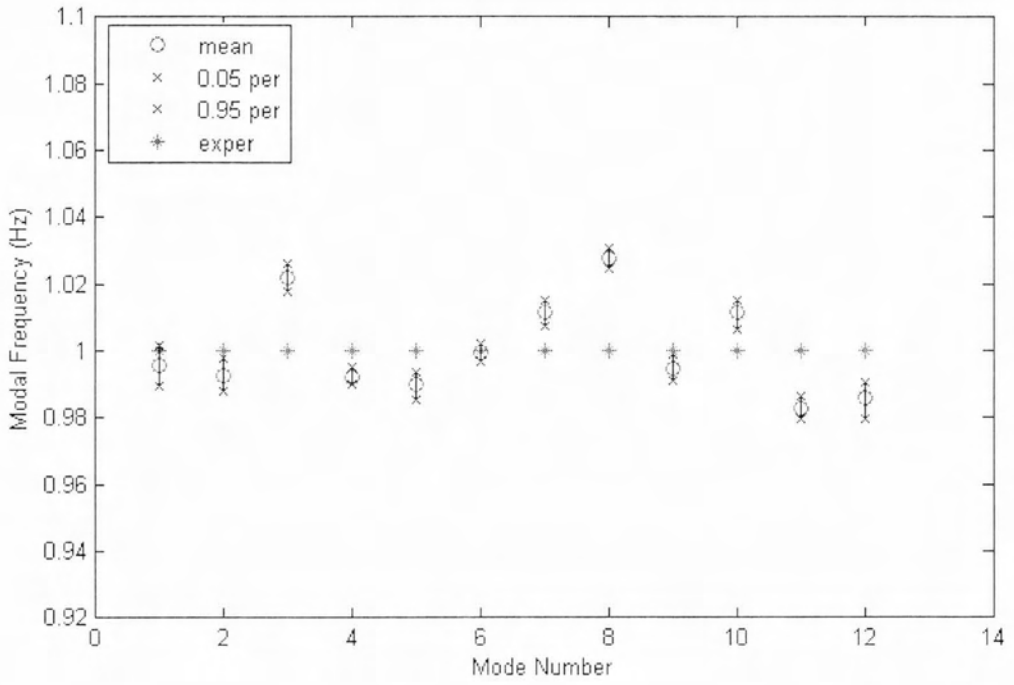

Figure 5.29: Uncertainty propagation to the output frequencies of model class 1

Model class 2

Model class 2 has four springs and the springs in x and y direction were replaced by fixed boundary conditions resulting in four less parameters compared to model class 1. In order to keep the parameter space smooth, the parameters associated with the springs were defined as the exponents of 10. Uniform priors were assigned for the model parameters.

- Load P (Pa): $P = P_{nom} * \theta_P, P_{nom} = 1.67e7Pa, \theta_P \in [0.5, 5]$
- Spring stiffness k_1 (N/m): $k_1 = 10^{\theta_k}, dk \in [5, 12]$
- Spring stiffness k_2 (N/m): $k_2 = 10^{\theta_k}, \theta_k \in [5, 12]$
- Spring stiffness k_3 (N/m): $k_3 = 10^{\theta_k}, \theta_k \in [5, 12]$
- Spring stiffness k_4 (N/m): $k_4 = 10^{\theta_k}, \theta_k \in [5, 12]$
- Prediction error $\sigma : \sigma \in [0, 1]$ assumed the same for all modes

Figures 5.30 and 5.31 present the marginal distributions of model class 2 parameters. From the marginal posterior distributions of k_2 and k_3 we can see that the model is very insensitive in their values. This could be related to the small area where the k_2 and k_3 springs are distributed compared to the area covered by the springs k_1 and k_4. We note that the marginal posterior distributions of k_1 and k_4 are multimodal indicating two most probable values for each parameter. This can be also verified from the 2D samples projection of θ_{k1} vs. θ_{k4} in Figure 5.32. This figure suggests that the parameters θ_{k1} and θ_{k4} are correlated and can take the values $\theta_{k1} = 7.5$, $\theta_{k2} = 9$ or $\theta_{k1} = 9$, $\theta_{k2} = 7.5$. This means there is a different stiffness in each side of the beam but because of the symmetry of the finite element model the methodology cannot distinguish the two sides from each other. The different stiffness could be explained in the physical structure because of the different foundation in each side as can be seen in Figure 1.1. Figure 5.37 presents the uncertainty propagation of the parameters to the output frequencies of the model. We notice that the predicted frequencies of this model are very close to those of model class 1, thus the springs of model class 1 in x and y direction do not have significant impact in the performance of the model.

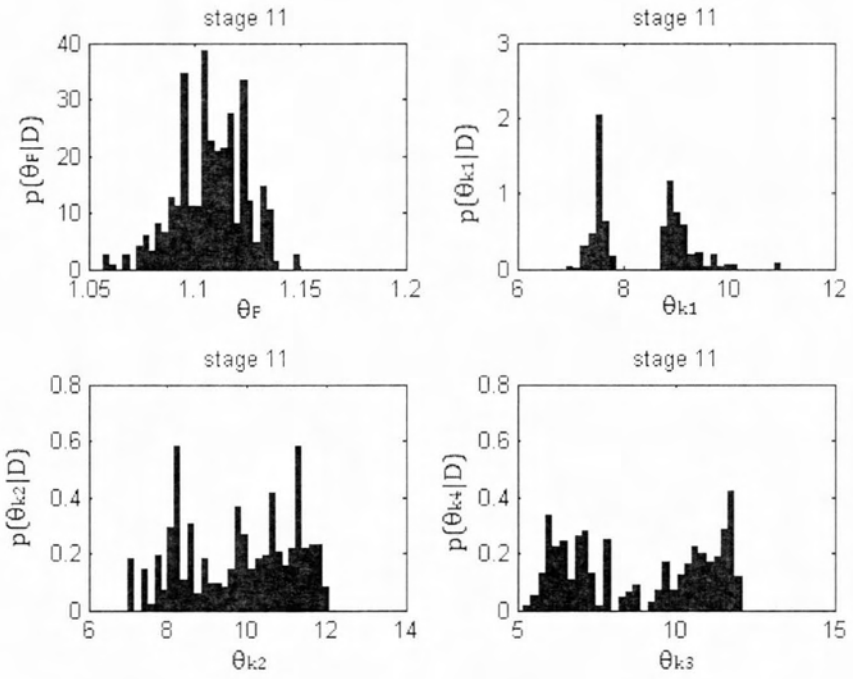

Figure 5.30: The marginal distribution of model class 2, parameters θ_P, θ_{k1}, θ_{k2}, θ_{k3}

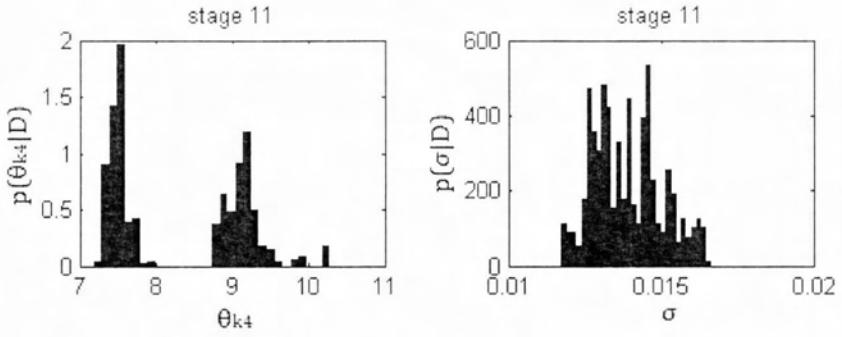

Figure 5.31: The marginal distribution of model class 2, parameters θ_{k4} , θ_{k4}

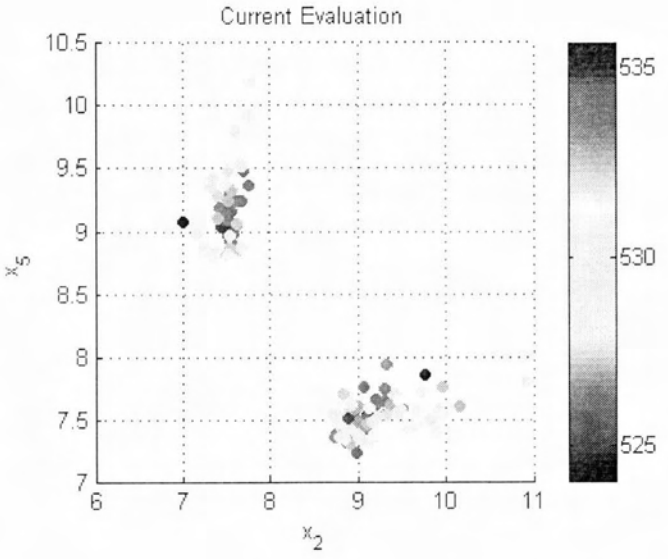

Figure 5.32: The marginal distribution of model class 1, parameters θ_{k4} , θ_{k1}

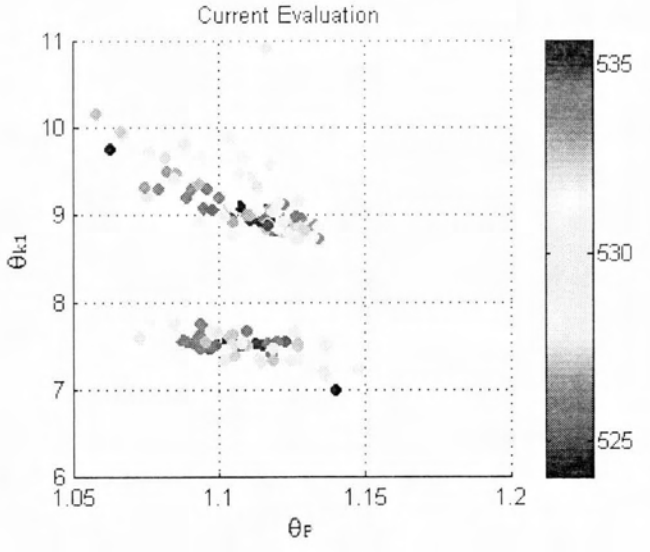

Figure 5.33: 2D sampe projection of model class 2, θ_{k1} vs. θ_P

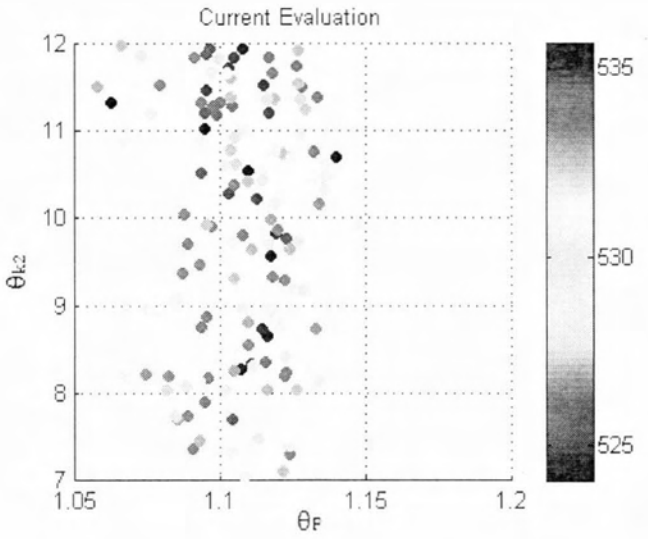

Figure 5.34: 2D sampe projection of model class 2, θ_{k2} vs. θ_P

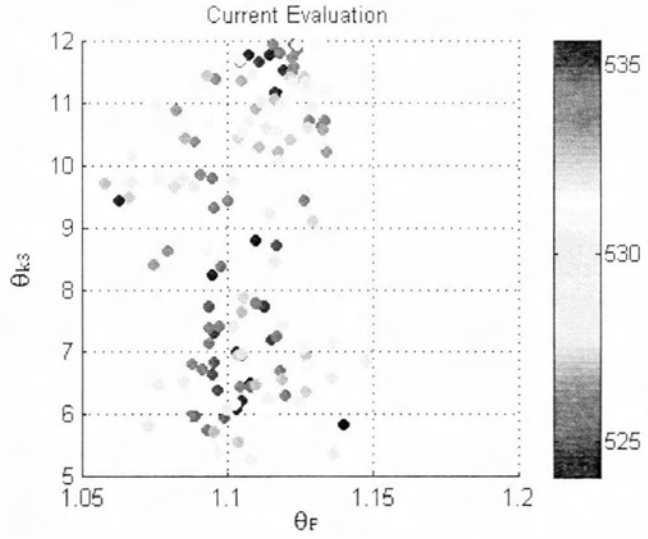

Figure 5.35: 2D sampe projection of model class 2, θ_{k3} vs. θ_P

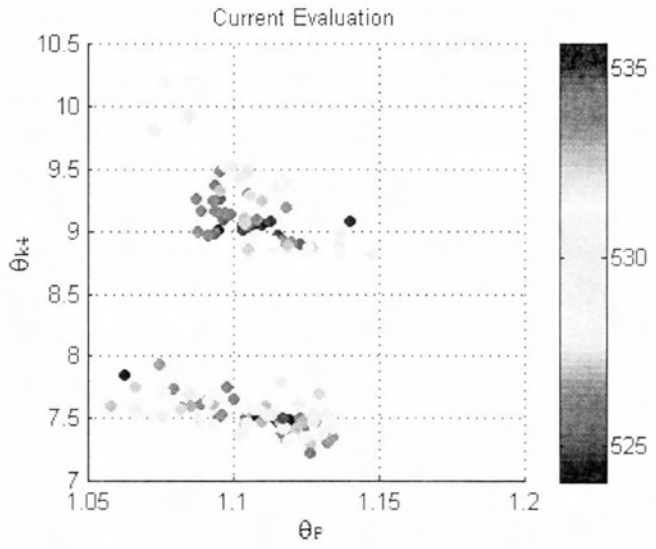

Figure 5.36: 2D sampe projection of model class 2, θ_{k4} vs. θ_P

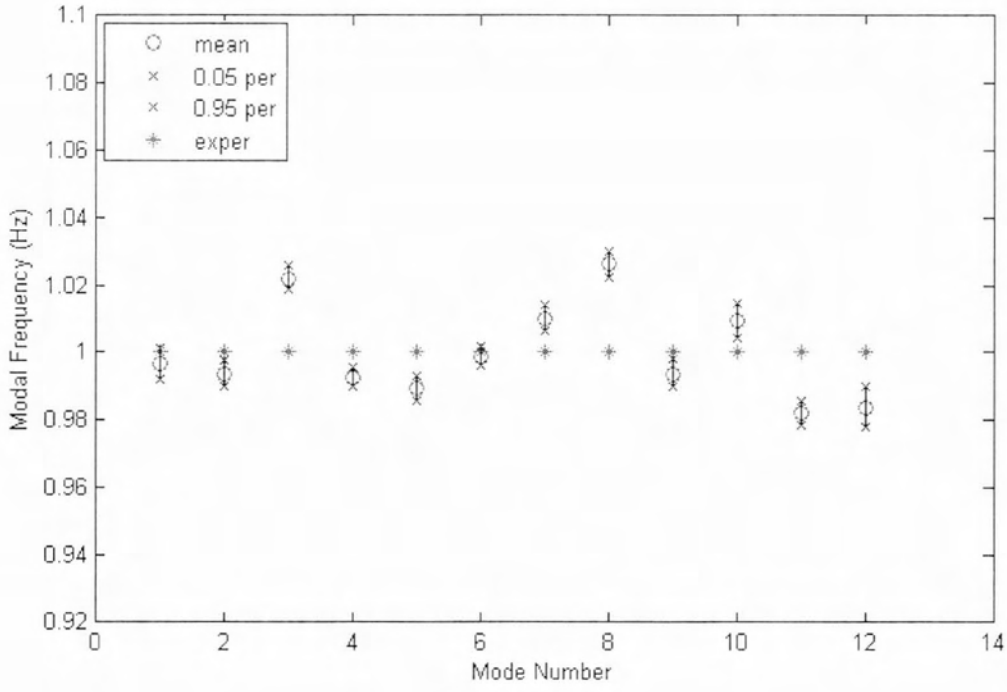

Figure 5.37: Uncertainty propagation to the output frequencies of model class 2

5.3 Bayesian model selection results

The evidence $P(D|M)$ for each model was calculated by the TMCMC algorithm and the results are presented in the following table.

Table 5.1: The evidence of the models

Model class	Evidence
Beam 1	434.49
Beam 2	497.11
0	385.04
1	512.58
2	515.42

According to equation 4.17 the most model whose results are probably the most accurate, for the given data D, is the one with the largest evidence. Thus, we conclude that the most suitable model is model class 2 which is the finite element model with the four springs. It is important to note that even though model class 1 gives essentialy the same results with model class 2, it has a smaller evidence associated with it. That is because the evidence $P(D|M)$ defined in equation 4.18 takes into account the number of parameters of the model, and penalizes the model with the more parameters that yields similar results. The analytical models also score lower evidences because they have an additional parameter (the length of the beam) and provide a slightly worse fit.

Chapter 6

Conclusions

This thesis examined methods of estimate the tension in bridge hangers via measured modal frequencies. Both analytical and finite element models were developed and examined separately. Moreover, a thorough analysis of boundary conditions was realized, by considering both fixed and flexible hanger ends. The models were compared with each other and with experimental data. Subsequently, the models were integrated into a TMCMC algorithm to estimate the uncertainty of their parameters, thus achieving the objectives of this project.

6.1 Findings

It is evident from the results that the boundary conditions affect significantly not only the output of the models but also its uncertainty. The results in the investigated models are summarized in Table 6.1.

Table 6.1: Summary of all the models examined

Model class	Model evidence	Deviation from nominal load	Evaluation time
Model class beam 1	434.49	5 %	5 min
Model class beam 2	497.11	-4%	5 min
Model Class 0	385.04	-20%	24 hours
Model class 1	512.58	4 %	36 hours
Model class 2	515.42	1 %	48 hours

Models where compared based on their evidence score in the Bayesian analysis, which is an indicator of their accuracy. The most accurate model for tension estimation in the examined hanger is therefore Model class 2, which is the the finite element model with four rotational springs ,as shown in Table 6.1.

It is evident that the fixed BC models are substantially less accurate than the ones that take flexibility into account. The use of spring elements is therefore deemed important in the model developing. However, Model class 1, which has additional springs in x and y direction in comparison to Model class 2, did not score as high as expected, despite the fact that it uses the most descriptive boundary conditions. This is a result of the penalty method for the extra parameters in the TMCMC algorithm. Therefore, fixed boundary

conditions in x and y directions seem to be a reasonable approximation for the simulation of the investigated hanger's end supports.

It needs to be noted at this point that even though model numerical models are not as effective in simulating a hanger as their FEA counterparts, their computational time is up to 1000 times lower. The time required for the analysis is very important, as the model has to run many times in the TMCMC algorithm, thus the selection of the most appropriate model should take into account this parameter as well. Especially the analytical model with flexible BC, which scored very close to Model class 2, is still useful for limited time studies, where a rough but quick estimation is required. Furthermore, numerical models can be used to get quick estimations for the problem parameters, which can then reduce the range of those parameters in the FEA models, hence building a very effective hybrid model.

6.2 Future work

Although the study reaches its aims, a few recommendations for future works are made here, based on the findings of this project:

- Excessive study of the beam numerical model with flexible ends in the area of large ξ in order to obtain reliable results for a wider range of hangers
- Optimize the mesh of the finite element models in order to obtain advantageous results in less computational time
- Examine the possibility of a hybrid model, with a numerical rough estimation and an FEA model for accurate results.

Bibliography

[1] Y-C.Chen J.Ching. Transitional markov chain monte carlo method for bayesian model updating, model class selection, and model averaging. *Journal of Engineering Mechanics*, 133(7):816–832, 2007.

[2] L.S. Beck, J.L. Katafygiotis. Updating models and their uncertainties. i: Bayesian statistical framework. *Journal of Engineering Mechanics*, 124(4):455–461, 1998.

[3] Papadimitriou C. Koumoutsakos Angelikopoulos, P. Bayesian uncertainty quantification and propagation in molecular dynamics simulations: A high performance computing framework. *The Journal of Chemical Physics*, 137(14):455–461, 2012.

[4] Yuen.K.Y. Beck, J.L. Model selection using response measurements: Bayesian probabilistic approach. *Journal of Engineering Mechanics*, 130(2):192–203, 2004.

[5] Y.Namita H.Zui, T.Shinke. Practical formula for estimation of cable tension by vibration method. *Journal of Structural Engineering*, 122(6):651–656, 1996.

[6] Wei-Hua Hu Wei-Xin Ren, Gang Chen. Empirical formulas to estimate cable tension by cable fundamental frequency. *Structural Engineering and Mechanics*, 20(3):363–380, 2005.

[7] G. Zheng Y.Q. Ni, J.M. Ko. Dynamic analysis of large diameter sagged cables taking into account flexural rigidity. *Journal of Sound and Vibration*, 257:301–319, 2010.

[8] Carlos A. Prato Marcelo A. Ceballos. Determination of the axial force on stay cables accounting for their bending stiffness and rotational end restraints by free vibration tests. *Journal of Sound and Vibration*, 317:127–141, 2008.

[9] A. Fasana-L. Garibaldi A. Bellino, S. Marchesiello. Cable tension estimation by means of vibration response and moving mass technique. *Mcanique et Industries*, 11:505–512, 2010.

[10] A. Fasana-L. Garibaldi A. Bellino, S. Marchesiello. Tension estimation of cables with different boundary conditions by means of the added mass technique. *UTC compiegne*, 2011.

[11] T.T. William. *Theory of vibration with applications*. Prencise Hall, 2nd edition.

[12] M.Petrolo E.Carrera, G.Guinta. *Beam Structures, Classical and Advanced theories*. Willey.

[13] Jagmohan L.Humar. *Dynamics of Structures.* A.A. Balkema, 2001.

[14] M.Breiner A.Biean. *Matlab 6 for Engineers.* Prencise Hall, 2002.

[15] K.V. Yuen. *Bayesian Methods for Structural Dynamics and Civil Engineering.* Wiley, 2010.

[16] J-S.Wang W.S. Kendall, F.Liang. *Marcov Chain Monte Carlo, Innovations and Applications.* World Scientific Publishing Co.Pte.Ltd., 2005.

Appendix A

Detailed Results

A.1 Convergence test of model class s1

Table A.1: Frequencies (Hz) of model class s1 under 5.35e7 Pa tension in various mesh densities

Elements	600	1000	3500	6200	9500	11200
Direction	x -y	x-y	x-y	x -y	x-y	x-y
Mode 1	5,02	5,58	5,57	5,57	5,57	5,57
Mode 2	11,68	13,46	13,44	13,44	13,44	13,44
Mode 3	20,79	24,3	24,35	24,4	24,51	24,51
Mode 4	35,58	39,04	38,98	38,97	38,98	38,98
Mode 5	47,13	57,00	56,89	56,89	56,9	56,9
Mode 6	64,47	78,42	78,3	78,28	78,28	78,28
elapse time (sec)	4	7	31	51	78	125

A.2 Convergence test of model class s2

Table A.2: Frequencies (Hz) of model class s2 under 5.35e7 Pa tension in various mesh densities

Elements	700	1500	3200	4500	9100	13000	14500
Direction	x -y	x-y	x-y	x -y	x-y	x -y	x -y
Mode 1	6,76	6,99	7,23	7,39	7,48	7,51	7,51
Mode 2	16,26	16,65	17,71	18,21	18,49	18,56	18,56
Mode 3	29,65	30,78	32,63	33,67	34,23	34,39	34,39
Mode 4	47,03	49,53	52,19	53,96	54,91	55,17	55,17
Mode 5	68,62	71,25	76,44	79,11	80,55	80,95	80,95
Mode 6	94,36	97,5	105,37	109,11	111,13	111,69	111,69
Elapse time	6	11	24	36	78	90	98

A.3 Convergence test of model class 0

Table A.3: Frequencies (Hz) of model class under 1.67$e7$ Pa tension in various mesh densities

Elements	A		B		C		D	
Direction	x	y	x	y	x	y	x	y
mode 1	5,98	5,99	5,99	5,60	5,97	5,97	5,97	5,97
mode 2	14,72	14,72	14,74	14,74	14,68	14,68	14,68	14,68
mode 3	27,17	27,18	27,20	27,21	27,10	27,10	27,10	27,10
mode 4	43,38	43,40	43,43	43,46	43,26	43,27	43,25	43,26
mode 5	63,13	63,16	63,21	63,25	62,93	62,95	62,91	62,93
mode 6	86,17	86,22	86,32	86,40	85,86	85,89	85,83	85,87
Elapse time (sec)	14,5		18,2		28,2		38	

Elements	E		F		G	
Direction	x	y	x	y	x	y
Mode 1	5,96	5,96	5,96	5,96	5,96	5,96
Mode 2	14,67	14,67	14,66	14,66	14,66	14,66
Mode 3	27,10	27,10	27,08	27,08	27,0	27,08
Mode 4	43,24	43,24	43,23	43,23	43,22	43,22
Mode 5	62,90	62,90	62,87	62,87	62,86	62,86
Mode 6	85,80	85,80	85,76	85,76	85,75	85,75
Elapse time (sec)	67.7		122		295	

A.4 The effect of the spring stiffness to the finite element moels with flexible boundaries

Model class 1

Table A.4: The frequencies of model class 1 (Hz) under various spring stiffnesses (N/m) in comparisson to the experimental and the model class 0 results

	E+07		E+08		E+09		E+10		E+11	
	x	y	x	y	x	y	x	y	x	y
Mode 1	5,23	5,23	5,71	5,71	5,91	5,91	5,94	5,94	5,94	5,94
Mode 2	12,91	12,91	14,04	14,04	14,53	14,54	14,61	14,61	14,62	14,62
Mode 3	23,62	23,63	25,81	25,81	26,80	26,81	26,96	26,96	27,00	26,98
Mode 4	37,05	37,06	40,86	40,86	42,69	42,70	42,99	43,00	43,02	43,03
Mode 5	52,87	52,89	58,89	58,90	61,92	61,93	62,45	62,46	62,51	62,52
Mode 6	71,03	71,07	79,90	79,91	84,23	84,27	85,09	85,10	85,18	85,20

	E+26		MC 0	Experimental	
	x	y	x- y	x	y
Mode 1	5,94	5,94	5,95	5,82	6,09
Mode 2	14,62	14,62	14,66	13,85	14,86
Mode 3	26,98	26,98	27,08	26,17	27,07
Mode 4	43,03	43,03	43,22	40,47	41,8
Mode 5	62,51	62,52	62,86	59,3	61,5
Mode 6	85,19	85,21	85,74	81,63	85,68

Model class 2

Table A.5: The frequencies of model class 2 under various spring stiffnesses (N/m)

	E+26 to E+13		E+12		E+11		E+10		E+09	
	x	y	x	y	x	y	x	y	x	y
Mode 1	5,94	5,94	5,94	5,94	5,94	5,94	5,94	5,94	5,91	5,91
Mode 2	14,62	14,62	14,62	14,62	14,62	14,62	14,61	14,61	14,54	14,54
Mode 3	26,98	26,98	26,98	26,98	26,98	26,98	26,96	26,96	26,81	26,81
Mode 4	43,03	43,03	43,03	43,03	43,02	43,03	42,99	43,00	42,70	42,71
Mode 5	62,51	62,52	62,51	62,52	62,51	62,52	62,45	62,46	61,94	61,95
Mode 6	85.19	85.19	85.19	85.21	85.18	85.20	85.09	85.10	84.28	84.30

	E+08		E+07		E+06		E+05		MC 0	Experimental	
	x	y	x	y	x	y	x	y	x - y	x	y
Mode 1	5,71	5,71	5,23	5,23	4,61	4,63	4,00	4,05	5,95	5,82	6,09
Mode 2	14,05	14,05	12,92	12,93	11,20	11,24	9,99	10,07	14,66	13,85	14,86
Mode 3	25,82	25,82	23,67	23,68	20,28	20,34	18,82	18,88	27,08	26,17	27,07
Mode 4	40,90	40,89	37,18	37,19	31,99	32,50	30,64	30,69	43,22	40,47	41,8
Mode 5	58,96	58,97	53,16	53,20	46,63	46,68	45,54	45,57	62,86	59,3	61,5
Mode 6	80.02	80.03	71.62	71.67	64.69	64.71	63.85	63.89	85.74	81.63	85.68

A.5 Numerical models vs. Finite element models

Table A.6: Frequencies (Hz) of Model class s1 vs. Model blass beam 1 for $5.35e7$ Pa tension

	MC S1	MC B1
Mode 1	5.57	5.64
Mode 2	13.44	13.56
Mode 3	24.51	24.68
Mode 4	38.98	39.23
Mode 5	56.90	57.31
Mode 6	78.28	78.93

Table A.7: Frequencies (Hz) of Model class s2 vs. Model class beam 1 for $5.35e7$ Pa tension

	MC S1	MC B1
Mode 1	7.48	7.70
Mode 2	18.49	19.11
Mode 3	34.23	35.2
Mode 4	54.91	57.15
Mode 5	82.55	84.09
Mode 6	111.13	116.35

Appendix B

The modeshapes of hanger 3

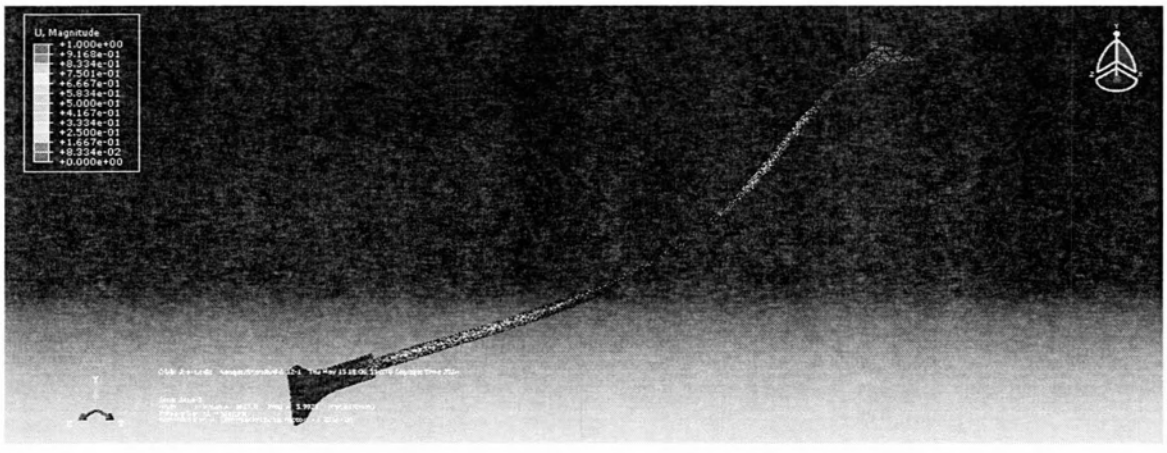

Figure B.1: Mode 1 in x direction of Model 4 under 1.67e7 Pa tension

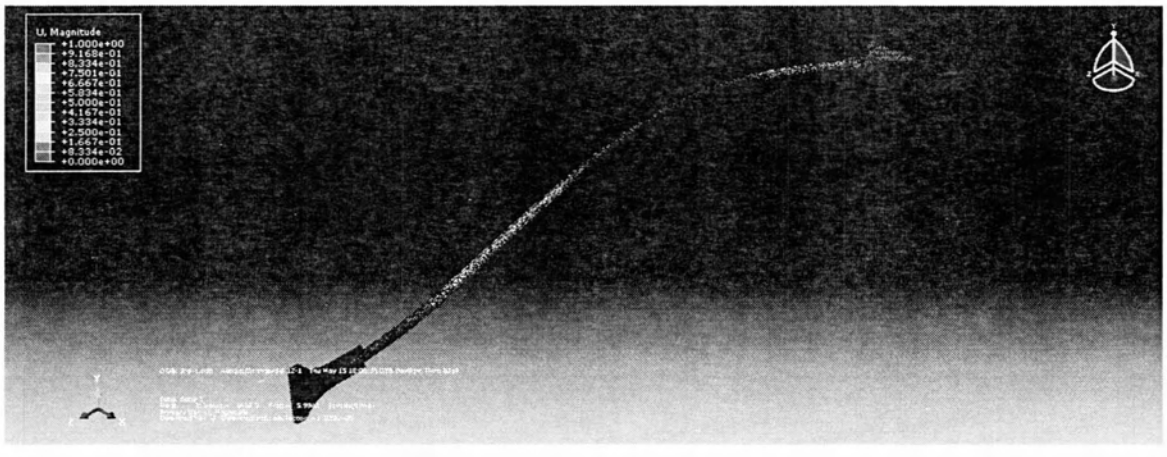

Figure B.2: Mode 1 in y direction of Model 4 under 1.67e7 *Pa* tension

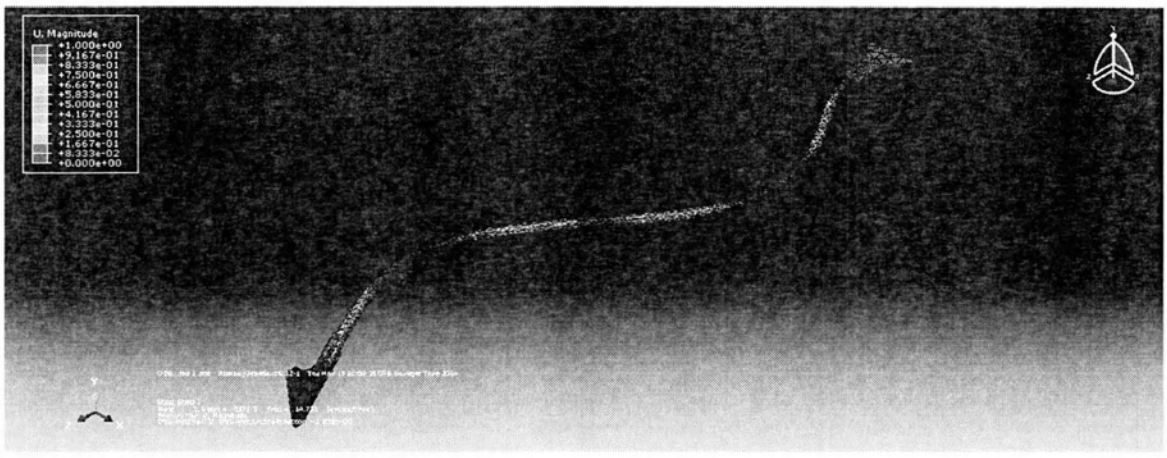

Figure B.3: Mode 2 in x direction of Model 4 under 1.67$e7$ Pa tension

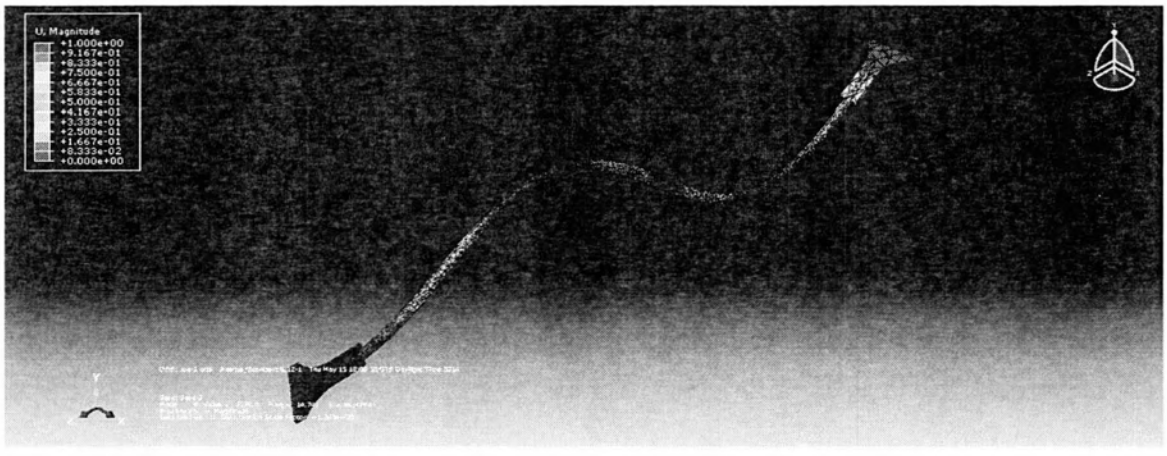

Figure B.4: Mode 2 in y direction of Model 4 under 1.67$e7$ Pa tension

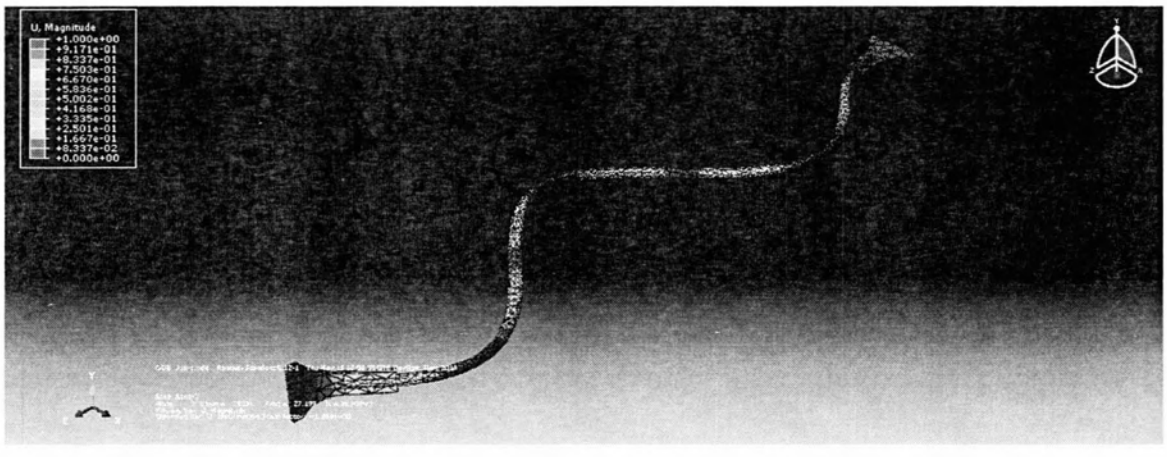

Figure B.5: Mode 3 in x direction of Model 4 under 1.67$e7$ Pa tension

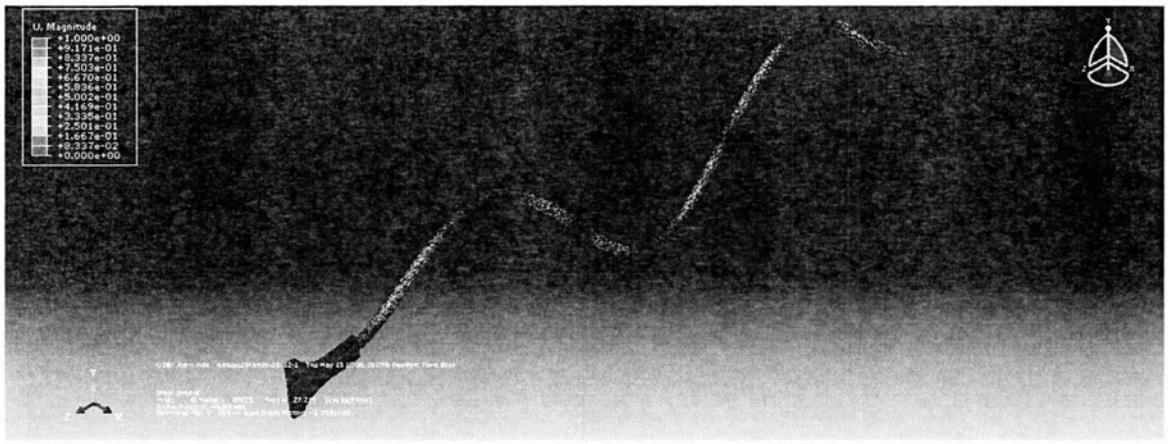

Figure B.6: Mode 3 in y direction of Model 4 under 1.67$e7$ Pa tension

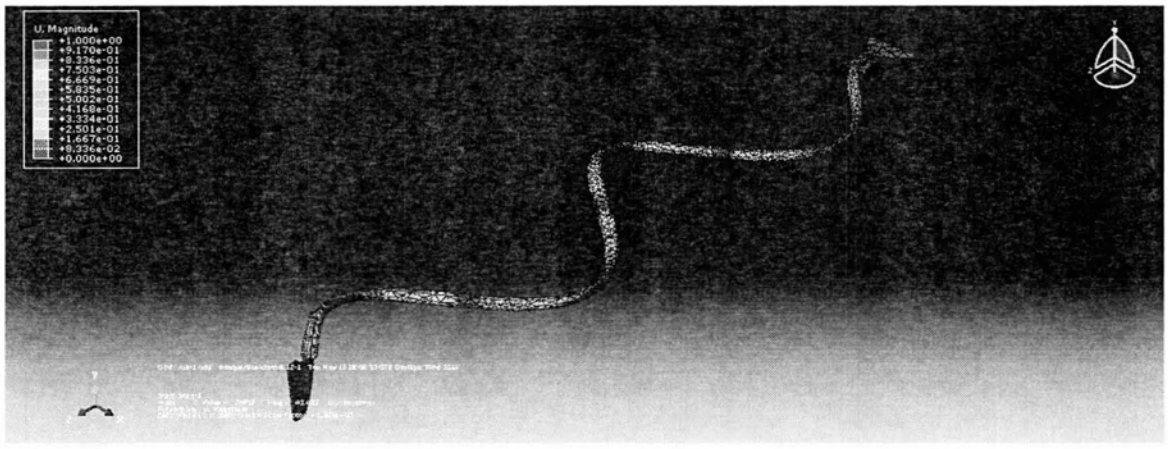

Figure B.7: Mode 4 in x direction of Model 4 under 1.67$e7$ Pa tension

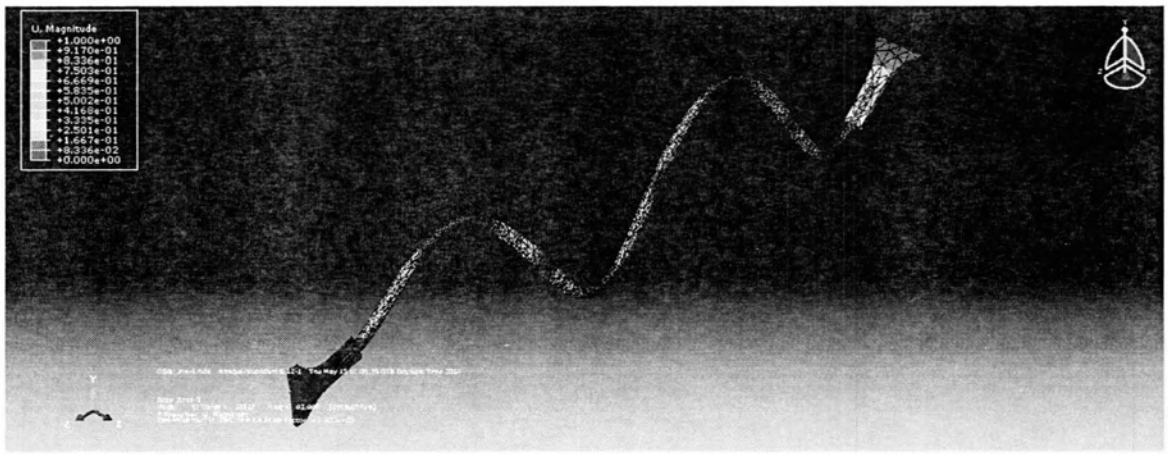

Figure B.8: Mode 4 in y direction of Model 4 under 1.67$e7$ Pa tension

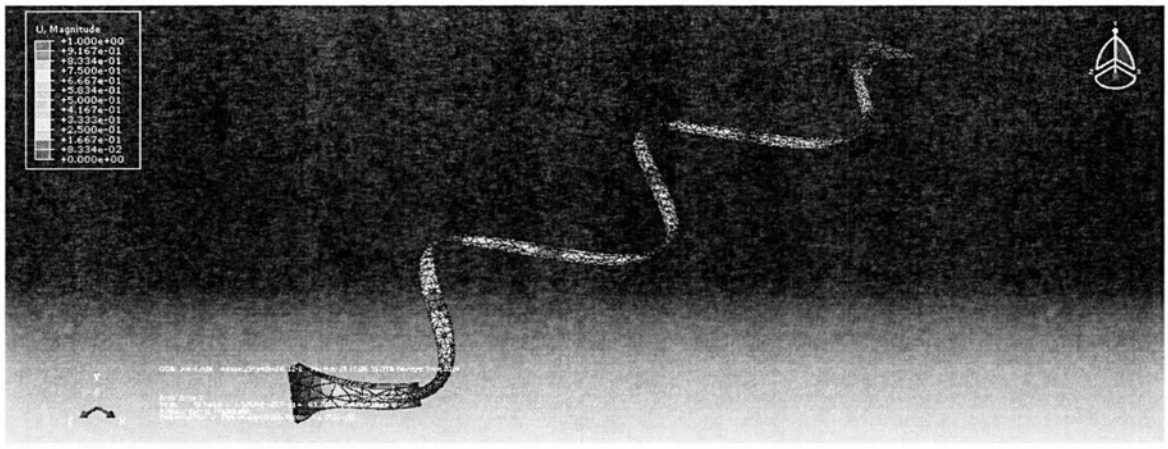

Figure B.9: Mode 5 in x direction of Model 4 under 1.67e7 Pa tension

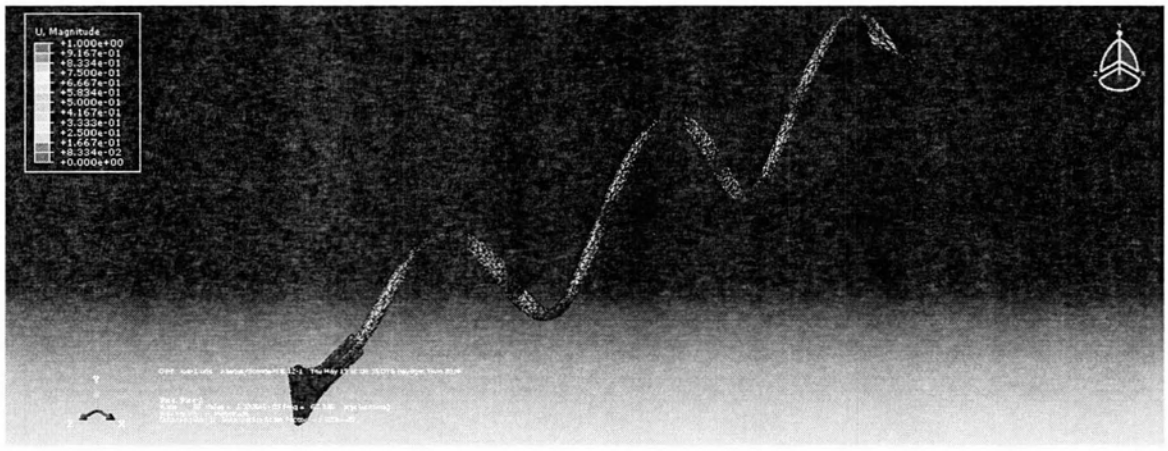

Figure B.10: Mode 5 in y direction of Model 4 under 1.67e7 Pa tension

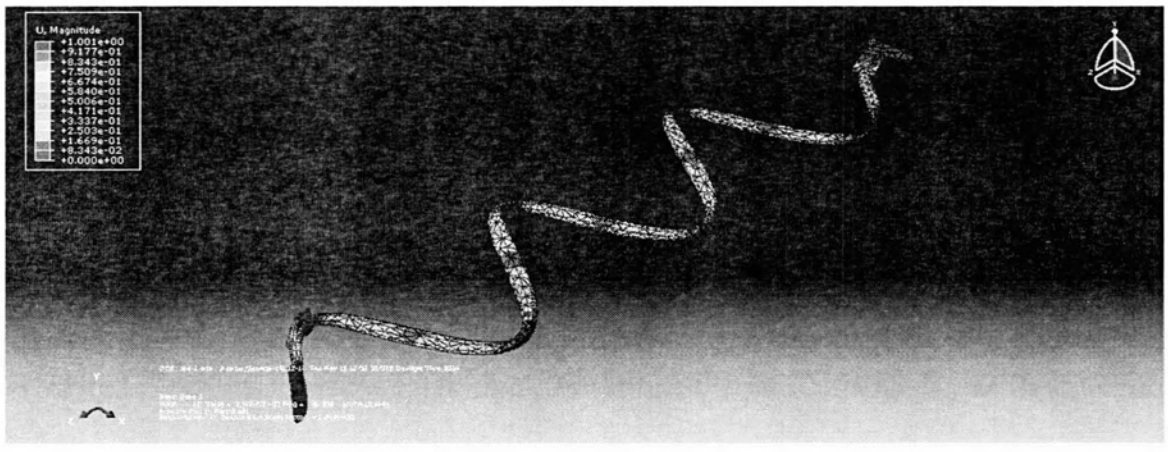

Figure B.11: Mode 6 in x direction of Model 4 under 1.67e7 Pa tension

Figure B.12: Mode 6 in y direction of Model 4 under 1.67e7 Pa tension

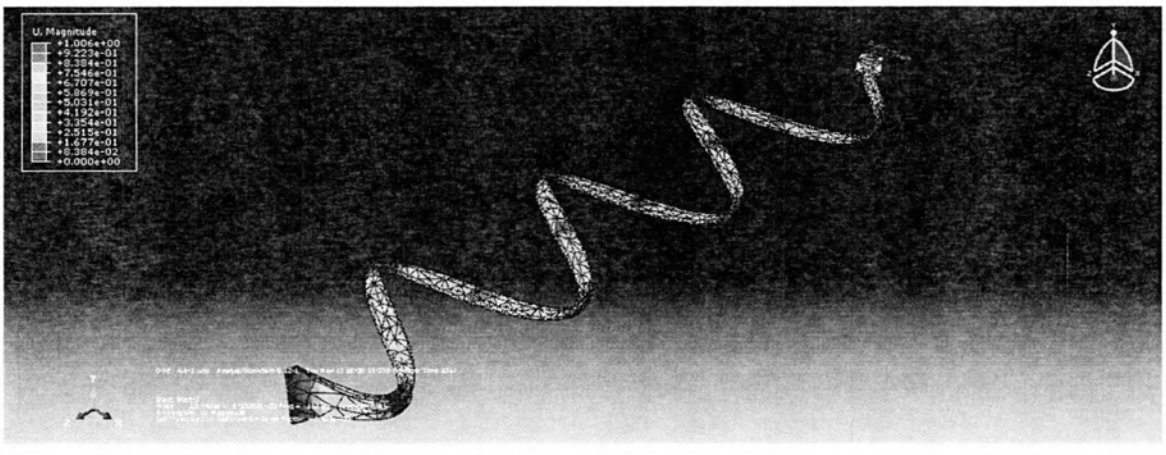

Figure B.13: Mode 7 in x direction of Model 4 under 1.67e7 Pa tension

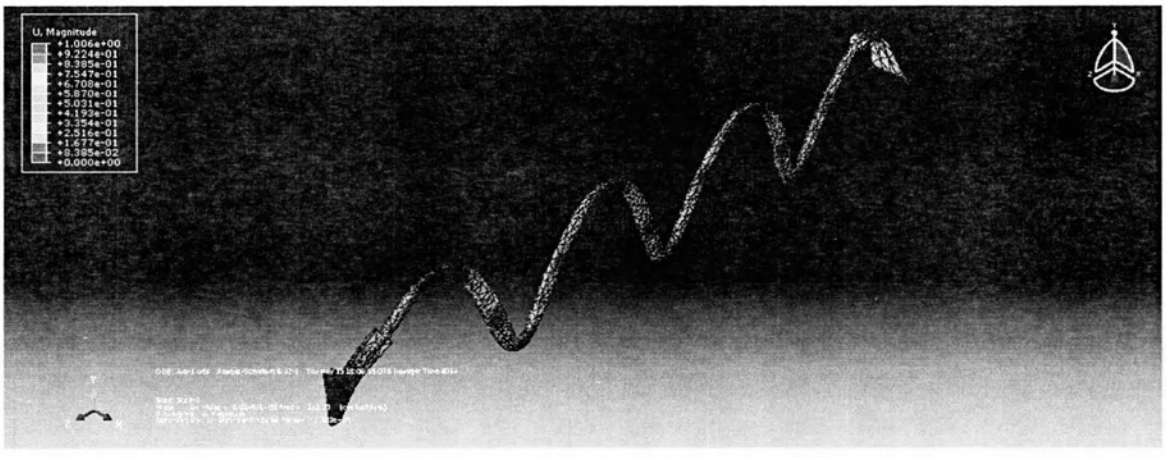

Figure B.14: Mode 7 in y direction of Model 4 under 1.67e7 Pa tension